

MATTHEW THOMAS FERREIRA

**Metabólitos da 15-lipoxigenase Influenciam
Crescimento, Migração e Potencial Invasivo de
Células de Glioblastoma.**

Tese apresentada ao Programa de Pós-Graduação em Biologia de Sistemas do Instituto de Ciências Biomédicas da Universidade de São Paulo, para obtenção do Título de Doutor em Ciências.

São Paulo
2019

MATTHEW THOMAS FERREIRA

**15-Lipoxygenase Metabolites Influence Growth,
Migration and Invasive Potential of
Glioblastoma cells**

Tese apresentada ao Programa de Pós-Graduação em Biologia de Sistemas do Instituto de Ciências Biomédicas da Universidade de São Paulo, para obtenção do Título de Doutor em Ciências.

Área de concentração: Biologia Celular e Tecidual

Orientadora: Profa. Dra. Alison Colquhoun

Versão corrigida

São Paulo
2019

CATALOGAÇÃO NA PUBLICAÇÃO (CIP)
Serviço de Biblioteca e informação Biomédica
do Instituto de Ciências Biomédicas da Universidade de São Paulo

Ficha Catalográfica elaborada pelo(a) autor(a)

Ferreira, Matthew Thomas
15-Lipoxygenase Metabolites Influence Growth,
Migration and Invasive Potential of Glioblastoma
Cells / Matthew Thomas Ferreira; orientadora Dra.
Alison Colquhoun. -- São Paulo, 2019.
113 p.

Tese (Doutorado) -- Universidade de São Paulo,
Instituto de Ciências Biomédicas.

1. Fatty acid metabolism. 2. Matrix
Metalloprotease Activity. 3. Lipoxygenase
synthesis. 4. Cyclooxygenase synthesis. 5.
Glioblastoma metabolism. I. Colquhoun, Dra. Alison,
orientador. II. Título.

UNIVERSIDADE DE SÃO PAULO
INSTITUTO DE CIÊNCIAS BIOMÉDICAS

Candidato(a): Matthew Thomas Ferreira

Título da Dissertação/Tese: 15-Lipoxygenase Metabolites Influence Growth, Migration and Invasive Potential of Glioblastoma Cells

Orientador: Dra. Alison Coluqhoun

A Comissão Julgadora dos trabalhos de Defesa da Dissertação de Mestrado/Tese de Doutorado, em sessão pública realizada a/...../....., considerou o(a) candidato(a):

() **Aprovado(a)** () **Reprovado(a)**

Examinador(a): Assinatura:
Nome:
Instituição:

Examinador(a): Assinatura:
Nome:
Instituição:

Examinador(a): Assinatura:
Nome:
Instituição:

Presidente: Assinatura:
Nome:
Instituição:



Cidade Universitária "Armando de Salles Oliveira", Butantã, São Paulo, SP - Av. Professor Lineu Prestes, 2415 - ICB III - 05508 000
Comissão de Ética em Pesquisa - Telefone (11) 3091-7733 - e-mail: cep@icb.usp.br

CERTIFICADO DE ISENÇÃO

Certificamos que o Protocolo CEP-ICB nº **980/2018** referente ao projeto intitulado: "*Os efeitos dos produtos de 15-LOX-1/2 em GBM in vitro*" sob a responsabilidade de **Matthew Tomas Ferreira** e orientação do(a) Prof.(a) Dr.(a) **Alison Colquhoun**, do Departamento de Biologia Celular e do Desenvolvimento, foi analisado pela **CEUA** - Comissão de Ética no Uso de Animais e pelo **CEPSH** - Comitê de Ética em Pesquisa com Seres Humanos, tendo sido deliberado que o referido projeto não utilizará animais que estejam sob a égide da Lei nº 11.794, de 8 de outubro de 2008, nem envolverá procedimentos regulados pela Resolução CONEP nº 466/2012.

São Paulo, 17 de agosto de 2018.

Prof. Dra. **Luciane Valéria Sita**
Coordenadora CEUA ICB/USP

Prof. Dra. **Camila Squarzoni Dale**
Coordenadora CEPSH ICB/USP

ACKNOWLEDGEMENTS

Firstly, I would like to thank my God and Savior Jesus Christ for putting me in this program and for keeping me, sustaining me, and guiding me until the end. To Him be the glory.

To my wife, Marcela, thank you for all your support, patience, prayers and for your unparalleled love. You are the one of greatest blessings to me, because you are the manifestation of God's grace and mercy to me. I love you and appreciate you very much.

To Dr. Alison Colquhoun, thank you for your guidance, pattern and patience. You are an excellent advisor and an amazing person. You have inspired me with your genuineness as a person, patience as an advisor and, especially, your integrity as a scientist. These are rare qualities and it has been an honor to learn from you.

I also thank Marley Januário da Silva for her support, pleasant attitude and willingness to always help. Your motherly love for us is a crucial element for the success of the entire laboratory.

To Felipe de Costa Souza, thank you for being a good friend and pleasure to work with for all these years. Also, thank you for teaching me how to open my mind, criticize, properly debate and learn from others with different points of view. This is an essential characteristic of a balanced human being. Thank you and I wish you all the best, my friend.

To Janaína Alessandra Silva, we entered into this doctoral program together as complete strangers, and now we are good friends. Thank you for reminding me to breath and call on Jesus when I was stressed, anxious or nervous. Believe it or not, this is one of the greatest forms of salvation. Your reminders helped to save me from so many negative things. You are an amazing person and wonderful friend.

To Lucas Barbosa Rossetti, thank you for being calm and rational at every turn, this influenced me a lot. Your willingness to help, flexibility and diligent attitude are key features of great scientist.

I would also like to thank Laís Mendes Goes for teaching me more than I could ever teach her. You have so much knowledge and you are a hard worker, that is why I know you will be an amazing scientist and a great professor.

To my family and friends in the USA, thank you for releasing me and supporting me to follow my dreams. I love you all and miss you all.

Finally, I would like to thank all of my colleagues who have contributed practically, emotionally, psychologically and spiritually to my experience here: Gustavo, Ivonir, Suzane, Renata, Luciana, Raony, Katrin, Ari, Ana Flavia, Gabriela, Ana, Michelle, Uri, Suelen, Fernanda, Cecilia, and all of the Professors that I have come to know during these years. Thank you very much.

I would like to thank CAPES for financially supporting me during this project (2015-2019).

“Keep your heart with all vigilance, for from it are the issues of life. Put away from you crooked speech and put perverse talk far from you. Let your eyes look directly ahead, and let your gaze be straight in front of you. Make straight the path of your feet, and all your ways will be established.” -Proverbs 4:23-26

ABSTRACT

Ferreira MT. **15-Lipoxygenase Metabolites Influence Growth, Migration and Invasive Potential of Glioblastoma cells** [Thesis (Ph.D. thesis in Systems Biology: Cell and Tissue Biology)]. São Paulo: Instituto de Ciências Biomédicas, Universidade de São Paulo; 2019.

Introduction and Objectives: Understanding the interaction between extremely aggressive cancers, like glioblastoma (GBM), and fatty acid metabolism could contribute to improve anti-tumoral therapies. 15-Lipoxygenase-1 (15-LOX-1), a linoleic acid (LA) and arachidonic acid (AA) metabolizing enzyme, induces both pro- and anti-tumorigenic effects in different cancer types. Its role in glioblastoma has not yet been clearly described. The aim of this study was to describe the influence of 15-LOX and its metabolites on GBM cell growth, migration and invasive potential.

Experimental Design: Two GBM cell lines were cultivated and treated *in vitro* with 15-LOX metabolites (13(S)-Hydroxyoctadecadienoic Acid (13-HODE), 9-HODE and 15(S)-Hydroxyeicosatetraenoic Acid (15-HETE)) and/or 15-LOX inhibitors (LUT and NDGA). MTT viability curves (HODEs [0.1-1 μ M]) and dose response curves (HODEs [1-10 μ M]; LUT [7.5-15 μ M]; NDGA [20-40 μ M]) were performed over 24h, 48h, 72h. Next, conventional and/or quantitative RT-PCR's (15-LOX and related downstream mRNAs: PPARs, GPR132, MMPs) of the cells were performed. Wound healing assays were performed after 12h of treatment (HODEs [5 μ M]; LUT [15 μ M]; NDGA [40 μ M]) to examine migration. Then, gelatin zymography (10mg/mL) and western blots (40 μ g of protein/sample) were performed to identify the influence of these metabolites and inhibitors on GBM invasive capacity (defined here as the presence/activity of MMPs). **Results and Discussion:** The 15-LOX pathway is present and active in the GBM cell lines. Both 13-HODE [5 μ M] and 9-HODE [5-10 μ M] increased cell count in U87MG (n=3). 13-HODE and 15-LOX-1 inhibitors, LUT [15 μ M] and NDGA [40 μ M], decreased migration in cell line T98G, and NDGA reduced matrix metalloprotease (MMP2) activity and increased the latent form of MMP2. 13-HODE/9-HODE treatments increase MMP2 mRNA in T98-G and U87-MG, respectively. All data were plotted and analyzed using GraphPad Prism 5.0. Analysis between two groups was performed with Student's T test, and a two-way ANOVA with Bonferroni post-test was used to compare multiple groups. The differences were considered statistically significant at $p < 0.05$. **Conclusions and Perspectives:** 13-HODE and 9-HODE influence GBM cell growth, 13-HODE and 15-LOX inhibition decreased migration, and 13-HODE/9-HODE increased invasive potential, while 15-LOX inhibition decreased invasive potential. 15-LOX and its LA-derived metabolites exercise a certain pro-tumorigenic influence on GBM cells *in vitro*. Further studies will clarify if these relationships positively correlate with malignancy.

Keywords: Glioblastoma. Lipoxygenases. Lipid Mediators. Cancer. MMPs.

RESUMO

Ferreira MT. **Metabólitos da 15-lipoxigenase Influenciam Crescimento, Migração e Potencial Invasivo de Células de Glioblastoma.** [Tese (Doutorado em Biologia de Sistemas: Biologia Celular e Tecidual)]. São Paulo: Instituto de Ciências Biomédicas, Universidade de São Paulo; 2019.

Introdução e Objetivos: Compreender a interação entre cânceres extremamente agressivos, como o glioblastoma (GBM), e o metabolismo dos ácidos graxos poderia contribuir para a melhora de terapias anti-tumorais. A 15-lipoxigenase-1 (15-LOX-1), uma enzima que metaboliza o ácido linoleico (LA) e o ácido araquidônico (AA), induz efeitos pró ou anti-tumorigênicos em diferentes tipos de câncer. Seu papel no GBM ainda não foi claramente descrito. O objetivo deste estudo foi descrever a influência da 15-LOX e seus metabólitos no crescimento, migração e potencial invasivo de células de GBM. **Delineamento Experimental:** Duas linhagens celulares de GBM foram cultivadas e tratadas *in vitro* com metabólitos da 15-LOX (Ácido 13(S)-Hidroxiocetadecadienoico (13-HODE), 9-HODE e Ácido 15(S)-Hidroxi-eicosatetraenoico (15-HETE)) e/ou inibidores de 15-LOX (LUT e NDGA). Curvas de viabilidade com MTT (HODEs [0,1-1 μ M]) e curvas de dose-resposta (HODEs [1-10 μ M]; LUT [7,5-15 μ M]; NDGA [20-40 μ M]) foram realizadas por 24h, 48h, 72h. Em seguida, foram realizados RT-PCR convencional e/ou quantitativo das células (RNAm's de 15-LOX e seus correspondentes *downstream*: PPARs, GPR132, MMPs). Os ensaios de fechamento de ferida foram realizados após 12 horas de tratamento (HODEs [5 μ M]; LUT [15 μ M]; NDGA [40 μ M]) para avaliar a migração. Em seguida, foram realizadas zimografias em gelatina (10mg/mL) e western blot (40 μ g de proteína/amostra) para identificar a influência desses metabólitos e inibidores no potencial invasivo do GBM (definida aqui como a presença/atividade das MMPs). **Resultados e Discussão:** A via de 15-LOX está presente e ativa nas linhas celulares de GBM. 13-HODE [5 μ M] e 9-HODE [5-10 μ M] aumentaram a contagem de células em U87MG (n = 3). Inibidores de 13-HODE e 15-LOX-1, LUT [15 μ M] e NDGA [40 μ M], diminuíram a migração na linhagem celular T98G, e NDGA reduziu a atividade de MMP2 e aumentou a forma latente de MMP2. Os tratamentos com 13-HODE / 9-HODE aumentam o RNAm de MMP2 em T98G e U87-MG, respectivamente. Todos os dados foram plotados e analisados usando o GraphPad Prism 5.0. A análise entre dois grupos foi realizada com o teste T de Student, e a ANOVA de duas vias com pós-teste de Bonferroni foi usado para comparar mais de dois grupos de dados. As diferenças foram consideradas estatisticamente significativas quando p < 0,05. **Conclusões e Perspectivas:** 13-HODE e 9-HODE influenciam o crescimento de células de GBM, 13-HODE e 15-LOX inibiram a migração, e 13-HODE/9-HODE aumentaram o potencial invasivo, enquanto a inibição de 15-LOX diminuiu o potencial invasivo. 15-LOX e seus metabólitos derivados de LA exercem uma influência pró-tumorigênica sobre as células de GBM *in vitro*. Novos estudos esclarecerão se essas relações se correlacionam positivamente com a malignidade. **Palavras-chave:** Glioblastoma. Lipoxigenases. Mediadores lipídicos. Câncer. MMPs.

LIST OF FIGURES

Figure I1 – Review of Biochemistry and Fatty Acid Synthesis	21
Figure I2 – Summary of PUFA Metabolism.....	23
Figure I3 – Mechanism for lipoxygenation of a <i>cis,cis</i> -1,4-pentadiene	26
Figure I4 – Schematic representation of linoleic acid metabolism	27
Figure I5 – Summary of the classifications and structures of mammalian MMPs.....	32
Figure R1 – Gel electrophoresis of cDNA	44
Figure R2 – Annealing Temperature Tests	44
Figure R3 – Conventional RT-PCR on 15-LOX Pathway in five GBM cell lines	46
Figure R4 – Colorimetric assay of U87-MG cells treated with 9-HODE and 13-HODE over a 72-hour period	48
Figure R5 – Exogenous 13-HODE treatments on U87-MG and T98-G over 72 hours	50
Figure R6 – Exogenous 9-HODE treatments on U87-MG and T98-G over 72 hours	51
Figure R7 – Exogenous 15-HETE treatments on U87-MG and T98-G over 72 hours	51
Figure R8 – Treatment with Lipoxygenase inhibitors Luteolin and NDGA	52
Figure R9 – Western Blots of 15-LOX-1 expression after treatments with LOX inhibitors Luteolin (LUT) and Nordihydroguaiaretic acid (NDGA) for 72 hours	53
Figure R10 – U87-MG treated with Lipoxygenase inhibitors Luteolin and NDGA	55
Figure R11 – T98-G treated with Lipoxygenase inhibitors Luteolin and NDGA	56
Figure R12 – Concomitant Treatments of HODEs with Lipoxygenase inhibitors in U87-MG	58
Figure R13 – Wound Healing Assay graphs for cell line T98-G Graphs	59
Figure R14 – Wound Healing Assay in cell line T98-G	60
Figure R15 – RT-PCR primer standardization of MMPs	62
Figure R16 – Conventional RT-PCR of MMP expression profile in 5 GBM Cell Lines	62
Figure R17 – Real Time quantitative RT-PCR of MMP expression profile in 5 GBM Cell Lines	63
Figure R18 – Zymograms of endogenous MMP expression	64
Figure R19 – Real Time quantitative RT-PCR expression of MMP2 and MMP14	65
Figure R20 – Western Blot and relative band intensities of U87-MG and T98-G cells treated with LUT or NDGA	67

Figure R21 – Gelatin Zymography and relative band intensities of GBM cells treated with LUT or NDGA	68
Figure R22 – Western Blots of 15-LOX-1 expression after treatments with a COX-1 inhibitor (SC560) and a COX-2 inhibitor (NS398) for 24 hours	70
Figure R23 – Western Blots of 15-LOX-1 expression after treatments with PGE₂ for 24 hours	71
Figure R24 – Conventional RT-PCR expression of MMP-2, MMP-14, MMP-9	72
Figure R25 – Quantitative Real Time PCR of MMP-2 and MMP-14 gene expression	73
Figure R26 – Western Blot and relative band intensities of MMPs in U87-MG and T98-G cells treated with SC560 or NS398	74
Figure R27 – Western Blot and relative band intensities of U87-MG cells treated with PGE₂	75
Figure R28 – COX Inhibitor Gelatin Zymography	76
Figure S1 – LC\ EIS-MS/MS of the Products	103
Figure S2 – 15-LOX-1 mRNA and protein expression observed by the Human Protein Atlas Project	104
Figure S3 – 15-LOX-2 mRNA and protein expression observed by the Human Protein Atlas Project	105
Figure S4 – TCGA database information concerning 15-LOX-1 and 15-LOX-2 mRNA expression and survival curves	106
Figure S5 – PPAR beta/delta mRNA and protein expression observed by the HPA and TCGA	107
Figure S6 – MMP-2 mRNA and protein expression observed by the Human Protein Atlas Project	108
Figure S7 – MMP-14 mRNA and protein expression observed by the Human Protein Atlas Project	109
Figure S8 – MMP-9 mRNA and protein expression observed by the Human Protein Atlas Project.....	110

**Figure S9 – TCGA database information concerning 15-LOX-1 and 15-LOX-2 mRNA
expression and survival curves111**

LIST OF TABLES

Table I1 – Summary of 15-LOX`s expression and influence on tumor progression in different models of cancer	30
Table M1 – Protein Quantification Standard Curve	39
Table M2 – Composition of Western Blot electrophoresis Separating Gel	39
Table M3 – Composition of Western Blot electrophoresis Loading Gel	39
Table M4 – Composition of Zymogram electrophoresis Separating Gel	42
Table M5 – Composition of Zymogram electrophoresis Loading Gel	42
Table R1 – Primer sequences, annealing temperatures, and band sizes for RT-PCR	45
Table R2 – Characteristics of U87-MG and T98-G GBM cell lines	47
Table R3 – MMP Primer sequences, annealing temperatures, and band sizes for RT-PCR	61
Table S1 – Summary of mRNA/Protein Expression identified by the Human Protein Atlas and TCGA Databases	112

LIST OF ACRONYMS

AA – Arachidonic Acid
cAMP – cyclic Adenosine Monophosphate
COX – Cyclooxygenase
CYP – Cytochrome P450
DMSO – Dimethyl sulfoxide
ECM – Extracellular Matrix
GBM – Glioblastoma
GPR 132 – G Protein Coupled Receptor 132
HETE – Hydroxyeicosatetraenoic Acid
HODE – Hydroxyoctadecadeinoic Acid
HPA – Human Protein Atlas
IDH1 – Isocitrate dehydrogenase
LA – Linoleic Acid
LOX – Lipoxygenase
LUT – Luteolin
MMP – Matrix Metalloprotease
MTT - Tetrazolium dye (3-(4,5-Dimethylthiazol-2-yl)-2,5-diphenyltetrazolium bromide)
NDGA - Nordihydroguaiaretic acid
PC – Phosphatidylcholine
PGE₂ – Prostaglandin E2
PL – Phospholipase
PPAR – Peroxisome Proliferator-Activated Receptor
ProMMP – Latent Form Matrix Metalloprotease
PUFA – Polyunsaturated Fatty Acid
RT-PCR – Reverse Transcription Polymerase Chain Reaction
TCGA – The Cancer Genome Atlas

CONTENTS

1 INTRODUCTION	17
1.1 CLASSIFICATION	17
1.2 FATTY ACIDS AND LIPID MEDIATORS	19
1.2.1 Polyunsaturated Fatty Acid Synthesis (Linoleic Acid/Arachidonic Acid)	22
1.3 ENZYME FAMILIES	24
1.3.1 Cyclooxygenases	24
1.3.2 Cytochrome P450 Epoxygenase	25
1.3.3 Lipoxygenase	25
1.3.4 5-Lipoxygenase (5-LOX)	27
1.3.5 12-Lipoxygenase (12-LOX)	27
1.3.6 15-Lipoxygenase (15-LOX)	28
1.3.7 15-LOX Products	28
1.4 TUMOR INVASION	31
1.4.1 Matrix Metalloproteases (MMPs)	31
2 JUSTIFICATION	34
3 MATERIALS AND METHODS	35
3.1 Cell Culture	35
3.2 Dose-Response Curve/ Trypan Blue Staining	35
3.3 MTT (3-(4,5-Dimethylthiazol-2-yl)-2,5-diphenyltetrazolium bromide) Assay	35
3.4 Total RNA Extraction	36
3.5 cDNA Synthesis	36
3.6 Conventional RT-PCR	37
3.7 Quantitative Real-Time PCR	37
3.8 Protein Extraction and Quantification	37
3.8.1 Sample Preparation	38
3.8.2 Protein Extraction	38
3.8.3 Protein Quantification	38
3.9 Western Blot	39
3.9.1 Gel Preparation	39
3.9.2 Running Samples	40
3.9.3 Blocking and Antibodies	40
3.10 Zymography Assay	40
3.11 Scratch Assay	42
3.12 Statistical Analysis	42
4 RESULTS	44

4.1	15-Lipoxygenase Pathway	44
4.1.1	RT-PCR of 15-LOX Pathway	46
4.1.2	Cell Line Selection	47
4.1.3	Cell Viability and Growth	47
4.2	15-Lipoxygenase Inhibitors	52
4.2.1	HODEs + 15-LOX Inhibitors in U87-MG	57
4.3	T98-G Cell Migration.....	59
4.4	Metalloproteases and Invasive Potential	61
4.4.1	HODEs and MMP expression	65
4.4.2	15-LOX Inhibitors and MMP expression	66
4.5	The Influence of COX and PGE2 on 15-LOX-1 and MMPs	69
5	DISCUSSION	77
5.1	15-LOX Pathway in GBM	77
5.2	15-LOX Products and Cell Viability and Growth	81
5.3	Lipoxygenase Inhibitors and Influence on GBM	82
5.4	15-LOX and Migration	84
5.5	Invasive Potential	85
5.6	The influence of COX on LA metabolism and Invasive Potential	86
6	CONCLUSION	88
	REFERENCES	89
	APPENDEX – SUPPLEMENTAL DATA	102

1 INTRODUCTION

Cancer is a collection of related diseases in which cellular dysregulation occurs to a point where cell death is not occurring adequately, cell proliferation is upregulated and cells begin to invade nearby tissues (1)(2). More than 18 million people were diagnosed with cancer in 2018, and the World Health Organization/ International Agency for Research on Cancer (WHO/IARC) predicts that this number will reach an estimated 24.5 million by 2030. Of these 18 million people, nearly 296 thousand were diagnosed with cancer in the brain or nervous tissue in 2018 and this number will likely increase to 350 thousand cases by 2030 (3). Gliomas, which are the most common form of brain tumors, are denominated by their similarity to glial cells in the nervous tissue, however, whether the cell of origin that produces the heterogenous tumor mass are glial cells (i.e. astrocytes, oligodendrocytes, microglia and ependymal cells) or neural stem cells or oligodendrocyte progenitor cells continues to be a topic for discussion in the literature (4).

1.1 CLASSIFICATION

The glioma grading system established by the World Health Organization (WHO) uses four grades (I, II, III, IV). Traditionally, the classification of primary brain tumors depended exclusively on a consensus reached after examining a tumor's histological characteristics (5). This histological exam first determines whether the tumor is diffuse (Grades II-IV) or not. Other aspects examined, i.e. in the case of malignant gliomas, include regions of necrosis and endothelial proliferation. Unfortunately, this type of cytological classification is prone to variability due to the subjective nature of histological interpretation.

However, in 2014, a meeting held in the Netherlands hosted by the International Society for Neuropathology gathered many of the world's experts to discuss the incorporation of molecular aspects into the diagnostic process of brain tumor classification (6). This meeting officially opened the way for a more complete, effective and modernized process of tumor classification. Hybridizing the diagnostic process, examining both genotypic and phenotypic aspects, was incorporated into the *World Health Organization Classification of Tumours of the Central Nervous System: Revised 4th Edition* (6).

The definition of clinically less frequent Grade I gliomas, generally classified as pilocytic tumors, were not altered. However, the new classification of other astrocyte-derived tumors

subdivided each grade, diffuse gliomas (Grade II), anaplastic gliomas (Grade III), and Glioblastomas (Grade IV), into three additional subclassifications: IDH-mutant, IDH-wild type and NOS. Isocitrate dehydrogenase (IDH) exists as different isoforms within the mitochondria, cytosol and peroxisomes. IDH1, one of the main producers of cytosolic NADPH, is found in the cytosol and peroxisomes. IDH1 mutations convert α -ketoglutarate to D-2-hydroxyglutarate (D-2HG). D-2HG can then increase DNA and histone methylation, thus, producing a potentially tumorigenic situation (7). IDH1 is a known biomarker of early astrocytoma development (8).

After histological examination, the status of IDH is determined through immunohistochemistry, and if the results are inconclusive the *not otherwise specified* (NOS) class is designated (6)(9). The other tumor types that were reclassified, but are not covered in the present study, can be reviewed in the WHO's 2016 publication (6). Using histology together with genomics opens the way for incorporating molecular cancer biology into clinical environments. Moreover, including proteomics and lipidomics could improve the classification process and even the therapeutic approach, however, accessible, cost-effective technologies for measuring these parameters are currently not available. Furthermore, identifying specific biomarkers and understanding their roles in and response to pharmacotherapies are still being explored.

About 28% of all central nervous system (CNS) tumors and 80% of all malignant CNS tumors are gliomas, and 45.2% of all malignant gliomas are classified as glioblastomas (GBM) (10). According to Matias *et al.* (2018) the typical characteristics that define GBM histological diagnostics are “nuclear atypia, cellular pleomorphism, mitotic activity, diffuse growth pattern, microvascular proliferation, and/or necrosis” (11). As for the IDH1 status in primary glioblastomas (90% of cases), IDH1 is not mutated, and in secondary glioblastoma (10% of cases) IDH1 mutations are identified (6).

As an attempt to treat GBM, conventional therapies applied are surgical resections, radiation therapy and chemotherapy. Unfortunately, the efficacy of these combined treatments is short-lived and the overall survival for most of these patients is between 12-15 months (11). There are a number of theories that try to explain the temporary effectiveness of current therapies, ranging from cancer stem cells (12) to tumor invasiveness (13), or from multiple drug resistance (14) to taking advantage of immune cell responses (15). Due to the heterogenous nature of glioblastoma cell composition, the involvement of all these factors, and others, have been demonstrated (16)(17).

The 2011 publication of Hanahan and Weinberg's "Hallmarks of Cancer: The Next Generation" included tumor-promoting inflammation as an enabling characteristic of cancer (18). Later, Fouad and Aanei (2017) revisited and even reorganized these classic hallmarks proposing a new definition of a cancer hallmark as "acquired evolutionary advantageous characteristics that complementarily promote transformation of phenotypically normal cells into malignant ones, and promote progression of malignant cells while sacrificing/ exploiting host tissue" (19). One of their proposed hallmarks is called "metabolic rewiring". In a review by Pavlova and Thompson, metabolic rewiring can be further separated into 6 hallmarks, one of which is the use of opportunistic modes of nutrient acquisition (20). This opportunistic nutrient acquisition includes scavenging free fatty acids from the microenvironment (21)(22). Both tumor-promoting inflammation and metabolic rewiring involve fatty acid-derived lipid mediators.

1.2 FATTY ACIDS AND LIPID MEDIATORS

Fatty acids are one of four basic building blocks in the cell; the others are sugars, amino acids and nucleotides. Fatty acids constitute fats, lipids and membranes, and they also serve as a source of energy. For periods of long-term fasting, fatty acids are stored as triacylglycerol lipid droplets in adipocytes. When energy is needed, and glucose metabolism is not adequate, fatty acid oxidation often occurs, although not exclusively, in the mitochondria; as is the case with the heart and liver (23). Panov *et al.* (2014) emphasize in their review that "20% of the brain's energy metabolism is supplied by the β -oxidation of fatty acids in astrocytic mitochondria" (24). Fatty acids used in nervous tissue metabolism for ATP synthesis can also be used, with the help of certain oxidases, to produce bioactive oxidized fatty acids called lipid mediators. The lipid mediators produced in both mitochondria and cytosol of many cell types, including astrocytes, are responsible for an array of signaling cascades involved in homeostasis, stress responses and disease pathology (25). As the literature clearly demonstrates, bioactive lipid mediators are directly involved in regulating the immune response to pathogens and lesions, as well as regulating inflammation (26)(22).

Fatty acid sources, most frequently localized in lipid membranes, vary in their number of carbons, the number of double bonds they possess, the location of their unsaturated carbons (double bonds) and hydroxylation sites (sites containing an -OH group). The composition of the cell membrane is very diverse, including glycerophospholipids, sphingolipids and cholesterols (27).

According to Harayama and Riezman's review (2018), there are two types of lipid diversity: 1) chemical and 2) compositional. Chemical diversity includes the individual structure of a lipid, e.g. stereoisomers; whereas compositional diversity considers the ratio of different lipids present in the membrane. They, together with Hayashi *et al.* (2014), describe how the position of a lipid group on the glycerol backbone within the cytoplasmic membrane can determine where a fatty acid becomes saturated, desaturated and elongated, and the subsequent biochemical signaling pathways that follow it. For example, considering Phosphatidylcholine (Figure I1), along the glycerol backbone there are 3 binding sites (Sn1, Sn2, Sn3); the third of which possess a phosphate group forming a glycerol-3-phosphate moiety. The Sn1 and Sn2 sites link with fatty acids. In the Sn1 position, the linked fatty acids tend to be saturated and monounsaturated fatty acids; while in the Sn2 position, unsaturated fatty acids may be found (27)(28). The enzymes involved with fatty acid remodeling in the membrane, e.g. transacylases, have been reported as being involved with polyunsaturated fatty acid accumulation (28). (Figure I1 briefly reviews biochemical principles and fatty acid synthesis cited in this thesis).

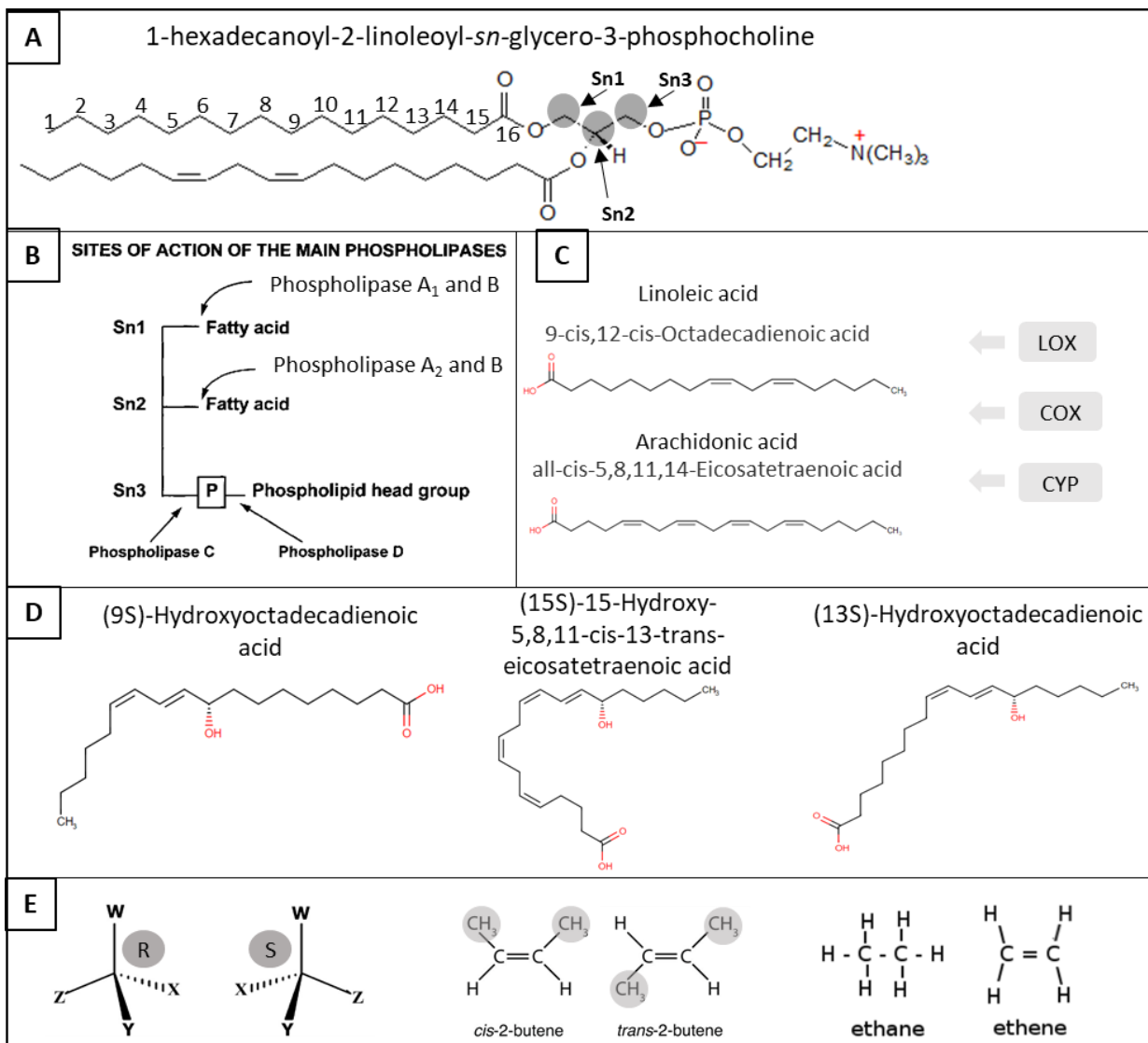


Figure 11. Review of Biochemistry and Fatty Acid Synthesis. [A] An example of a typical phospholipid: 1-hexadecanoyl-2-linoleoyl-*sn*-glycero-3-phosphocholine (PC). At the Sn1 site is a monounsaturated fatty acid, palmitic acid (16:0) (PA), while at the Sn2 site is a PUFA, linoleic acid (18:2n6) (LA). The classification of PUFAs are based upon the first unsaturated carbon of the membrane-bound fatty acyl group [ex. omega-6 fatty acid; 6th Carbon from the methyl group]. Moreover, the numbering applied (ex. Linoleic Acid = 18:2) refers to the number of carbons (18) and the number of double bonds (2) present. [B] Phospholipase A₂ hydrolyzes the LA to release it from the glycerol's Sn2 position. [C] LA and arachidonic acid (20:4n6 AA; another common example of a Sn2 bound PUFA) become available for oxygenation by lipoxygenases (LOX), cyclooxygenase (COXs) and/or cytochrome P450 epoxygenase (CYPs). [D] The products yielded can be referred to as lipid mediators when examining biological activities. In this case, the denomination of these lipids depends on the carbon at which the hydroxyl group is added (ex. 9-HODE; 9th carbon from the carboxyl end). [E] [Left-to-Right] These are examples of chiral structures (S) and (R); *cis*- and *trans*- conformations, which are responsible for the bends in a PUFA's structure; and unsaturated (ex. Ethene) and saturated (ex. Ethane) structures. Fatty acid chemical structures were acquired from The Human Metabolome Database (<http://www.hmdb.ca/>).

1.2.1 Polyunsaturated Fatty Acid Synthesis (Linoleic Acid/Arachidonic Acid)

Certain, basic polyunsaturated fatty acids (PUFAs) cannot be synthesized, *de novo*, by mammals and, therefore, must be consumed in one's diet. The intake of PUFAs, followed by their assimilation into cellular membranes subsequently alter the bioavailability of certain fatty acid substrates and their lipid mediator products. PUFAs are fatty acids that have more than one double bond in their carbon chain. The fatty acid nomenclature depends on the carbon of the first double bond closest to the methyl terminus or the omega end, e.g. omega-3 (Carbon 3 = docosahexaenoic acid), omega-6 (Carbon 6 = arachidonic acid). PUFAs in the brain are represented by omega-3 (n3) and omega-6 (n6) fatty acids (29). (Figure I1)

Once incorporated in the cell membrane, PUFAs are made available for metabolism with the aid of a superfamily of enzymes called phospholipases (PL). There are three main classes of phospholipases according to their hydrolytic cleavage sites: PLA, PLC and PLD. PLA cleaves fatty acyl ester bonds at either the sn1 (PLA1) or sn2 (PLA2) position (30). There are four main types of PLA2's: secretory (sPLA2), calcium-independent (iPLA2), lipoprotein (Lp-PLA2) and cytosolic (cPLA2). Cytosolic PLA2 is of interest due to its role in fatty acid metabolism and lipid mediator production, as well as its association with chemoresistance in GBM (31). Membrane-bound fatty acids, like linoleic acid and arachidonic acid, can be hydrolyzed and released by cPLA2 and, with the help of other enzymes, subsequently processed into bioactive lipid mediators.

Linoleic acid (LA) is an 18 carbon, long chain fatty acid (LCFA = that which contains 14-18 carbons) with two *cis*(Z) double bonds beginning from the 6th carbon (18:2n6) (Figure I1). This PUFA is the precursor of all the omega-6 (n6) fatty acids and can be synthesized *de novo* by Δ 12-desaturase; however, mammals lack this enzyme. Therefore, LA must originate from the diet and is thus referred to as an essential fatty acid. LA can be found in corn and soy oils and is one of the most abundant fatty acids in the Western diet. Regarding lipid mediator production, the metabolic destiny of LA may either be hydroxylation (which will be described ahead) or further desaturation and elongation to form other n6 PUFAs. With the aid of Δ 6-desaturase, LA can be converted into gamma-linolenic acid (GLA 18:3n6). Then the enzyme elongase 5 adds 2 more carbons forming dihomo-gamma-linolenic acid (DGLA 20:3n6). Next, DGLA is converted into arachidonic acid (AA 20:4n6) by means of Δ 5-desaturase. AA can be synthesized *de novo* or introduced by dietary means (ex. eggs and meat). Each of these PUFAs can be metabolized to form an array of bioactive

lipid mediators. However, LA and AA are among the most common PUFAs and are the focus of this study (32). Figure I2 summarizes PUFA metabolism.

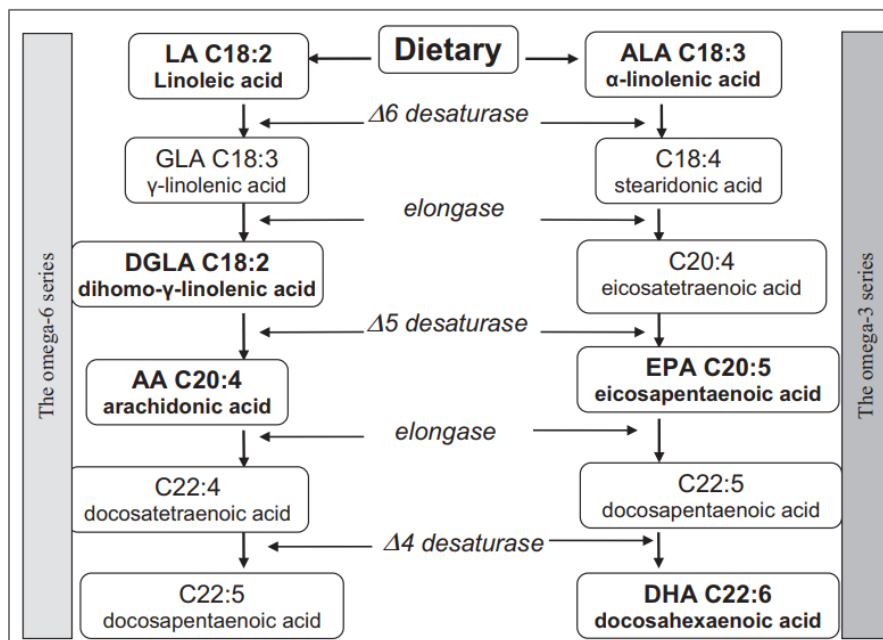


Figure I2. Summary of PUFA metabolism (32)

1.3 ENZYME FAMILIES

1.3.1 Cyclooxygenases

As previously mentioned, the transformation of LA and AA into lipid mediators occurs both enzymatically and nonenzymatically (33)(34). Due to AA's four *cis*-double bonds, it possesses a number of sites at which peroxidation may occur. There are three families of enzymes responsible for AA peroxidation. The first group is the cyclooxygenase (COX) family. There are two main isoforms of COX in humans designated as COX-1 and COX-2. Although a splice variant of COX-1, COX-3, has been discovered in human brain tissue, it is poorly understood (35)(36). These two main isoforms (COX-1 and COX-2) are responsible for converting AA into bioactive eicosanoids. These 20-carbon bioactive lipid mediators operate in an autocrine and paracrine manner with their respective receptors on the plasma membrane (G-protein couple receptors [GPRs]) as well as the nuclear envelope (ex. peroxisome proliferator-activated receptors [PPARs]). However, these eicosanoid receptors are able to bind with more than one type of eicosanoid, thus receiving a reputation of "promiscuity" (37). The main products of COX activity are prostaglandins and thromboxane A₂ and are often referred to as "prostanoids" due to the fact that prostanoic acid is their base structure (34)(38).

First, COX introduces two O₂ molecules to arachidonic acid by hydrogen abstraction, which, after oxygenation, becomes a free radical to bind with an oxygen molecule. Next, it forms an unstable cyclic endoperoxide-hydroperoxide compound referred to as prostaglandin G₂ (PGG₂). PGG₂ quickly rearranges as a less unstable prostaglandin, PGH₂, which then undergoes peroxidation by varying enzymes to produce an array of prostaglandins (PGs) (39).

COX-1 is generally considered a house-keeping enzyme that maintains the basal synthesis of prostanoids for homeostatic reasons. However, COX-2 is an enzyme that is highly expressed at sites of inflammation. Sustained COX-2 expression in tumorigenesis has been associated with tumor progression and poor prognosis. That is why COX enzymes have been studied extensively as targets for treatments related to inflammation and cancer. Non-steroid anti-inflammatory drugs (NSAIDs), like ibuprofen, inhibit COX activity effectively. However, its long-term use has proven to be harmful to the liver and GI tract and has been abandoned as a long-term chemotherapeutic approach (40). COX-targeting therapies continue to be of extreme interest since the pro-

tumorigenic lipid mediator, PGE₂, identified in many cancer types, including gliomas, has proven to be upregulated and very influential in cell growth, migration and invasion (41)(42).

1.3.2 Cytochrome P450 Epoxygenase

The second family of enzymes that metabolizes AA is the monooxygenated epoxygenase, cytochrome P450 (CYP). According to the CYP Nomenclature Committee, “CYP refers to heme-containing proteins characterized by a maximum absorption wavelength of 450 nm in the reduced state in the presence of carbon monoxide” (43). This carbon monoxide binding pigment was initially described in 1958 by Klingenberg (44). Over the following decades, the cytochrome P450 super family has been gradually elucidated, establishing over 13,000 genes represented by over 400 gene families among all the biological kingdoms (43).

Mammalian CYP450 is bound to either mitochondrial or endoplasmic reticulum membranes (43). It is suggested that the reaction mechanism of this oxygenation occurs in two steps. In the first step, P450, bound to the substrate, receives an electron reducing the heme iron. The second electron then activates the heme-bound oxygen molecule on CYP450 by splitting the O-O bond. From there, one oxygen atom becomes part of a water molecule and the other oxygen is incorporated into the substrate (45). Its general reaction with AA produces epoxyeicosatrienoic acids (EETs) and hydroxyeicosatetraenoic acids (HETEs), which often regulate blood pressure control (46)(47). Some of the other main eicosanoids produced by the CYP family are thromboxane A₂ (by TXA₂ synthase) and prostacyclin I₂ (by PGI₂ synthase), the latter of which is an important anti-inflammatory mediator (48)(49).

1.3.3 Lipoxygenases

The third family of enzymes involved in LA and AA metabolism into lipid mediators is the lipoxygenase (LOX) family. Lipoxygenases are a family of nonheme iron-containing dioxygenases that insert, in a stereospecific way, molecular oxygen into polyunsaturated fatty acids that contain at least two *cis*-double bonds (15)(50). There are 3 main functions of lipoxygenases: 1) signaling pathways; 2) peroxidation reactions and 3) mobilization of lipids. The first function involves forming single free fatty acid products from esterified substrates, such as leukotrienes and HETEs. The second function involves the quick formation of mixed products of acids or esters. The enzymes involved in this activity have a quick turnover and the subsequent products may cause structural and pathological changes. The third function involves oxygenating unsaturated fatty

acids esterified in triglycerides. This releases the fatty acids for β -oxidation and energy production (50).

Lipoxygenase biochemistry typically depends on free-radical oxidation. Figure I3 is an example of the typical mechanism involved in lipoxygenase activity on a *cis,cis*-1,4-pentadiene (51). Lipoxygenases are denominated according to the carbon on the AA/LA chain at which oxygenation and hydroperoxyl radical formation occurs. There are 3 main human lipoxygenases: 5-LOX, 12-LOX (also called platelet-type 12-lipoxygenase) and 15-lipoxygenase (15-LOX, subtypes -1 and -2) that are accompanied by a few, less-studied isozymes. Figure I4 represents lipoxygenation of LA.

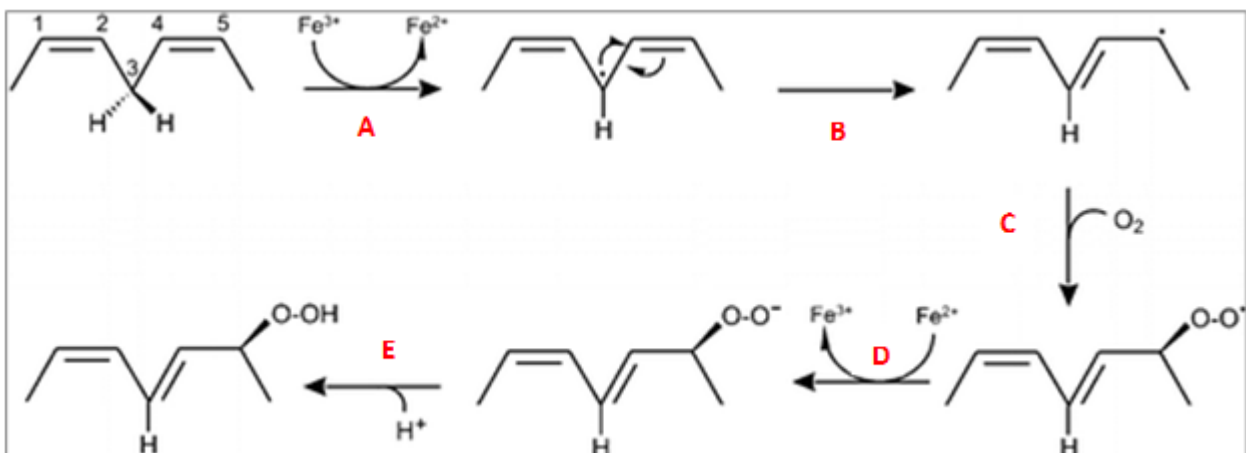


Figure I3. Mechanism for lipoxygenation of a *cis,cis*-1,4-pentadiene. **A)** First hydrogen abstraction occurs due to the activity of iron Fe^{3+} (ferric form), thus, forming a radical and Fe^{2+} (ferrous form; inactive). **B)** This radical then draws the electron of the neighboring double bond (carbons 4 – 5) forming a radical on the sixth carbon. **C)** Binding quickly with an oxygen molecule, a peroxy radical is formed. **D)** Next, the active site iron (Fe^{2+}) donates an electron forming a peroxy anion, which **E)** is then protonated to form a hydroperoxide. (Figure adapted from Haeggstrom and Funk, 2011) (51).

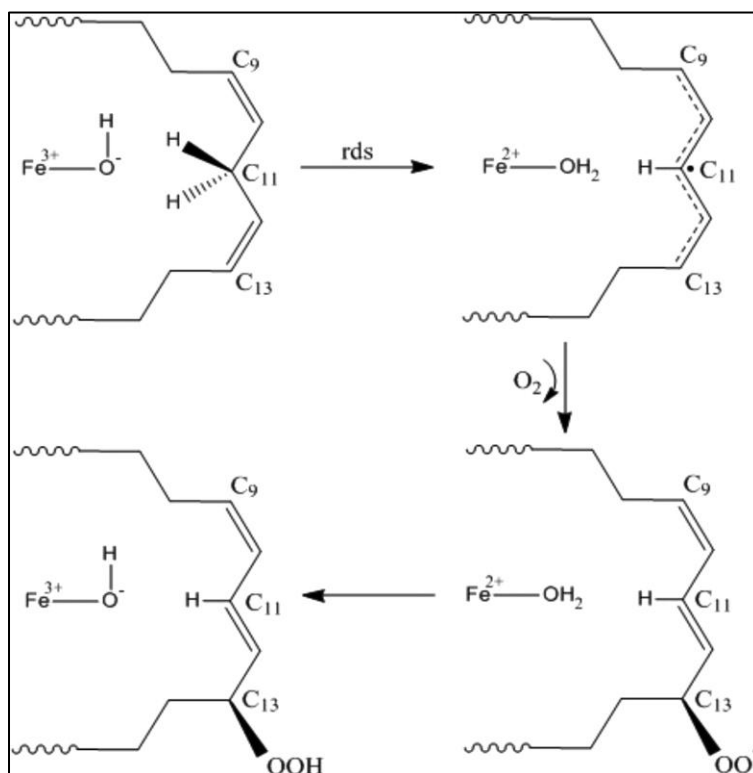


Figure I4. Schematic representation of Linoleic Acid metabolism by non-heme iron-containing lipoxygenases as designed by Soler *et al.* (160).

1.3.4 5-Lipoxygenase

The 5-LOX enzyme is the most well characterized of the LOX family. It is responsible for converting AA into 5-hydroperoxyeicosatetraenoic acid (5-HpETE), which is an unstable and inactive precursor of 5-hydroxyeicosatetraenoic acid (5-HETE) (52). The 5-LOX product, 5-HpETE, can be further processed to form Leukotrienes A₄ (LTA₄) and then B₄ (LTB₄), as well as the cysteinyl leukotrienes C₄ (LTC₄), D₄ (LTD₄) and E₄ (LTE₄), which are structurally similar but functionally different (53). 5-LOX's activity depends on a co-factor, 5-lipoxygenase activating protein (FLAP). FLAP is located on the nuclear membrane and is responsible for facilitating 5-LOX access to AA (54). When FLAP is inhibited, a noticeable decrease of 5-LOX products can be observed (55).

1.3.5 12-Lipoxygenase

There are three isoforms of 12-lipoxygenase in mammals and they are distinguished by their tissues of origin: platelet, leukocyte and epidermal. 12-LOX is responsible for converting AA

into 12-hydroperoxyeicosatetraenoic acid (12-HpETE) first, which is unstable and inactive, and subsequently into 12-hydroxyeicosatetraenoic acid (12-HETE) (50). 12-HETE's biological activities vary depending on the lipoxygenase and tissue, and are associated with vasoconstriction/vasodilation, platelet aggregation, inflammatory mediator production and adipogenesis during inflammation and tissue repair (56).

1.3.6 15-Lipoxygenase

Fatty acid metabolism through 15-LOX occurs by two functional isomeric enzymes designated as either 15-LOX-1 and 15-LOX-2. The first, 15-LOX-1, is expressed principally in reticulocytes, eosinophils, macrophages, epithelial tracheobronchial cells, and in the skin (52). 15-LOX-1 metabolizes linoleic acid (LA) to hydroxyoctadecadienoic acids (13-HODE and 9-HODE), and it metabolizes AA to 15-hydroxyeicosatetraenoic acid (15-HETE). 15-LOX-1 is capable of binding to both AA and LA, however it has a much greater affinity toward LA (57). The 15-LOX relationship with AA and LA will be described in more detail further on. 15-LOX-1 also possesses an initiating role in production of the anti-inflammatory lipoxins derived from n-3 PUFAs (58). The down-regulation of 15-LOX-1 expression has already been linked to colorectal cancer progression (59). However, the overexpression of 15-LOX-1 has been associated with prostate cancer tumorigenesis (60).

The second type of 15-lipoxygenase, 15-LOX-2, is expressed in the prostate, lung, skin, and cornea tissues (61). 15-LOX-2 also metabolizes AA to 15-HETE, but does not effectively metabolize LA (62)(50). While both 15-LOX-1 and 15-LOX-2 were downregulated in breast cancer patients with metastases (63), it has been demonstrated that the reduction of 15-LOX-2 expression in primary prostate epithelial cells is inversely correlated with the tumor's cell cycle. This indicates that through 15-LOX-2 up-regulation the suppression of prostate cancer development could result from restricting cell cycle progression (64). Despite the conflicting reports of pro-/anti-tumorigenic activities resulting from 15-LOX metabolism, the evidence seen in GBM is limited. The relationship between 15-LOX-1 and 15-LOX-2 expression and activity in GBM, if thoroughly investigated, could serve as a therapeutic target.

1.3.7 15-Lipoxygenase Products

There are many products and intermediate products of lipoxygenase metabolism but only a few, more stable products are highlighted in this study. Both 15-LOX-1 and 15-LOX-2 are capable

of converting AA into 15-hydroperoxyeicosatetraenoic acid (15-HpETE), which is less stable and biologically inactive, and then into 15-HETE. 15-HETE is an endogenous signaling molecule that can bind to PPAR γ and PPAR β/δ that repress the expression of pro-inflammatory genes and possesses potent anti-inflammatory activities (65)(66). It is involved in upregulating platelet aggregation and thrombin generation (67) and inhibits cell cycle progression in prostate cancer (64). In non-small cell lung cancer, 15-HETE levels were reduced prior to the onset of tumors. This suggests that 15-HETE may have a role in lung cancer similar to its role in prostate cancer (68).

13-hydroxyoctadecadeinoic acid (13-HODE) is an 18-carbon lipoxygenase-derived monohydroxy fatty acid and the major metabolite in LA metabolism by 15-LOX-1. 13-HODE is a ligand for peroxisome-proliferator-activated receptor gamma (PPAR γ) (68). In colon cancer, 13-HODE has been shown to bind to PPAR γ and consequently inhibiting the formation of metastatic cancer (69). Also its presence decreases PPAR δ , which results in the recovery of apoptosis in human colorectal cancer (70). However, in prostate cancer the overexpression of 15-LOX-1/13-HODE is associated with tumor progression (60).

The other major metabolite of 15-LOX-1 metabolism of LA is 9-hydroxyoctadecadeinoic acid (9-HODE). 9-HODE can be synthesized at low levels from LA by 15-LOX-1. 9-HODE, along with 13-HODE, can also be generated non-enzymatically by means of heat or UV exposure (71). 9-HODE acts through PPAR γ also, but the consequences are different than 13-HODE. When PPAR γ was examined in mesangial cells, Negishi *et al.* determined that 9-HODE stimulates cell proliferation and extracellular matrix synthesis (72). The other 9-HODE receptor is G2A (or GPR132). Through G2A, in keratinocytes, 9-HODE produced an increased mobilization of intracellular calcium, secretion of cytokines and inhibition of accumulation (73). In addition, 9-HODE can inhibit cell proliferation of keratinocytes (71).

All three of the lipid mediators covered can be produced in their R and S conformations. Chiral isomers have identical chemical compositions but have an asymmetrical difference, also known as isomers. (refer to Figure I1). This slight conformational difference of fatty acids can result in different functions (74). However, in the present study, the lipid mediators examined were only those in their (S) conformation, thus, chiral conformation will not be included in the nomenclature used (ex. 13-HODE = 13(S)-HODE).

The role of 15-LOX and its products are unknown in glioblastoma metabolism and activity. Table II summarizes the influence of 15-LOX in different cancer types seen in the literature.

Table II. Summary of 15-LOX's expression and influence on tumor progression in different models of cancer.

Cancer type	15-LOX expression	Influence on Tumor	Reference
Breast Cancer	↓	Neg	(63)
Colon Cancer	↓	Neg	(59)
Prostate Cancer	↑	Pos	(62)
Glioblastoma	?	?	-

15-LOX expression: upregulated (↑), downregulated (↓).

Influence: Negative (Neg) = anti-tumorigenic; Positive (Pos) = pro-tumorigenic

1.4 TUMOR INVASION

1.4.1 Matrix Metalloproteases

One hallmark of cancer partially responsible for the lack of successful therapies, is invasiveness (18). GBM cells are capable of migrating and invading neighboring tissues quickly, and there are a number of pathways responsible for transformed cells to relocate (75). Matrix-metalloproteases (MMPs) are zinc endopeptidases mainly responsible for the alteration of the extracellular matrix (ECM) and its biophysical properties (76). The MMP family is a subgroup of proteolytic enzymes responsible for ECM remodeling. As seen in Figure I.5, MMPs can be classified by their domain organization (basic MMPs, matrilysins, gelatinases, membrane-type or furin-activatable MMPs) (76).

MMP-2 and MMP-9, are responsible for degrading type IV collagen in the ECM. Type IV Collagen is a crucial component of the basement membrane and is often up-regulated in glioma tissue (77). These two MMPs are zinc-dependent endopeptidases (78). When MMP-2 and MMP-9 are secreted, they are latent enzymes; 72kDa (proMMP2) and 92kDa (proMMP9). Both MMP-2 and MMP-9 are composed of a propeptide domain, a catalytic domain (containing three fibronectin motifs) and C-terminal hemopexin-like domain; refer to Figure I.5. Latency is believed to be maintained by the presence of Zinc on the catalytic domain bound to a sulfhydryl (SH) group present on a cysteine residue in the propeptide domain (78)(79). The disruption of this Zinc-cysteine pairing, resulting from proteolytic intervention or conformational changes, issues in the activation of these MMPs (80).

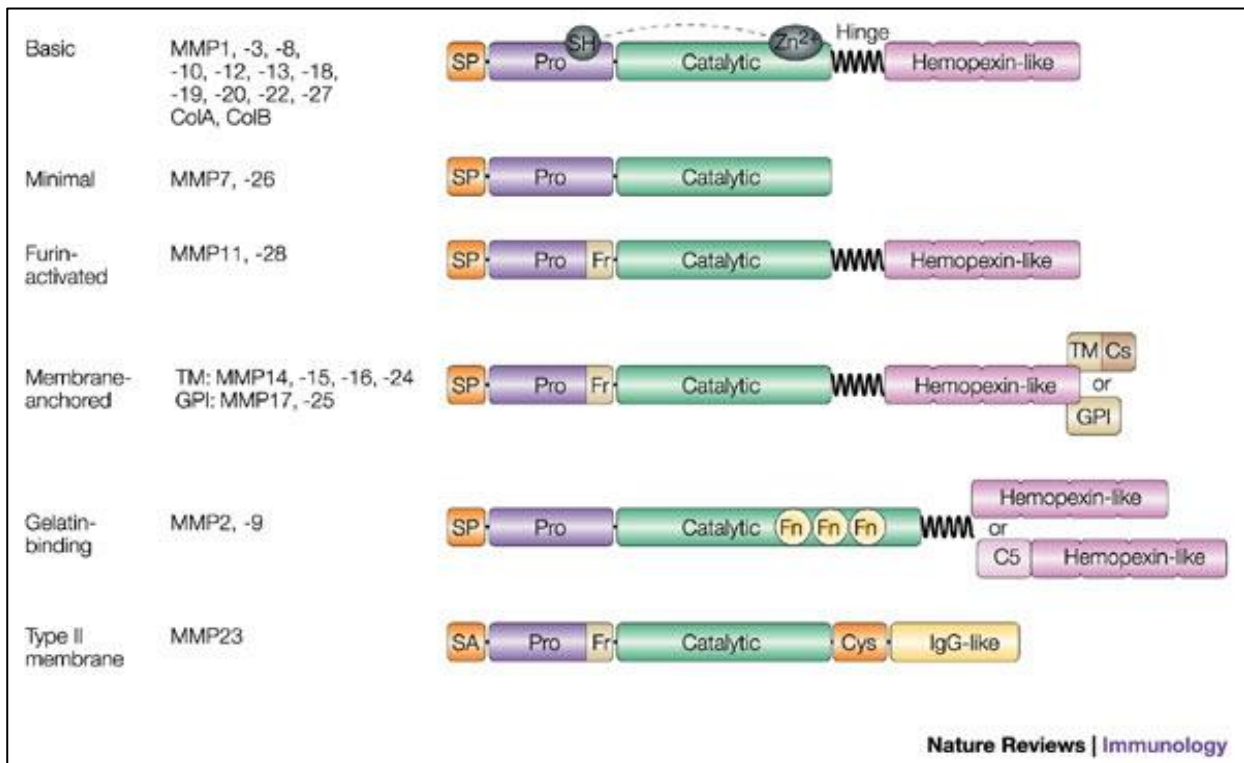


Figure I5. Summary of the classifications and structures of mammalian MMPs; created by Parks *et al.* (81).

The activation of MMP-2 and MMP-9 are slightly different. MMP-2's activation is mostly dependent upon MMP-14. MMP-14 (also known as MT1-MMP) is a membrane bound protein known for its involvement in upregulating the production of angiogenic factors (ex. vascular endothelial growth factor (VEGF)-A). It also interacts with cell adhesion molecules; for example, MMP-14 is responsible for shedding CD44, thus promoting cell migration. However, MMP-14 is most well-known for cleaving proMMP-2 into its active form, MMP-2. MMP-14 forms a homodimer and then pairs with tissue inhibitor of metalloproteases 2 (TIMP2). After one MMP-14 component pairs with TIMP2, proMMP-2 binds to the TIMP-2-free MMP-14 and is cleaved in the middle of its pro-domain creating its activated form, MMP-2 (62kDa) (82).

MMP-9 activation depends on conformational adjustments to release the Zn dependent active site. The intracellular form of MMP-9 (85kDa) is partially glycosylated, when it matures it is glycosylated and secreted (92kDa). Once in the extracellular environment a number of factors, the most potent of which is MMP-3, can cleave proMMP-9 into its active form, MMP-9 (82kDa) (83)(78). MMP-9 can suffer post-conformational changes producing a 62kDa inactive form as well as forming heterodimers (with TIMPs) and homodimers (~200kDa) (83).

As is seen in various types of aggressive cancer, these three MMP's are often upregulated and associated with tumor progression and invasion (84). Although there are studies demonstrating the influence of prostaglandins on MMPs (85)(86), there are no studies investigating 13-HODE and 9-HODE's influence on MMP-2 or MMP-9 expression/activity in GBM. Currently, there are only studies demonstrating a stimulatory effect of 15-HETE on MMP-2 upregulation in rheumatoid arthritis (87) and potentially in pulmonary arterial hypertension (88), and 13-HODE/15-HETE downregulating MMP-1/MMP-13 has been reported in osteoarthritis (89).

2 JUSTIFICATION

The influence of 15-LOX and its metabolites on GBM metabolism and cellular activities remains unclear. Due to the presence of HODEs and HETEs in GBM cells, it is hypothesized that they play a role in cellular activities. Therefore, this study aimed to elucidate the influence that 15-LOX and its products 13-HODE, 9-HODE and 15-HETE, may have in GBM cell growth, migration or invasion.

3 MATERIALS AND METHODS

3.1 Cell Culture

Human cell lines T98-G, U251-MG, A172, U138-MG and U87-MG were analyzed. Cell lines were kindly donated by Dr. Menck (U87-MG, U138-MG) and Dr. Costanzi-Strauss (U251-MG), Biomedical Sciences Institute and Dr. Maria-Engler (A172, T98-G), Pharmacy School, University of São Paulo. For comparative analyses at certain points of this study, a breast cancer cell line (MCF-7) was used, and a fibrosarcoma cell line (HT-1080) was kindly donated by Dr. Vanessa Freitas, Biomedical Sciences Institute, University of Sao Paulo. Cultivation was performed following a previously published protocol in our lab (90). Ideal growth concentrations were standardized for all five cell lines over 72 h and were determined to be 3×10^4 cells. *Data not shown*. All cell lines were cultured in DMEM (Dulbecco's Modified Eagle Medium - Gibco Inc.) supplemented with 10% (v/v) FBS (fetal bovine serum - Gibco Inc.), 50 units/mL penicillin, 50 $\mu\text{g/mL}$ streptomycin (Gibco Inc.). All the cells were maintained at 37°C in a humidified atmosphere with 5% CO_2 in both 25cm^2 and 75cm^2 flasks, until the desired confluency.

3.2 Dose-Response Curve / Trypan Blue Staining

To determine their impact on GBM growth, exogenous 13-HODE, 9-HODE and 15-HETE, were added to the cell lines in variable concentrations. Twelve hours after plating cells in 24-well plates, the medium was changed to medium containing different concentrations of 9-HODE (1 μM , 5 μM , 10 μM), 13-HODE (1 μM , 5 μM , 10 μM), or 15-HETE (0.1 μM , 1 μM , 2.5 μM). As for the lipoxygenase inhibitors treatments, Luteolin (7.5 μM or 15 μM) and Nordihydroguaiaretic acid (20 μM or 40 μM) were used. The negative controls in this experiment were cells treated with either Ethanol (HODEs) or DMSO (inhibitors). The treatments were applied in 24-hour intervals. The samples were collected at 24 h, 48 h and 72 h, and stained with 0.4% Trypan Blue. Then both the viable and unviable cells were counted in a Neubauer chamber. All treatments were tested at least three times in triplicates.

3.3 MTT (3-(4,5-Dimethylthiazol-2-yl)-2,5-diphenyltetrazolium bromide) Assay

Cells were seeded at 5×10^2 for U87-MG, in 96-well plates. After 24 hours cells were treated with 0.1 μM , 1 μM and 10 μM of the following lipid mediators: 13-HODE; 9-HODE and 100%

Ethanol (control). At 24, 48 and 72 hours of treatment, each well was incubated for 4 hours with 0.25mg/mL of tetrazolium at 37°C in a humidified atmosphere with 5% CO₂. At the end of incubation, cells were washed with warm PBS and lysed with 100 µl of 0.04 M HCl in isopropanol to solubilize the formazan. The absorbance was read at 590 nm in an Epoch Multi-Volume Spectrophotometer System (*BIOTEK, Winooski, VT, USA*).

3.4 Total RNA Extraction

For total RNA extraction, the five cell lines were processed following our previously established protocol (90) were each lysed with 1 mL of Trizol (Invitrogen) and left at room temperature for five minutes. After this period 0.2 mL of chloroform were added, and the samples were mixed for 15 seconds and left at room temperature for three minutes. Following this, the samples were centrifuged at 10,697 RCF (Relative Centrifugal Force) for 15 minutes at 4 °C. Next, the superior aqueous layer of the sample was removed and added to 0.5 mL of isopropanol to be centrifuged at 10,697 RCF for 10 minutes at 4 °C. The remaining precipitate was washed three times in 1 mL of 95% ethanol and centrifuged at 5344 RCF for five minutes at 4 °C. Finally, the precipitate was resuspended in 20 µL – 100 µL of diethylpyrocarbonate (DEPC) water that was previously deactivated by autoclaving. The concentration of RNA was determined using an Epoch microplate reader measuring the absorbency at a ratio wavelength of A260 nm/A280 nm as the standard value; all the RNAs used in this study presented between 1.8 and 2.0 purity. The purified RNA was stored and maintained in the -80 °C freezer.

3.5 cDNA Synthesis

Complementary DNA (20 µL) was obtained by using Moloney Murine Leukemia Virus Reverse Transcriptase (M-MLV RT) (*Invitrogen*) in a reverse transcription polymerase chain reaction (RT-PCR) with 2 µg of the RNA of interest. This reaction included 2 µL of a free nucleic acid mix (dNTP mix), 2 µL Random Primer, 1 µL of RNA inhibitor (RNase OUT), 2 µL Dithiothreitol (DTT), 4 µL RT buffer, and 1 µL MMLV (all reagents were purchased from *Thermo Fisher Scientific*). An *Eppendorf MasterCycler®* thermocycler was used to amplify the cDNA. Amplification was then confirmed by electrophoresis with a 1% agarose gel containing ethidium bromide revealed in a *Syngene G-Box* (UV light) and captured by the *GeneSys* program (*Syngene*).

3.6 Conventional RT-PCR

Primers were designed using the open-sourced *Perlprimer program* (91) and the NCBI Primer-BLAST tools. The primers were then purchased from *Thermo Fisher Scientific*. The protocol followed our previously published article (90). Annealing temperatures and band sizes were determined for each primer pair (**Table R2**). Next, the analysis of mRNA expression by conventional RT-PCR was performed. The following genes were amplified: the enzymes 15-LOX-1, 15-LOX-2, MMP-2, MMP-14, MMP-9 and the receptors PPAR γ , PPAR δ , GPR132. Amplification was confirmed by gel electrophoresis with 1% agarose containing ethidium bromide, and the product was viewed through a U.V. light capture system (*Syngene*). The internal control gene chosen was ribosomal subunit 18 (18s) due to its consistent endogenous expression in all glioma cell lines.

3.7 Quantitative Real-Time PCR

The traditional polymerase chain reaction is important for confirming the cell lines' ability to express the genes of interest and the optimal annealing temperatures at which the primer binds to the sample. To analyze the gene expression of the enzymes and receptors of interest, we used Real Time quantitative PCR (RT-qPCR). We obtained a standard curve showing the optimal quantities of cDNA and the concentrations of primers to be used in the experiments (Data not shown). Reactions were prepared containing Syber Green Mix (*Life Technologies*). The amplifications were performed through the 7300 REAL TIME PCR system (*Applied Biosystems*). Dissociation curves verifying amplification specificity were also performed. To evaluate the differential expression of the treated groups, the relative quantification method with 18s was used as a normalizer (endogenous control). The primers for MMP-2, MMP-9, and MMP-14 were first standardized, and then tested in five glioma cell lines (U87-MG, U251-MG, U138-MG, A172, T98-G) and a breast cancer cell line (MCF-7) and a fibrosarcoma cell line (HT1080), first using conventional RT-PCR and then confirmed by RT-qPCR.

3.8 Protein Extraction and Quantification

3.8.1 Sample Preparation

U87-MG and T98-G cells were cultivated in T-25 plates until they reached 80-90% confluency. At this moment, cells were treated with Luteolin (7.5 μ M or 15 μ M) or NDGA (20 μ M or 40 μ M) with their respective controls in duplicates for 24h and 72h following the methodology previously mentioned. Cells were then trypsinized and counted in a Neubauer chamber. Next a pellet was formed by centrifugation at 4°C for 3min at 410 RCF and washed with cold PBS 3x before snap-freezing the samples in liquid nitrogen. The samples were stored in a -80°C until the time of extraction.

3.8.2 Protein Extraction

The frozen pellet was slowly thawed on ice then centrifuge for 10min at room temperature and excess PBS was removed. Then the lysing buffer containing protease inhibitor was added (volume depending on the size of the pellet). The pellet was re-suspended in the buffer for 5 minutes and then sat in ice for 30 minutes. Next the sample was centrifuged at 9520 RCF in 4°C for 10min. After 10min the supernatant was remove and placed in a new tube.

3.8.3 Protein Quantification

First a concentration curve was created using 1mg/mL of Albumin in varying concentrations (see Table M1). Then 1 mL of Solution C (50:1 ratio of Solution A [Anhydrous Na₂CO₃ (w/v: 20g/L), NaOH (4g/L), NaK tartrate (0.2g/L)] and Solution B [CuSO₄ x 5 H₂O (5g/L)], respectively) to each sample standard, and the sample itself, for 15 minutes. After 15min, 100 μ L of Folin were added and the samples rested in ice for 30 minutes. Then 100 μ L of each sample was placed in a 96-well plate, in duplicate, for absorbance reading in the spectrophotometer BioTek. After recording the absorbance at 750nm, a concentration curve was calculated and the estimated protein content of the sample of interest was determined. Then the samples were aliquoted and 2x Laemmli sample buffer was added accordingly (1:1) and place in boiling water (or close to boiling) for 5 minutes. Then the samples were frozen at -80°C for long-term use.

Table M1. Protein Quantification Standard Curve

Protein Quantification Table			
Tube	Albumin 1mg/mL	H ₂ O	Resulting Protein
1	150 μ L	50 μ L	750
2	100 μ L	100 μ L	500
3	50 μ L	150 μ L	250
4	20 μ L	180 μ L	100
5	15 μ L	185 μ L	75
6	10 μ L	190 μ L	50
7	0 μ L	200 μ L	Blank

3.9 Western Blot

3.9.1 Gel Preparation

The gels used for electrophoresis were specifically prepared for each Western Blot. The running gel mix was prepared and added to the glass support where it was allowed to dry for 30-45 minutes (see Table M2). The loading gel was then mixed (see Table M3) with the well-forming comb and allowed to dry for 20-30 minutes. The gels were then placed inside the electrophoresis cube with fresh running buffer.

Table M2 (Gel#1) and Table M3 (Gel#2). Composition of Western Blot electrophoresis gels.

GEL #1 (Running Gel)		GEL #2 (Loading Gel)	
	10% Bis-Acrylamide		4% Bis-Acrylamide
	(2 Gels)		(2 Gels)
Distilled H ₂ O	7.9 mL	Distilled H ₂ O	3.4 mL
1.5M Tris-Buffer pH8.8	6.7 mL	1M Tris-Buffer pH6.8	830 μ L
40% Bis-Acrylamide	5 mL	40% Bis-Acrylamide	630 μ L
10% SDS	200 μ L	10% SDS	50 μ L
10% APS	200 μ L	10% APS	50 μ L
TEMED	8 μ L	TEMED	5 μ L

3.9.2 Running Samples:

Samples were added to each well according to the desired protein content. The loading gel ran at 75 V and 0.25 amps for 20-30min in Running Buffer (Glycine + UltraPure™ Tris (*Invitrogen*) + H₂O; pH 8.3). When all samples reached the running gel, the current was adjusted to 100 V for 2 hours in ice. After electrophoresis, the gel was immediately placed in the transfer apparatus and rested in fresh Blotting Buffer (TBS 1X + Methanol). The transfer ran at 100 V for up to 2 hours.

3.9.3 Blocking and Antibodies:

The transfer was confirmed by staining the membrane with Ponceau Red solution. After washing the membranes with TBS 1x to remove the stain, they were blocked with 5% Fat Free Milk + TBS Tween 20 for 1 hour. After removing excess milk with a wash in TBS 1x, the primary antibodies (15-LOX-1[1:700]; MMP-2 [1:2000]; MMP-14 [1:2000]; actin [1:3000]) were added to the membranes in clean plastic sacks and gently rocked on an agitator overnight in 4°C. The next morning, the membrane was removed and washed twice with TBS Tween 20 for 10 minutes each and once with TBS 1x for 5 minutes. Then, the secondary antibody was added (anti-sheep, anti-mouse, anti-rabbit [1:2000]) and the membrane was placed on an agitator for 2 hours (maximum) at room temperature. Finally, the membranes were washed twice with TBS Tween 20 for 10 minutes each and once with TBS 1x for 5 minutes and stored for revealing with enhanced chemiluminescence (ECL- *Bio-Rad Laboratories Inc., Sao Paulo, SP, Brazil*) in a Syngene G-BOX with its GeneSys program. In the case of 15-LOX-1, the secondary antibody possessed a biotinylated conjugate requiring an additional 3.5-hour incubation with streptavidin horseradish peroxidase conjugate (*ExtraAvidin Peroxidase; Sigma-Aldrich, St. Louis, MD, USA*) in order to have a reaction with the ECL solution.

3.10 Zymography Assay

Gelatin zymography assays measure degradation caused by gelatinase enzymes, such as Matrix Metalloproteases (MMPs). To identify if MMPs were produced by the cells, a zymogram was performed of the serum-free medium in which the cells were incubated. The 10% Gelatin Zymogram Gel was prepared (refer to Tables M4 and M5) and stored in Running Buffer (0.25M TrisBase pH8.3 + 10% SDS + Glycine + ddH₂O) as recommended by Toth and Fridman (83).

Fresh serum free samples were removed from cell culture after 21h of incubation and stored on ice. Older samples (no more than 1 week old) were removed from a -80°C freezer and slowly thawed on ice for 2 hours. The gels were placed in a running chamber with running buffer while the samples thawed. Once thawed, the samples were centrifuged at 10,000 RCF for 5 min at 4°C.

The supernatant was separated and used for the zymogram. Using various quantities, the samples were diluted 1:1 with 2x Sample (Laemmli) Buffer, not containing Dithiothreitol (DTT)/ mercaptoethanol, and were not boiled; all of which may denature the MMPs beyond recovery. After resting for 5 minutes, 25 µL of the sample were placed in the well of the loading gel. The gel ran for 2-3 hours at 100 V. The gels were washed with 2.5% Triton X-100 Buffer three times for 15 min on an agitator. Triton X-100 washes serve to remove the SDS present in the samples so that the proteins can be restored to their tertiary and potentially functional conformations. Then Development Buffer (1.5M Tris-HCl, pH8.8 + 1M CaCl₂ + 2% NaN₃ + ddH₂O) covered the gels and they were incubated for 17 hours. The negative control was a second gel washed with 10 mM Ethylenediaminetetraacetic acid (EDTA)-containing 2.5% Triton X-100 Buffer and incubated with 10 mM EDTA-containing development buffer. EDTA serves as a protease inhibitor by chelating the metal ions present which could activate the protease active sites (92). The next day, the gels were washed with Fixation Buffer and stained using 0.1% Coomassie Blue Staining Buffer (4.5:1:4.5 ratio of Methanol, Acetic Acid, ddH₂O + Coomassie Blue) for 30 min. Then the gels were washed in a Destaining Buffer (4.5:1:4.5 ratio of Methanol, Acetic Acid, ddH₂O) until bands could be seen. Images were captured in a *Syngene G:BOX - GeneSys* program (Maryland, USA).

Table M4 (10% Gel) and Table M5 (4% Gel). Composition of Zymogram Gels.

Separating Gel		Loading Gel	
10% Zymogram Gel		4% Gel	
ddH ₂ O	4.74 mL	ddH ₂ O	3.64 mL
1.5 M Tris-Buffer, pH8.8	2.50 mL	40% Bis-Acrylamide	640 µL
40% Bis-Acrylamide	2.51 µL	0.5 M Tris-Buffer, pH6.8	625 µL
1% Gelatin (10 mg/1mL)	100 µL	20% SDS	25 µL
20% SDS	50 µL	10% APS	40 µL
10% APS	50 µL	TEMED	20 µL
TEMED	5 µL		

3.11 Scratch Assay

Aiming to measure short-term migration in T98G cells treated with the 15-LOX products and LOX inhibitors, a wound healing assay was performed. First, the initial number of cells needed to reach 90-100% confluency in 12 h for an assay in a 24-well plate was determined (9×10^4 cells). Using a 1mL pipette tip, a streak was made in the middle of the well. After the medium was carefully changed to include previously determined concentrations of eicosanoids and drugs with their respective controls, then images of the plates were taken immediately (0 h), and later at 12 h. The images of the scratched sites were processed in ImageJ Software by calculating the number of cell-free pixels in the images at 0 h and comparing them with the number of pixels at 12 h. A reduction in the values between 0 h and 12 h imply that cell migration into the cell-free space occurred. The relative 0h/12h value for each treatment was then compared with the 0h/12h value of the DMSO treatment (positive control) and a value (%) was produced.

3.12 Statistical Analysis

Dose response tests are presented as the mean plus the SEM. Using the GraphPad Prism 5 software the significance was determined by a two-way ANOVA test with a Bonferroni post-test to compare between multiple data sets. Not assuming equal variances, one-tailed or two-tailed unpaired t-test was used with Welch's correction to compare specific pairs of data. Real time PCR

followed the Livak method of $2^{-\Delta\Delta CT}$ (93). Differences were considered significant with $p < 0.05$. The significance of the p-value is represented in the figures by “*” ($* < 0.05$, $** < 0.01$, $*** < 0.001$).

4. RESULTS

4.1. 15-Lipoxygenase Pathway

First, cell lines were cultivated, and stocks were created and stored in liquid nitrogen. After cultivation, total RNA extraction was performed, and cDNA was made for all five cell lines (Figure R1.) Before examining the mRNA expression of proteins involved in the 15-LOX pathway, cDNA primers were designed (Table R1) and ideal annealing temperatures for conventional RT-PCR were determined (Figure R2).

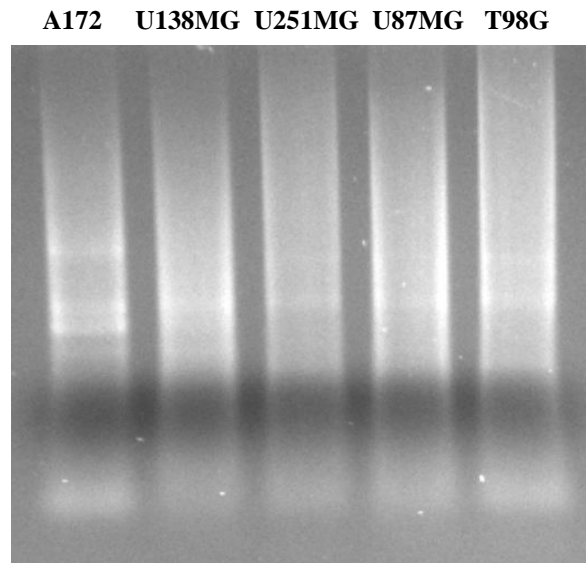


Figure R1. Gel electrophoresis of cDNA made from 5 GBM cell lines: A-172; U138-MG; U152-MG; U87-MG; T98-G

Annealing Temperature Tests

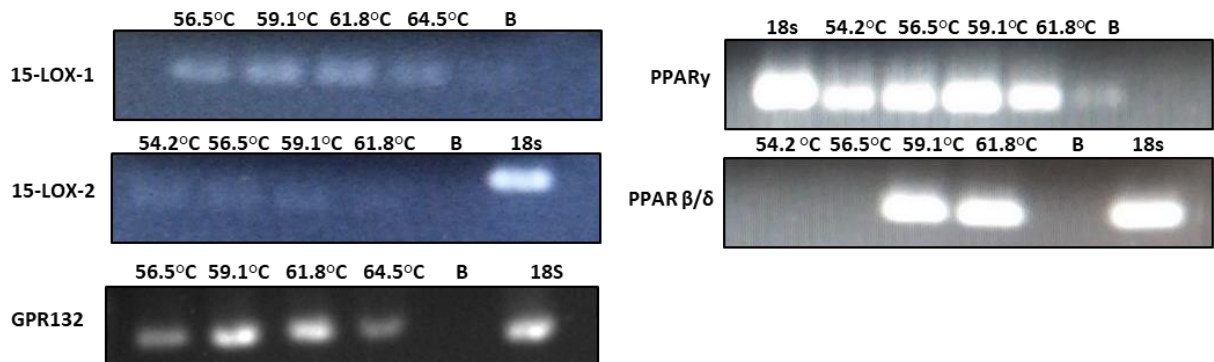


Figure R2. Annealing temperature tests after 40 cycles in a thermocycler for primers examined in this study. For temperatures were selected as a range for each primer based upon NCBI-BLAST/ Perl Primer simulated PCR results. The temperature of the most intense band was selected for PCR analysis. B = Blank; 18s = ribosomal subunit 18 as an endogenous control.

TABLE R1. Primer sequences, annealing temperatures, and band sizes for RT-PCR			
Primer	Sequence	Annealing Temp. (°C)	Band Size (base pairs)
18s sense	TGT GAT GCC CTT AGA TGT CC	59.1	244bp
18s anti-sense	CCT CAC TAA ACC ATC CAA TCG G		
15-LOX-1 sense	CTG TGA AAG ACG ACC CAG AG	59.1	107bp
15-LOX-1 anti-sense	TCC CGA GCC TGT AAA GAC AC		
15-LOX-2 sense	CTC AAT ATC AAA TAC TCC ACA GCC	56.5	129bp
15-LOX-2 anti-sense	TTT CAT CTC ATT CAG ACT CCT CC		
GPR132 sense	AAA TAT GCC AGG GAG GAA GGT	59.1	263bp
GPR132 anti-sense	ACG GTG TCA AGA ACA TGA GG		
PPAR delta sense	CTG GAG TAC GAG AAG TGT GAG	59.1	237bp
PPAR delta anti-sense	ATT GTA GAT GTG CTT GGA GAA GG		
PPAR gamma sense	GAC TTC TCC AGC ATT TCT ACT C	59.1	232bp
PPAR gamma anti-sense	CTT TAT CTC CAC AGA CAC GAC		

4.1.1. RT-PCR of 15-LOX Pathway

After standardization was performed, conventional RT-PCR was performed for 40 cycles in a thermocycler in five GBM cell lines (Figure R3). Messenger RNA of all the components for the 15-LOX pathway were present in all five GBM cell lines in varying degrees. 15-LOX-1's most intense band was seen in U138-MG. 15-LOX-2's strongest band was seen in A172. The 9-HODE receptor, GPR132, displayed its strongest band in T98-G. PPAR γ was absent from U138-MG but most intense in U87-MG and A172. PPAR β/δ was intense in all five cell lines.

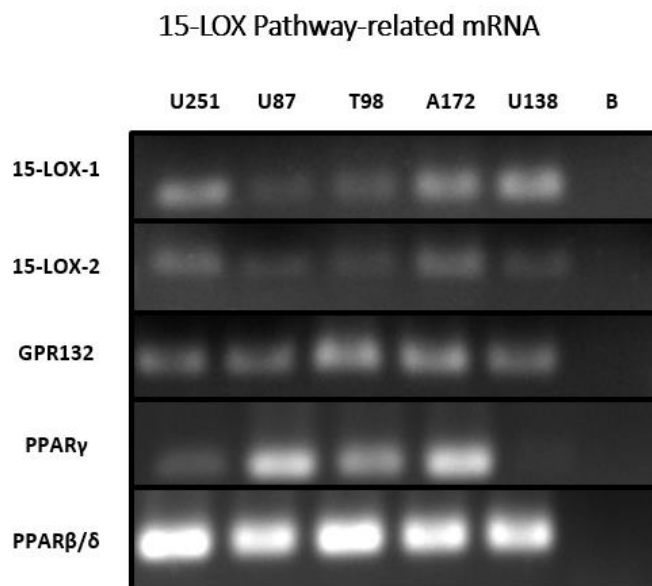


Figure R3. Conventional RT-PCR of 15-LOX pathway in five GBM cell lines. Cell lines U251-MG, U87-MG, T98-G, A172, U138-MG were used for genes associated with the 15-LOX pathway. All the genes were amplified in all cell lines after 40 cycles. Blank [B]. N=2.

4.1.2. Cell Line Selection

After identifying the presence of mRNA pertaining to the 15-LOX pathway in almost all five GBM cell lines, U87-MG and T98-G were selected for further testing due to their heterogenous profile as summarized in Table R2.

Table R2. Characteristics of U87-MG and T98-G GBM cell lines.

Characteristic	U87-MG	T98-G
TP53	Wildtype	Mutant
PTEN	Mutant	Mutant
Tumorigenic	YES	NO
In vitro growth	Individualistic/Spread	Clusters
Radiation therapy	More Sensitive	Less Sensitive
Chemotherapy	Less Resistent	More Resistent

4.1.3. Cell Viability and Growth

After U87-MG cells were cultivated in a 96-well plate, MTT colorimetric assays were performed to observe the mitochondrial capacity to produce formazan from MTT (tetrazole), which is typically associated with cell viability, under conditions of exogenous 13-HODE and 9-HODE over 24h, 48h and 72h (Figure R4). The concentrations applied were 0.1 μ M, 1 μ M and 10 μ M. Since the 10 μ M treatment caused the cell medium to contain 2% ethanol (the other treatments introduced <1% ethanol), a second vehicular control was used to determine the interference of ethanol in the cellular response. In this case, ethanol did mask the response caused by the 10 μ M treatments in all time periods. A significant reduction in MTT conversion was observed in all time periods of cells treated with both 13-HODE and 9-HODE. The 1 μ M treatments reduced viability after 24h, 48h and 72h, and the 0.1 μ M treatments reduced viability at 48h and 72h.

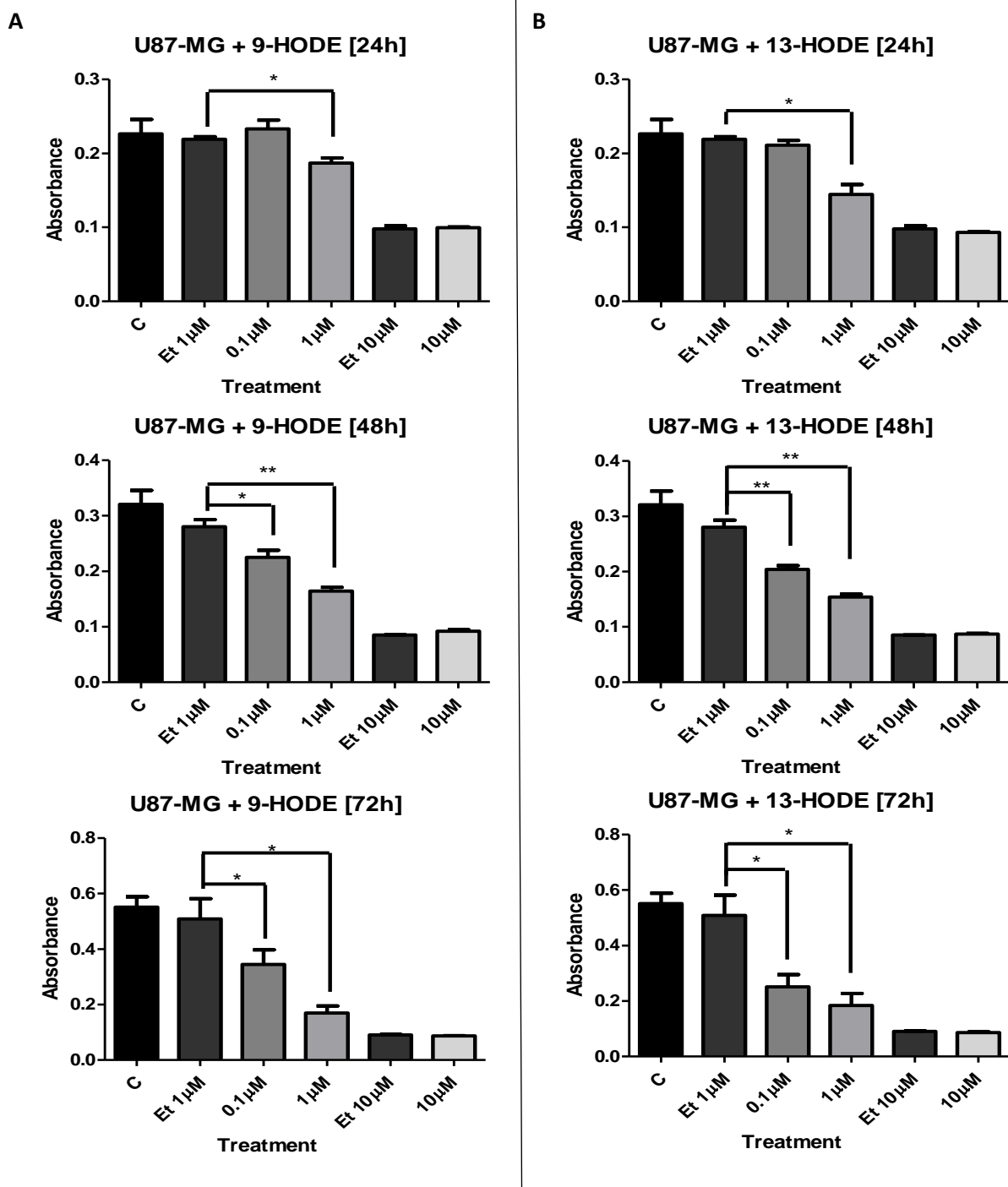


Figure R4. Colorimetric assay of U87-MG cells treated with 9-HODE and 13-HODE over a 72-hour period. Graphs show MTT absorbance after 24, 48 and 72 hours of exogenous 13-HODE or 9-HODE treatments on U87-MG. Cells treated with both 9-HODE (A) and 13-HODE (B) demonstrated significant decreases in cell viability with 0.1 μ M starting after 48 hours, and with 1 μ M treatments at all three time periods. However, the effects of 10 μ M treatments were masked by the effects of the ethanol vehicle as seen by the control. $p < 0.05$ (*), $p < 0.01$ (**). N=3 in duplicate.

Next, both U87-MG and T98-G cells were cultivated for 24h, 48h and 72h with either 13-HODE or 9-HODE at higher concentrations (1 μM , 5 μM and 10 μM), and T98-G cells were also treated with AA/15-LOX product 15-HETE (0.1 μM , 1 μM and 2.5 μM). Cells were then collected and counted with 0.4% Trypan Blue staining to record viable cells and cells with permeable cellular membranes (dead or dying cells). The stained cells counted constituted less than 1% of the representative cells counted in the Neubauer Chamber (*data not shown*). Significant increases in cell count were observed with 5 μM treatments of 13-HODE at 24h and 72h (U87-MG) and at 48h (T98) (Figure R5). The 9-HODE treatments significantly increased cell count in the U87-MG at 48h and 72h with both 5 μM and 10 μM treatments (Figure R6 [*top*]). The T98-G cells increased cell counts in response to 5 μM treatments at 24h and 48h (Figure R6 [*bottom*]). The 15-HETE treatment was only tested on the T98-G cell line for 24h, 48h and 72h at lower concentrations (0.1 μM , 1 μM and 2.5 μM) due to the dilution of the 15-HETE stock. Significant increases in cell count were observed in the 0.1 μM and 1 μM treatments at 24h and 48h (Figure R7).

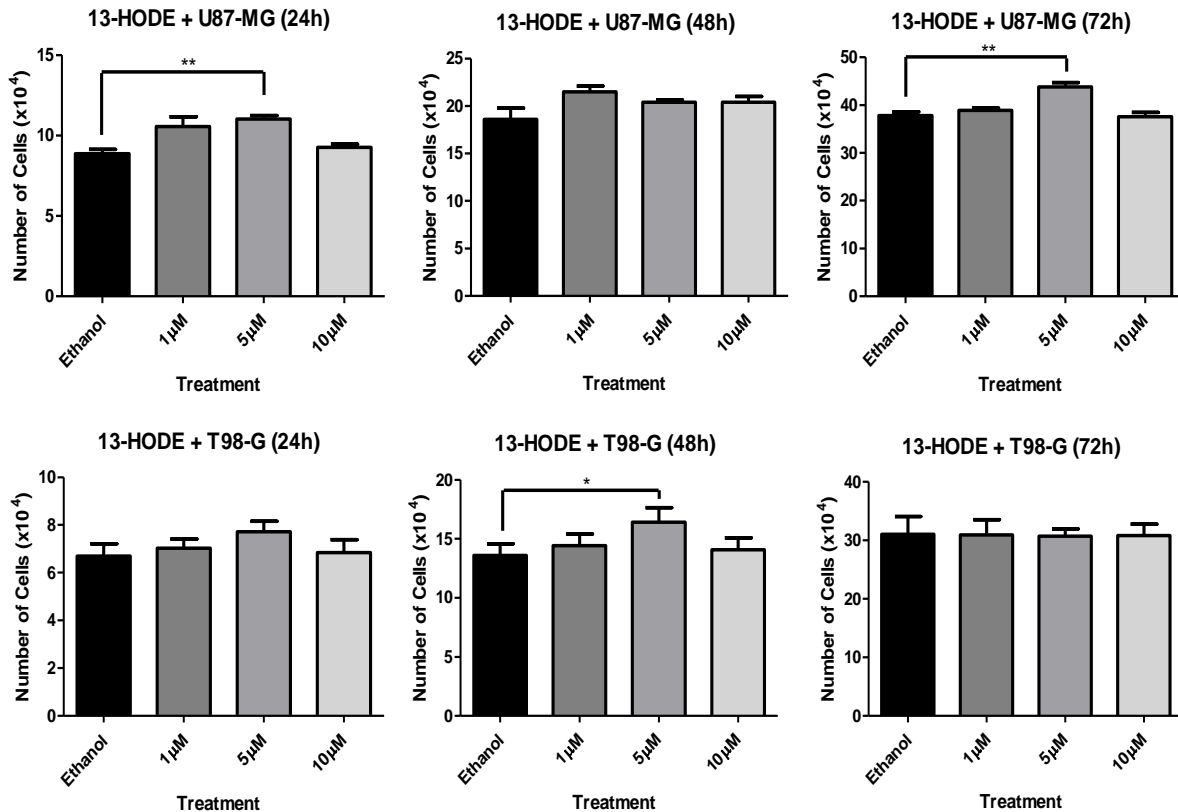


Figure R5. Exogenous 13-HODE treatments on U87-MG and T98-G over 72 hours. U87-MG cells [top row] treated with 13-HODE significantly increased cell number with the 5 μM treatments at 24h and 72h, while a significant effect was only seen at 48h in T98-G cells [bottom row] with the 5 μM treatment. An unpaired t-test with Welch's correction was performed and a p-value ≤ 0.05 was considered significant (*) and $p < 0.01$ was very significant (**). N=3, in triplicate.

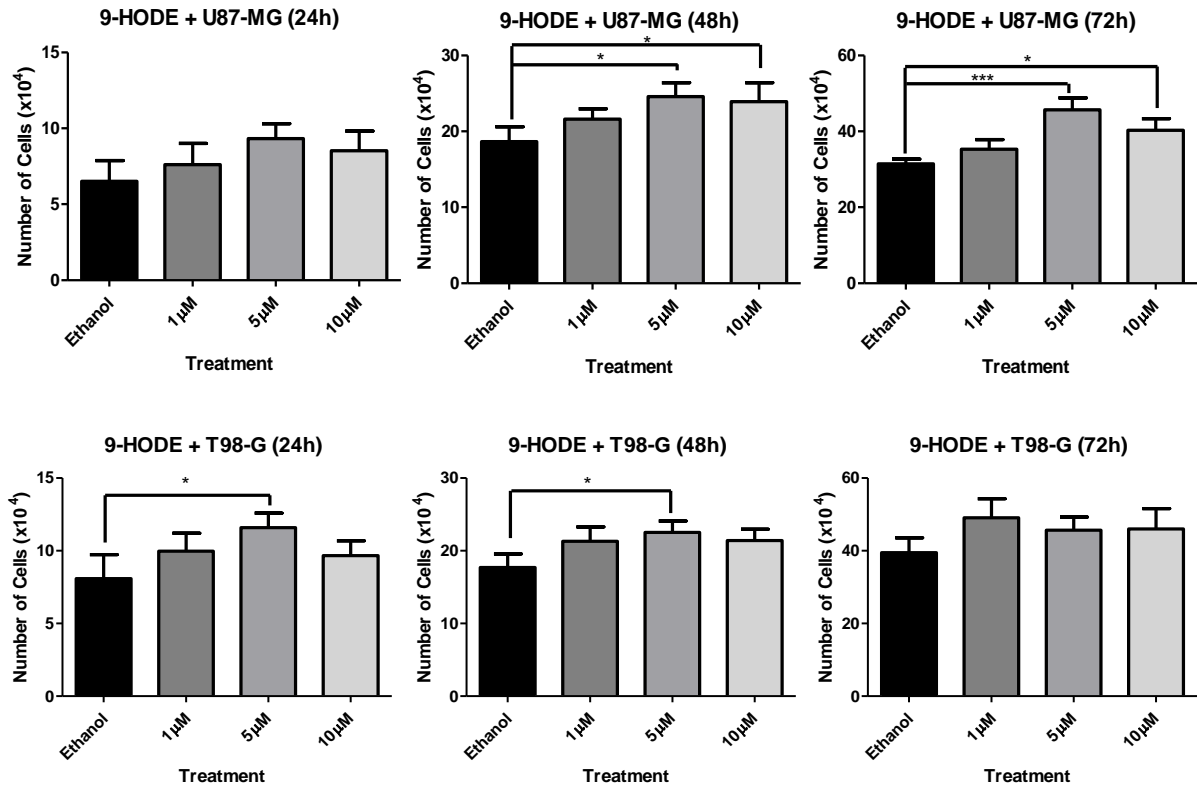


Figure R6. Exogenous 9-HODE treatments on U87-MG and T98-G over 72 hours. U87-MG cells [top row] treated with 9-HODE significantly increased cell number with the 5 and 10 μ M treatments at 48h and 72h, while a significant effect was seen at 24h and 48h in T98-G cells [bottom row] with the 5 μ M treatment. An unpaired t-test with Welch's correction was performed and a p-value ≤ 0.05 was considered significant (*) and $p < 0.001$ was very significant (**). N=3, in triplicate.

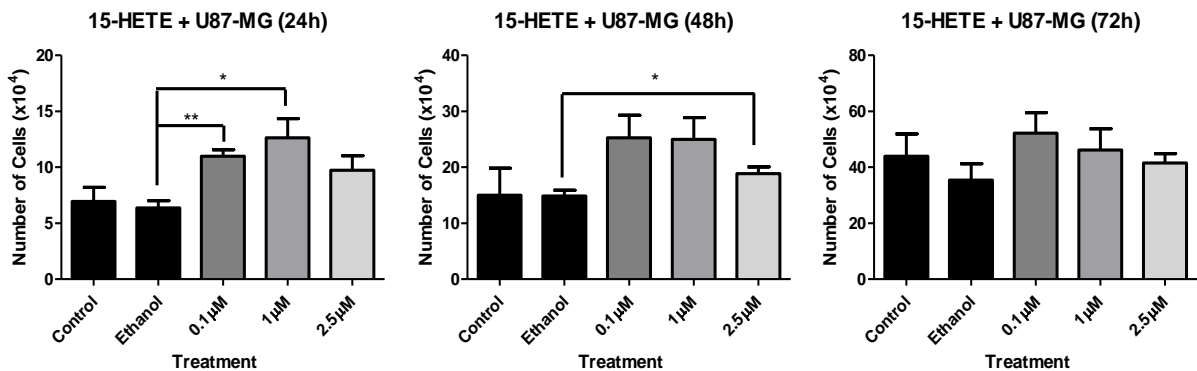


Figure R7. Exogenous 15-HETE treatments on U87-MG over 72 hours. U87-MG cells treated with 15-HETE significantly increased cell number with the 0.1 μ M and 1 μ M treatments at 24h and 48h. An unpaired t-test with Welch's correction was performed and a p-value ≤ 0.05 was considered significant (*) and $p < 0.01$ was very significant (**). N=3, in duplicate.

4.2. 15-Lipoxygenase Inhibitors

Two 15-LOX inhibitors were used on both U87-MG and T98-G cell lines; Luteolin (LUT) and Nordihydroguaiaretic acid (NDGA). Based on the literature and a previous study in the lab, different concentrations were used for LUT (7.5 μ M; 15 μ M) and NDGA (20 μ M; 40 μ M) over a 72-hour period (Figure R8). A slight tendency to reduce cell count was observed with the 15 μ M LUT and 40 μ M NDGA treatments, and little to no influence was observed on cell count over 72h for the 7.5 μ M LUT and 20 μ M NDGA treatments. Thus, 15 μ M LUT and 40 μ M NDGA were selected for further study. Western blot analysis of protein expression in the cells treated with 15 μ M LUT and 40 μ M NDGA demonstrate that: 1) 15-LOX-1 is present in these two cell lines and 2) that these pharmacological inhibitors do not influence the expression of 15-LOX-1 (Figure R9).

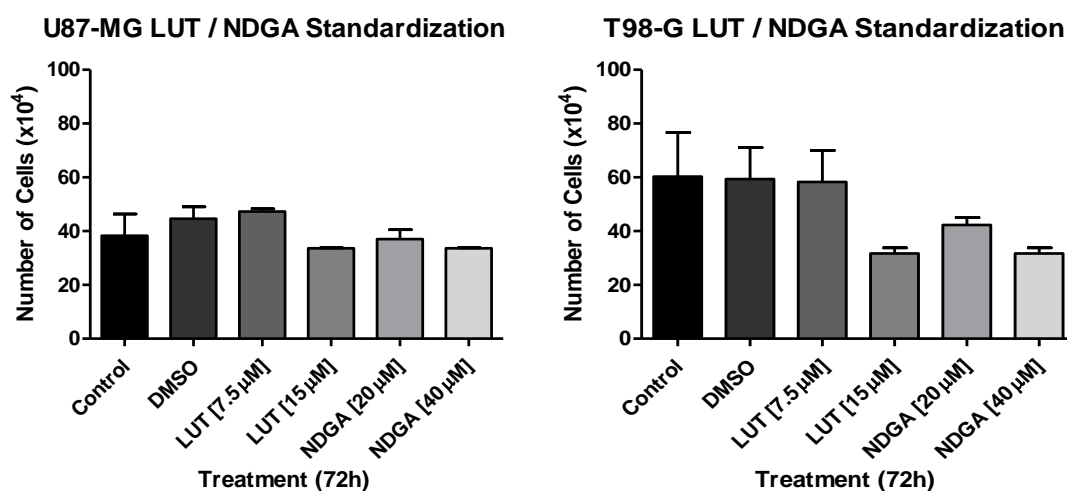


Figure R8. Treatment with Lipoxygenase inhibitors Luteolin and NDGA, in the U87-MG and T98-G cell lines. Graphs show the results after 72 hours of treatment with NDGA [20 and 40 μ M] and Luteolin [7.5 and 15 μ M], with the data analysis in relation to the control, showing a decreasing tendency in cell count. N=2, in triplicate.

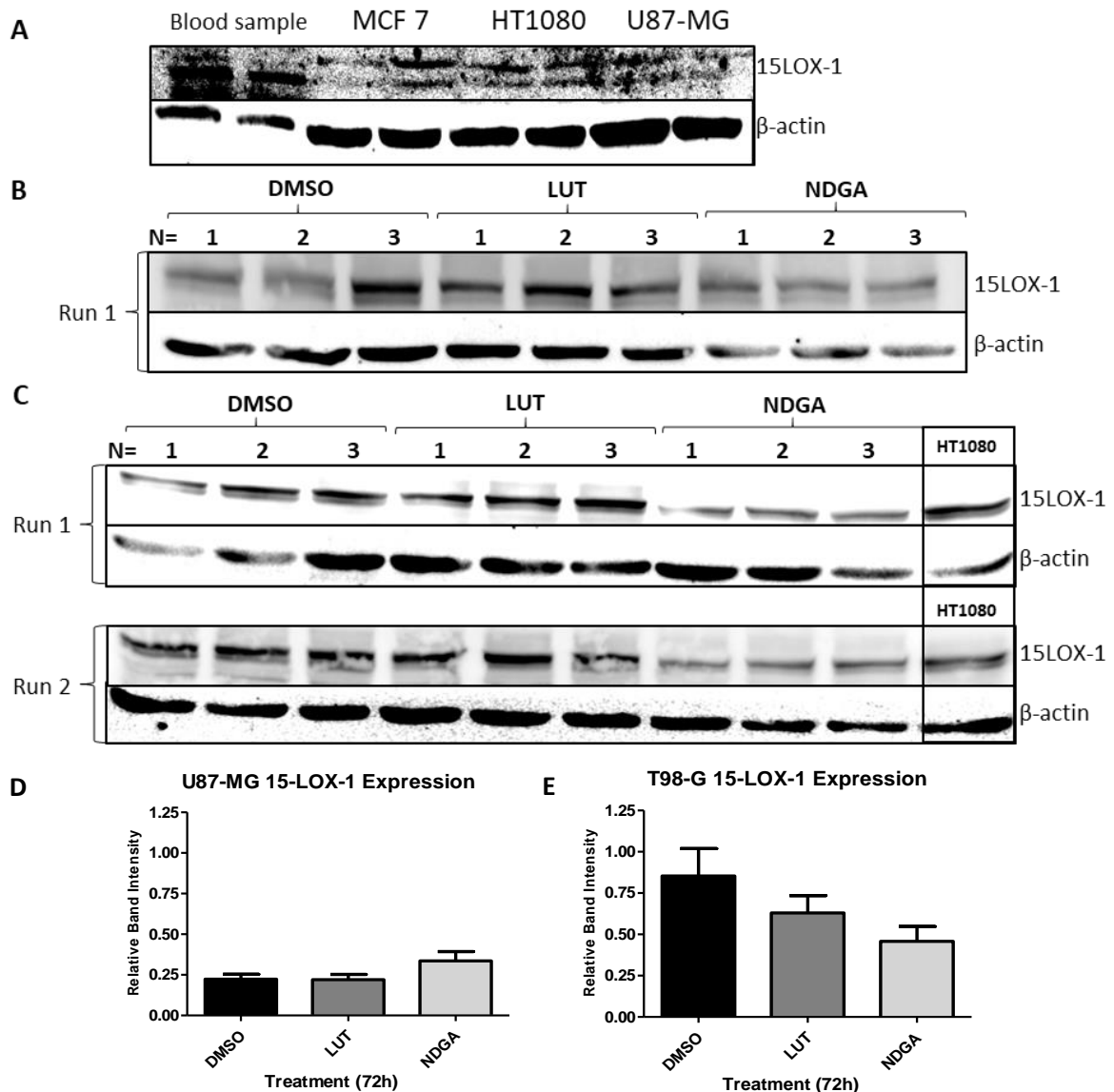


Figure R9. Western Blots of 15-LOX-1 expression after treatments with LOX inhibitors Luteolin (LUT) and Nordihydroguaiaretic acid (NDGA) for 72 hours. (A) Standardization of the 15-LOX-1 antibody (70kDa) in 80 µg (left lane) and 40 µg (right lane) of a blood sample, a breast cancer cell line (MCF7), a fibrosarcoma cell line (HT1080) and the GBM cell line (U87-MG). (B) U87-MG protein samples (40 µg) of treated cells. (C) T98-G protein samples (40 µg) of treated cells. The Western Blot protocol was performed twice using fresh samples and new nitrocellulose membranes (*Run 1*; *Run 2*). Each membrane possesses three separate trials of cells incubated in each treatment ($N=1,2,3$). The HT1080 cell line was used as a positive control. (D) U87-MG and (E) T98-G statistical analysis. The relative band intensities of 15-LOX-1 were normalized to the relative band intensities of the endogenous control, β-actin (42kDa). An unpaired t-test with Welch's correction was performed and a p-value ≤ 0.05 was considered significant (*).

The morphology of U87-MG (Figure R10) and T98-G (Figure R11) cells treated with the inhibitors over a 72-hour period with (two columns on the left) and without serum during the last 24h period of the 72h treatment (column on the right). Luteolin reduced cell confluency over the 72-hour period yet did not influence cell morphology in either 10% FBS medium or in serum-free medium. NDGA reduced cell confluency at both concentrations over 72h, and cells treated in medium containing 10% FBS demonstrated no obvious alterations to cell morphology. The cells were extremely sensitive to the inhibitors added to the serum-free medium. Luteolin reduced cell confluency in U87-MG, and T98-G displayed many detached cells. The T98-G cells that continued to adhere to the plate remained in their islet formations but were very morphologically altered and formed many vesicles in the cytoplasm. The cells treated with NDGA in serum-free medium (*bottom right corner*) were mostly attached to the plate demonstrating limited cell growth. However, there were very few detached cells and U87-MG cells appeared to have created more debris during this last 24h-period of the 72h treatment. Cell morphology was completely altered in both cell lines due to NDGA in serum-free medium.

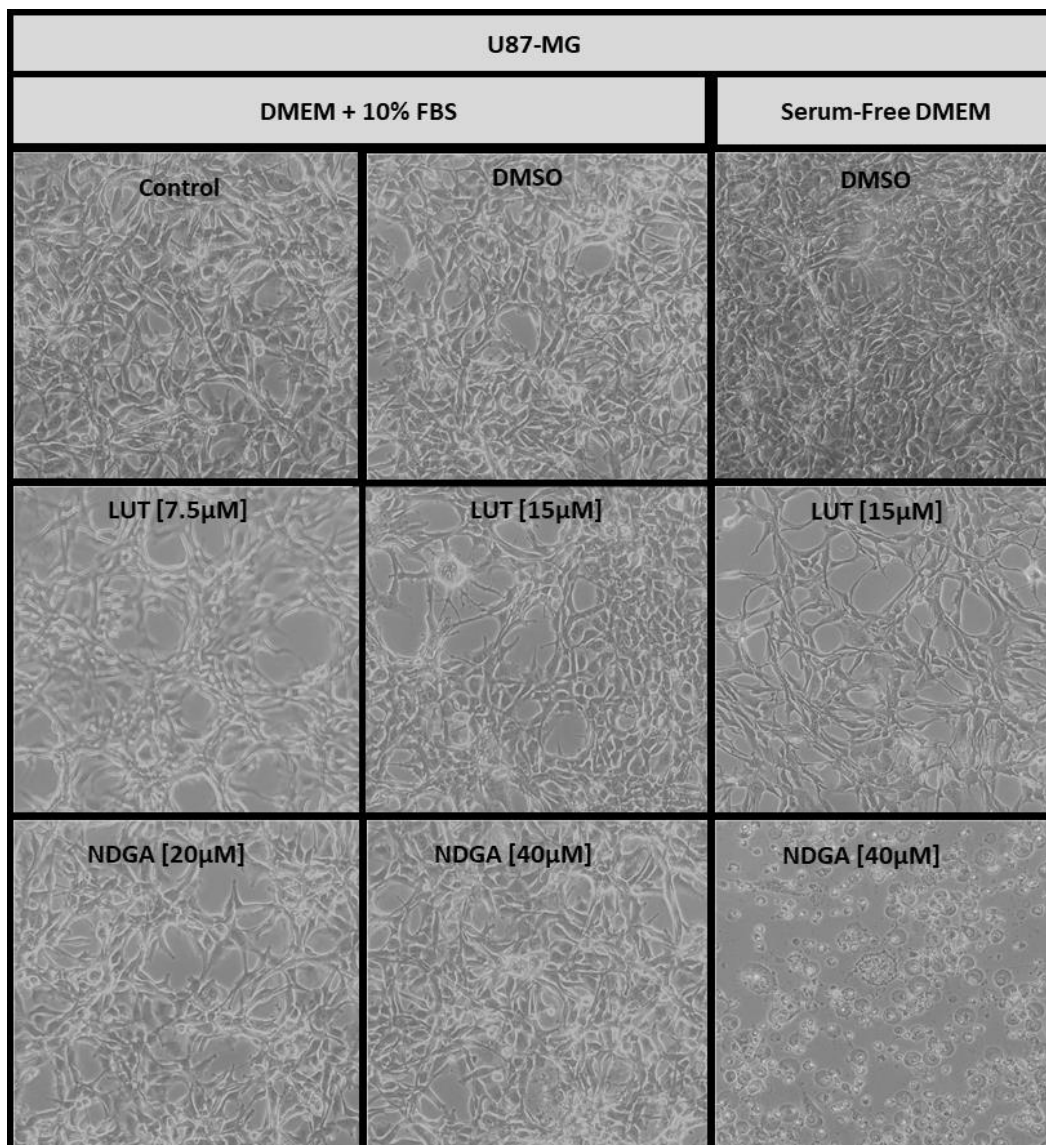


Figure R10. U87-MG treated with Lipoxygenase inhibitors Luteolin and NDGA, in the U87-MG cell line. Graphs show the results after 48 hours and 72 hours of treatment with NDGA [20 and 40 μ M] and Luteolin [7.5 and 15 μ M], with the data analysis in relation to the control, showing a decreasing tendency in cell count. Phase-contrast microscope images shows cell plate at 72 h immediately before collection.

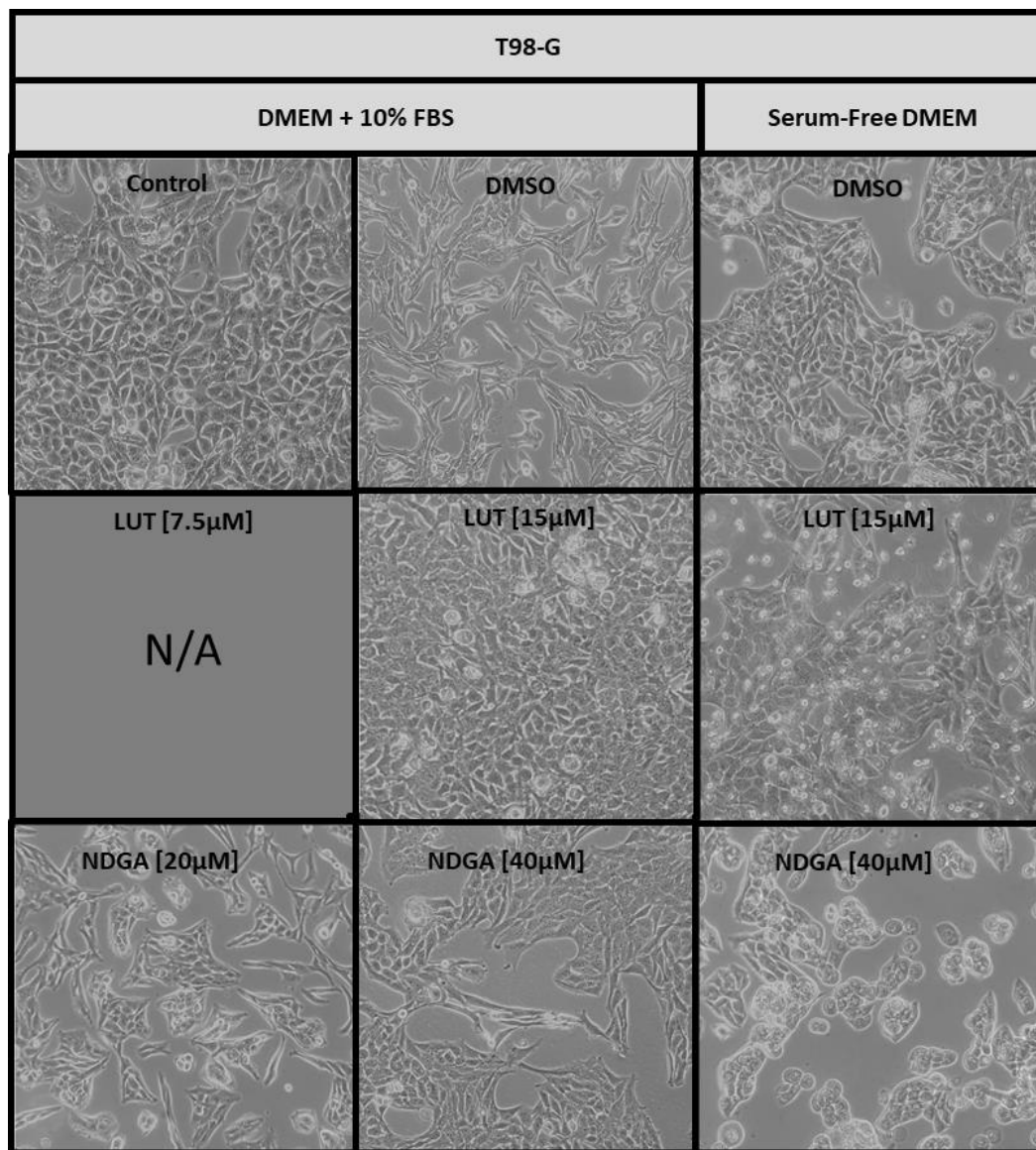


Figure R11. T98-G treated with Lipoxygenase inhibitors Luteolin and NDGA, in the T98-G cell line. Graphs show the results after 48 hours and 72 hours of treatment with NDGA [20 and 40 μ M] and Luteolin [7.5 and 15 μ M], with the data analysis in relation to the control, showing a decreasing tendency in cell count. Phase-contrast microscope images shows cell plate at 72 h immediately before collection.

4.2.1. HODEs + 15-LOX Inhibitors in U87-MG

Concomitant treatments of the 13-HODE/ 9-HODE with the 15-LOX inhibitors were performed over a 72-hour period (Figure R12) to identify any relationship between cell growth and 15-LOX inhibition. A tendency to increase cell count at 48h ($p=0.055$) and at 72h ($p=0.08$) was observed with the 13-HODE [$5\ \mu\text{M}$] treatment, as was expected. However, an increase in cell count was also observed when 13-HODE was added to the LUT treatment [*bottom*] ($p=0.05$) after 72h, implying that the presence of LUT did not interfere with 13-HODE's influence on cell count. No changes in cell count were observed by the other treatments.

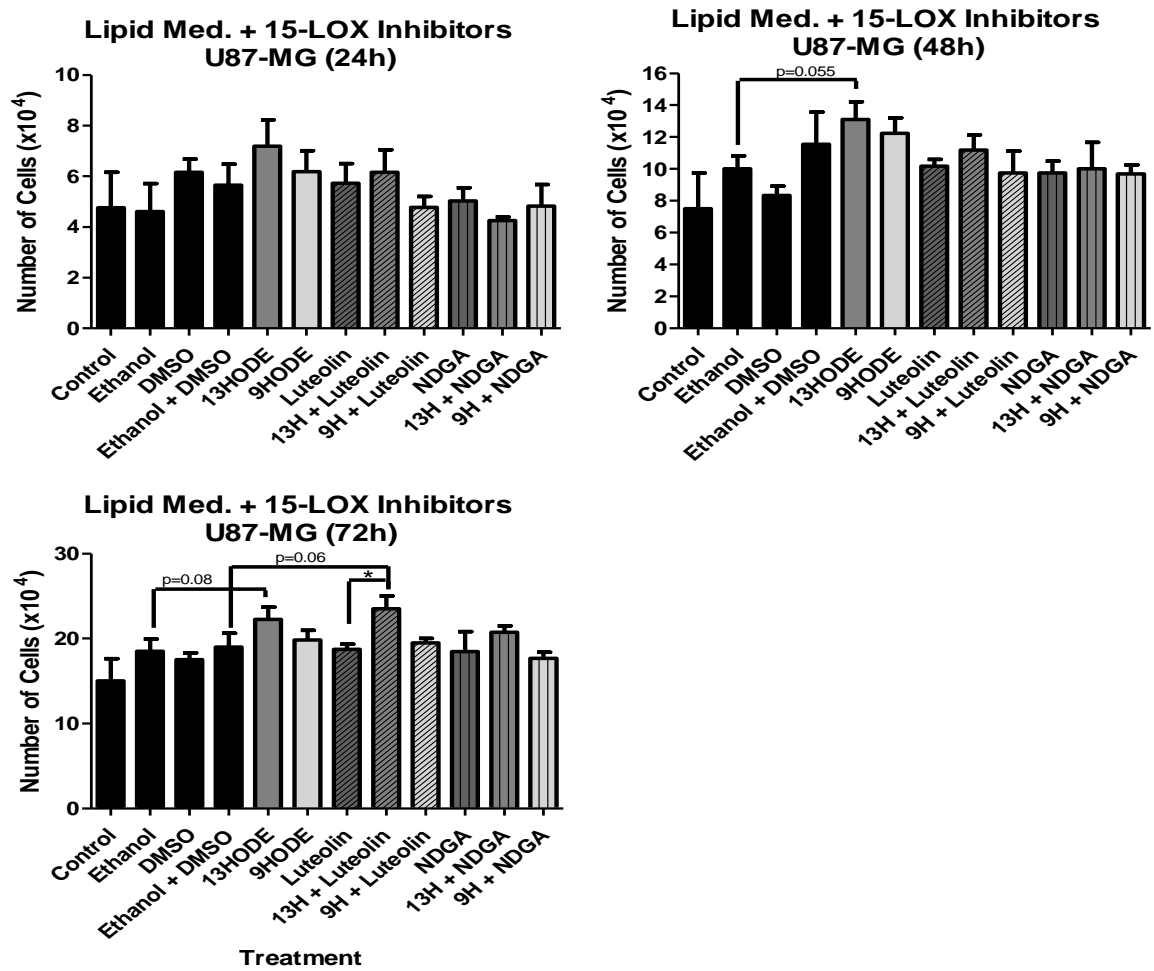


Figure R12. Concomitant Treatments of HODEs with Lipoxigenase inhibitors in U87-MG. Graphs show the influence of combined treatments of 13-HODE [5 μ M]/ 9-HODE [5 μ M] with LUT [15 μ M]/ NDGA [40 μ M] and their respective controls on cell count after 24h, 48h and 72 hours. An increasing tendency in cell count was observed at 48h and 72h with 13-HODE. A significant increase was also observed with the 13-HODE+LUT treatment compared with LUT alone. No other combined treatments displayed any alterations. * $p < 0.05$. N=3, in duplicate.

4.3. T98-G Cell Migration

Since T-98G cells did not appear to be as sensitive to the HODE treatments as U87-MG cells were, yet T98-G cells do produce HODEs (Figure S1), it is possible that the role of these lipid mediators may be found in other cellular activities, such as migration. T98-G cells were cultivated in 24-well plates and when 90-100% confluency was reached a streak was made on the plate and treatments with 13-HODE [5 μ M]/ 9-HODE [5 μ M]/ 15-HETE [1 μ M]/ LUT [15 μ M] /NDGA [40 μ M] were applied. A significant reduction in the migration was observed due to the 13-HODE treatment (23%), while 9-HODE and 15-HETE tended to increase migration compared to the control (Figure R13; *left graph*). The 15-LOX inhibitor treatments significantly reduced T98-G migration by 62% (LUT) and 29% (NDGA) (Figure R13; *right graph*). Pictures were taken at 0 hours and 12 hours, representative images are displayed in Figure R14.

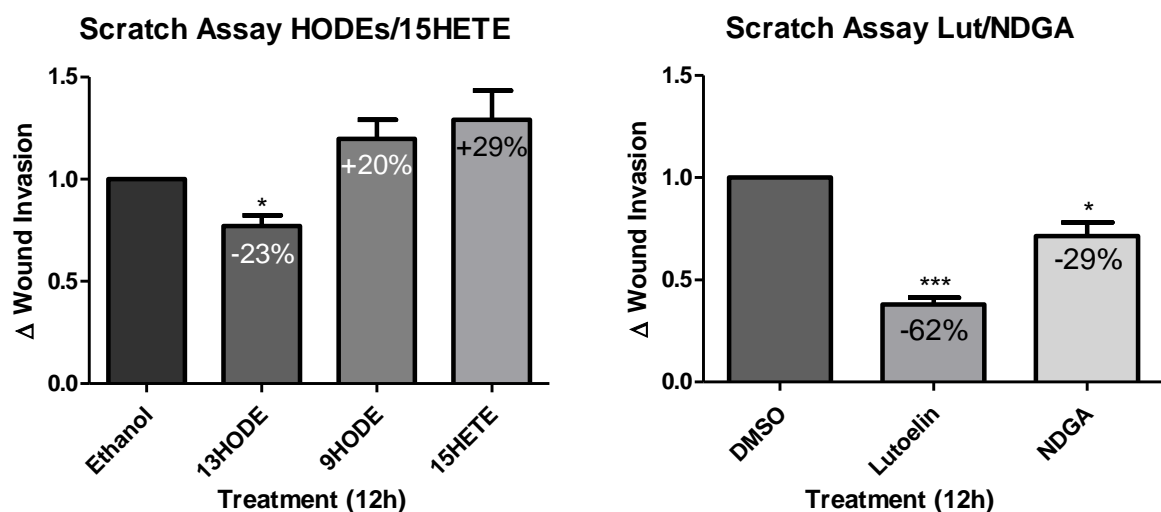


Figure R13. Wound Healing Assay graphs for cell line T98-G. Graphs show the effects of 13-HODE [5 μ M], 9-HODE [5 μ M] and 15-HETE [1 μ M] [*left*], and 15 μ M of Luteolin and 40 μ M NDGA [*right*] on T98G cell migration. A decrease in migration was observed in the 13-HODE treatment (23%), as well as in the Luteolin (62%) and NDGA (29%) treatments. N=3 in duplicate. * $p < 0.05$, *** $p < 0.001$.

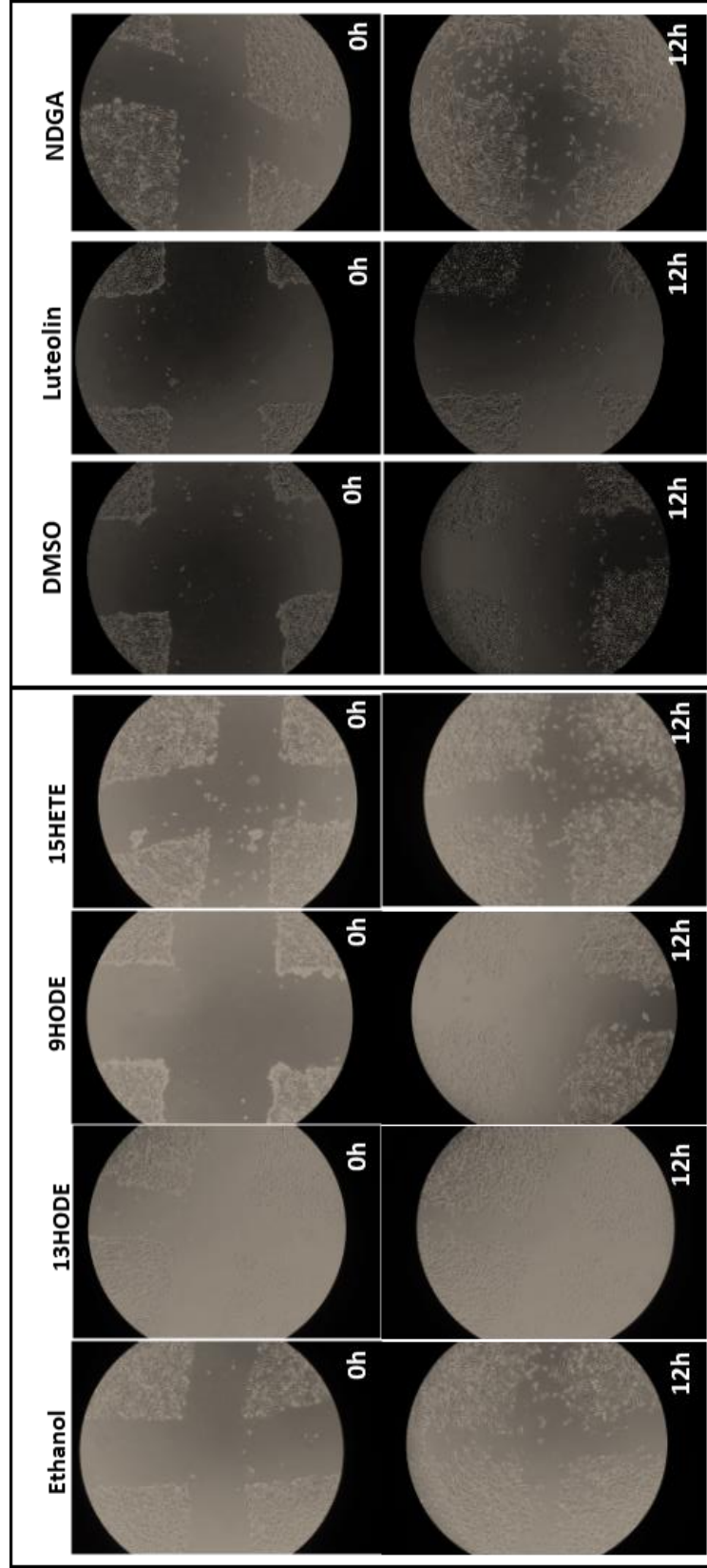


Figure R14. Wound Healing Assay in cell line T98-G. Representative photos of 13-HODE [5 μ M], 9-HODE [5 μ M] and 15-HETE [1 μ M] treatments [*left*], and 15 μ M of Luteolin and 40 μ M NDGA treatments [*right*] on T98G cell migration at 0h and 12h.

4.4. Metalloproteases and Invasive Potential

Cell migration depends on ECM remodeling in order to invade other tissues. Since a dramatic effect on cell invasion was observed by LUT and NDGA, the influence of these Lipoxygenase inhibitors on MMP expression and activity was explored. The primers were first standardized for conventional and Real Time Quantitative PCR analysis (Table R3 and Figure R15). Then, conventional RT-PCR was performed to determine MMP expression in five GBM cell lines (Figure R16). MMP-2 and MMP-14 were abundant in all GBM cell lines. MMP-9 expression was negligible in all the cell lines after 40 cycles were run. RT-qPCR also identified MMP2 and MMP14 in all 5 cell lines, most conspicuously in U87-MG and T98-G (Figure R17). However, since MMP-9 was poorly expressed, mRNA was below the detectable limit of RT-qPCR (data not shown).

TABLE R3. MMP Primer sequences, annealing temperatures, and band sizes for RT-PCR			
Primer	Sequence	Annealing Temp. (°C)	Band Size (base pairs)
MMP2 sense	GAC CAG AAT ACC ATC GAG ACC A	59.1	128 bp
MMP2 anti-sense	GTG TAG CCA ATG ATC CTG TAT GTG		
MMP9 sense	TTT GTT CAA GGA TGG GAA GTA CTG	59.1	124 bp
MMP9 anti-sense	CTC CTC AAA GAC CGA GTC CA		
MMP14 sense	CTT CAA AGG AGA CAA GCA TTG G	59.1	297 bp
MMP14 anti-sense	CCC TTG TAG AAG TAA GTG AAG AC		

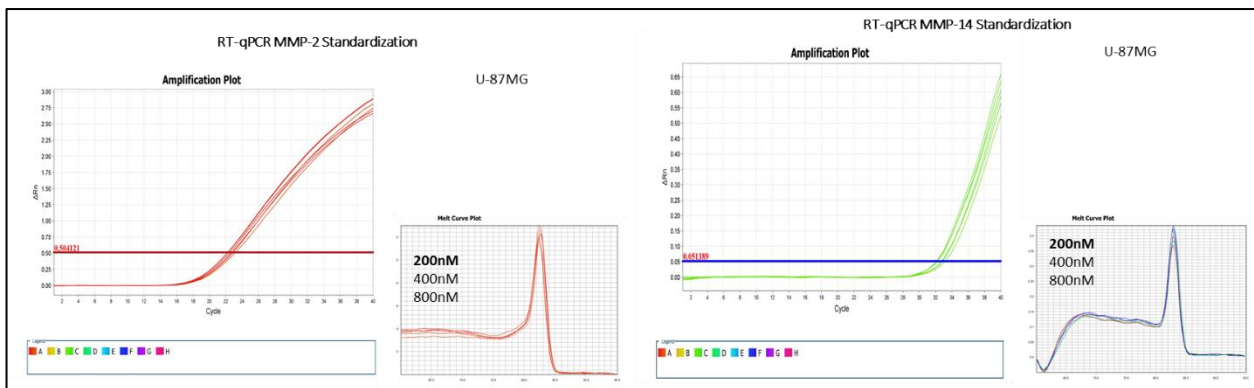
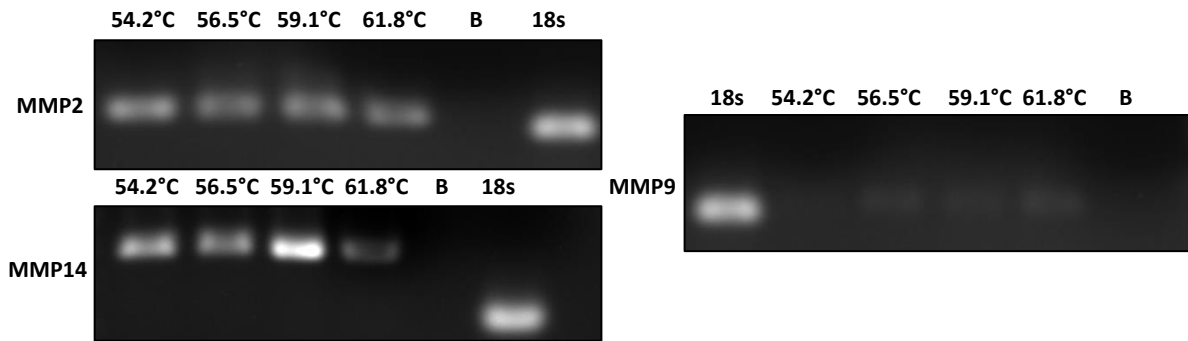


Figure R15. RT-PCR primer standardization of MMPs. Representative Gel electrophoresis of annealing temperatures for MMP-2, MMP-14 and MMP-9 [top]. Representative amplification curves and Melting Curve Plots for MMP-2 and MMP-14 [bottom]. MMP-9 expression was not detected by qPCR. All the genes were amplified in all cell lines after 40 cycles. Endogenous control was 18S. Blank [B]. N=3 in duplicate.

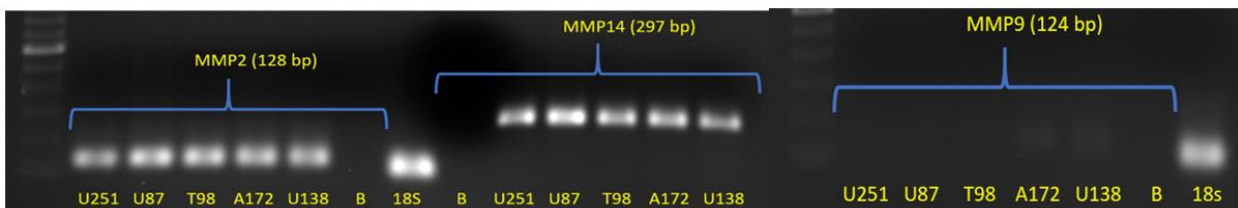


Figure R16. Conventional RT-PCR of MMP expression profile in 5 GBM Cell Lines. Cell lines U251-MG, U87-MG, T98-G, A172, U138-MG were examined for MMP expression. MMP-2 and MMP-14 were expressed in all cell lines. MMP-9 expression was negligible. All the genes were amplified in all cell lines after 40 cycles. Blank [B]. N=3 in duplicate.

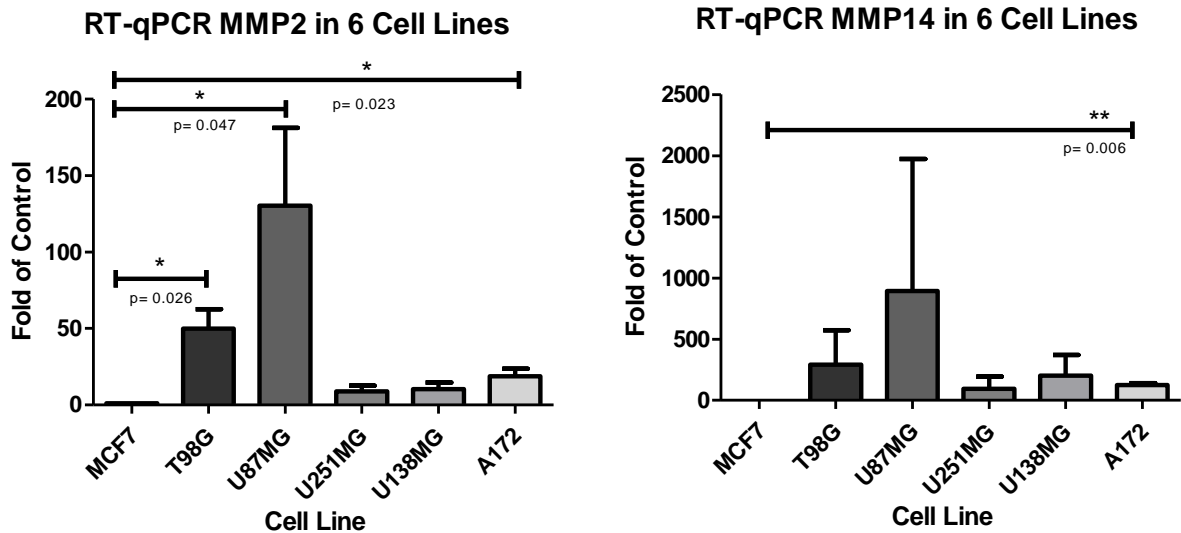


Figure R17. Real Time quantitative RT-PCR of MMP expression profile in 5 GBM Cell Lines. Cell lines U251-MG, U87-MG, T98-G, A172, U138-MG were examined in comparison with breast cancer cell line MCF-7 for MMP expression. MMP-2 and MMP-14 were expressed in all cell lines. MMP-9 expression was negligible. The fold of control was calculated by $2^{\Delta\Delta CT}$ considering MCF7 as the control. Blank [B]. N=3 in duplicate.

Further confirmation of MMP expression and activity in U87-MG and T98-G cell lines was performed through Gelatin Zymography (Figure R18). Both latent (ProMMP2) and active forms of MMP-2 were produced and secreted by both cell lines in the culture medium. When the band intensity was normalized to the number of cells in the well at the time of collection and to the expression of the fibrosarcoma cell line, HT1080, U87-MG appeared to have much more MMP2 (both active and latent) than T98-G. U87-MG cells were cultivated in both 2 mL of serum-free medium or 4 mL of serum-free medium for comparison of gelatin zymography band intensities (Figure R18; *bottom left*). T98-G cells were cultivated in 2 mL of serum-free medium for more intense bands (Figure R18; *bottom right*). As confirmed by RT-PCR/ qPCR, MMP-9 was neither present nor active in these two GBM cell lines.

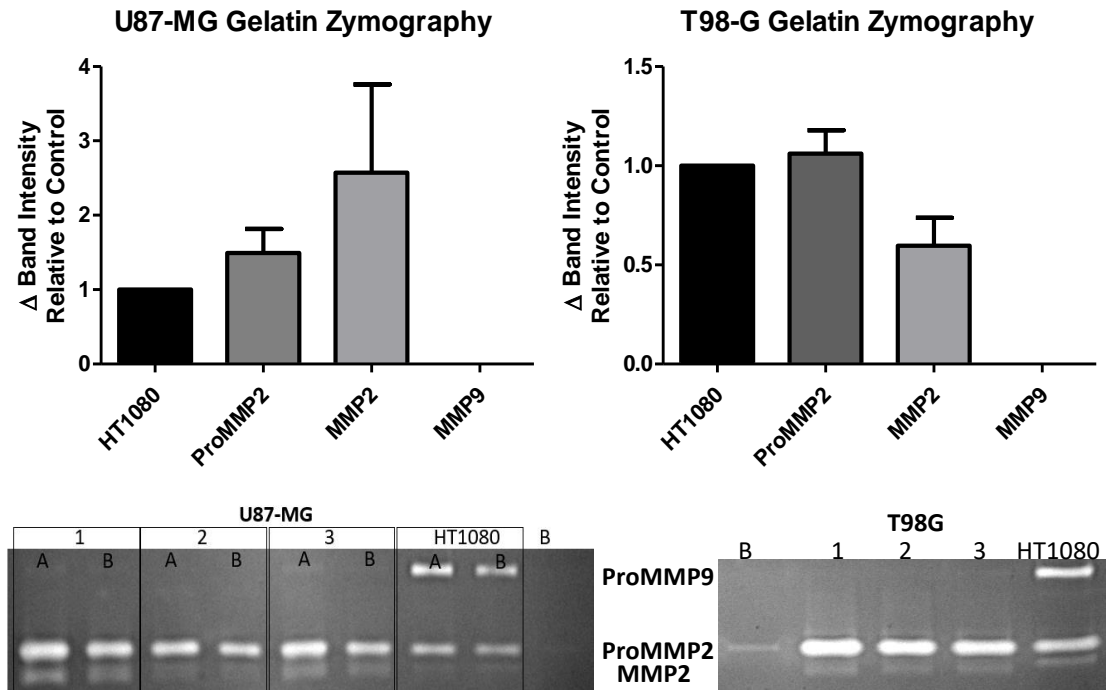


Figure R18. Zymograms of endogenous MMP expression in U87-MG [top left] and T98G [top right] cells by cultivation in T-25 plates with 2mL of serum-free DMEM for 21hrs. Relative intensities were adjusted by the number of cells counted in each plate when the medium was collected and compared with HT1080's relative MMP expression. Gelatin Zymography of U87-MG samples [bottom left] cultivated in either 2 mL (Lane A) or 4 mL (Lane B) of medium were run in duplicates. Each lane was a separately cultivated trial (N=1, 2, 3). Each band shows the relative activity of proMMP2 (72kDa), activated MMP2 (MMP2: 62kDa), proMMP9 (92-82kDa) compared with the HT1080 fibrosarcoma cell line. Zymography of T98-G cultivated in 2 mL of cell medium [bottom right]. B = blank. N=3 in duplicates.

4.4.1. HODEs and MMP expression

To determine the influence of the HODEs on MMP-2 expression, U87-MG cells were treated with 9-HODE and 15-HETE and T98-G cells were treated with 13-HODE for 72h and collected. Real Time quantitative PCR was performed to observe any alterations in mRNA expression (Figure R19). Both 9-HODE and 13-HODE significantly increased MMP-2 mRNA expression. 15-HETE appears to have no influence on MMP-2 expression.

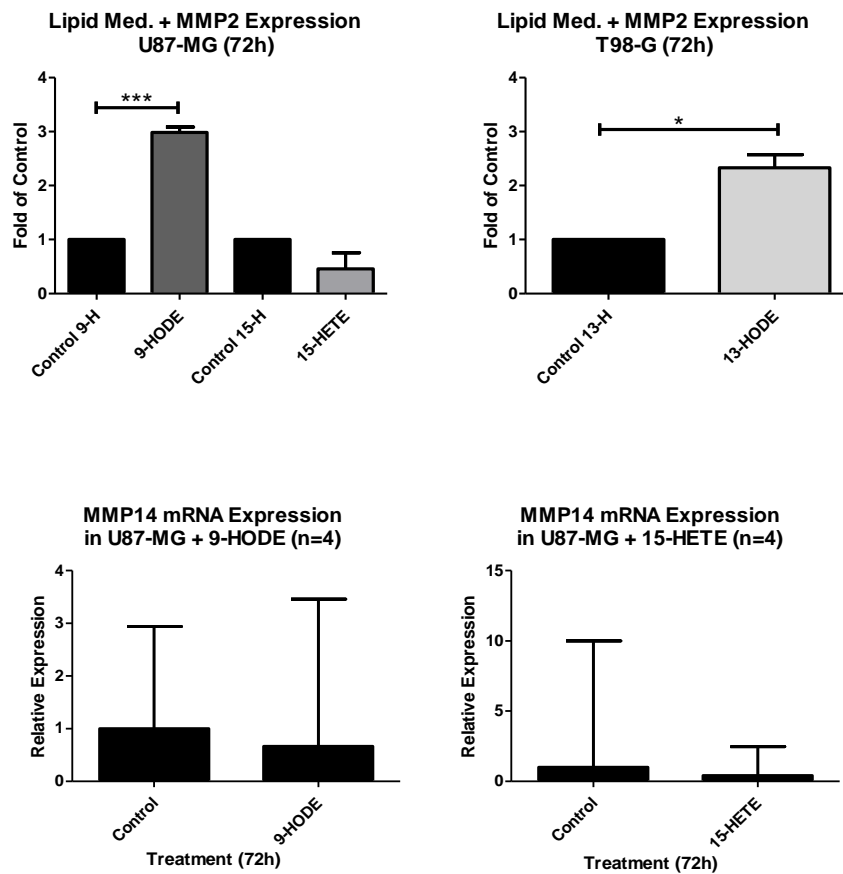


Figure R19. Real Time quantitative RT-PCR expression of MMP2 and MMP14 after 72h of treatments with HODEs and 15HETE; U87-MG [top left] and T98G [top right]. MMP-2 mRNA increased with HODE treatments and was not significantly altered by 15-HETE. MMP14 expression was not influenced by the treatments [bottom]. The fold of control was calculated by $2^{\Delta\Delta CT}$. Blank [B]. N=3 in duplicate.

4.4.2. 15-LOX Inhibitors and MMP expression

Since 15-LOX products appeared to influence MMP2 mRNA expression, cells were treated with LUT and NDGA in order to measure their influence on MMP expression and its extracellular activity through western blotting (Figure R20) and gelatin zymography (Figure R21), respectively. In U87-MG, LUT and NDGA did not influence the production of latent (ProMMP) or active forms of MMP2 or MMP14, however, NDGA did significantly inhibit the activity of ProMMP2. Concerning T98-G, Luteolin did significantly inhibit the synthesis of ProMMP2 and MMP2, but it did not influence MMP2's activity. Moreover, NDGA caused a significant increase in ProMMP2 production and significantly decreased ProMMP14 and ProMMP2 activity.

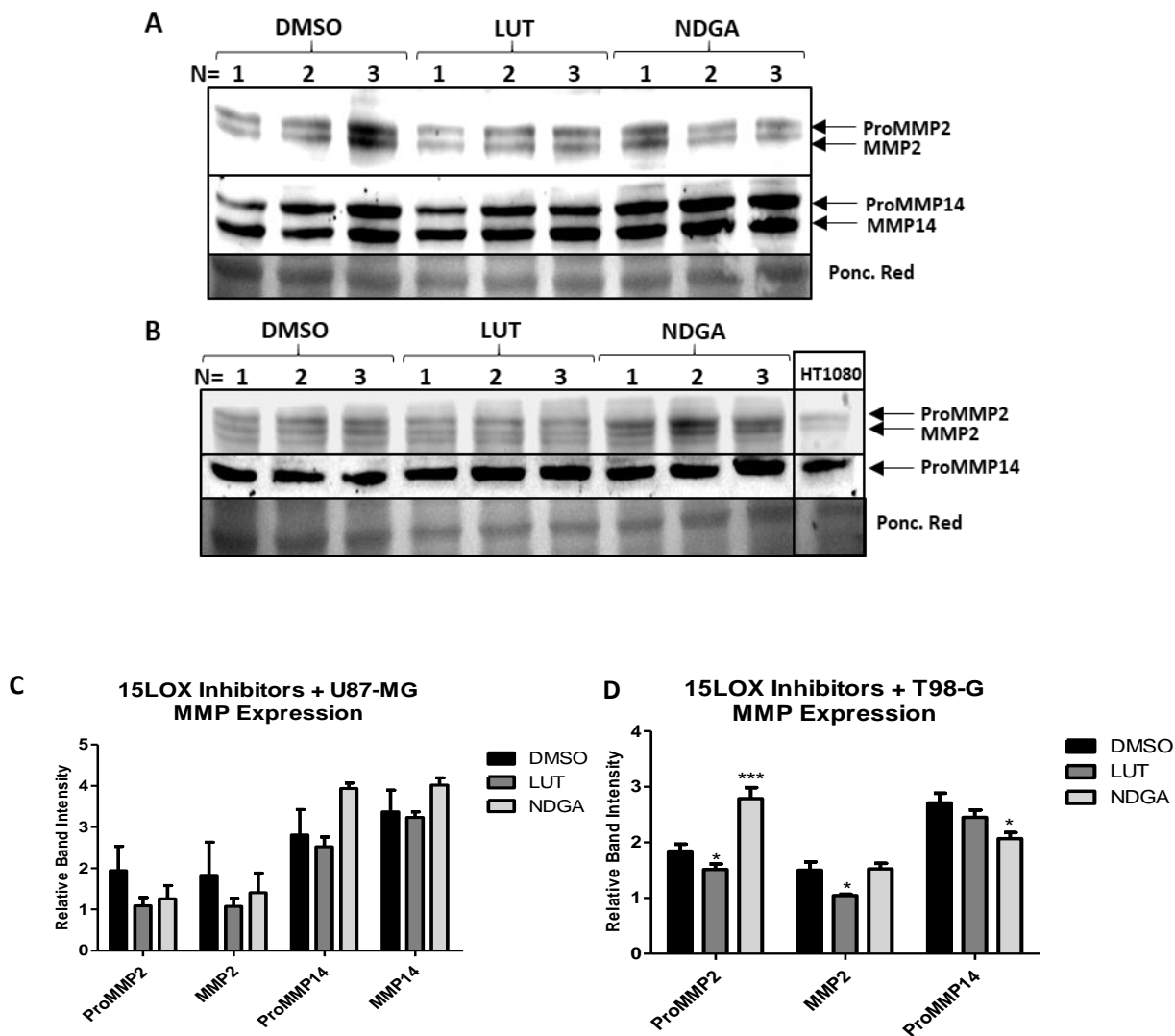


Figure R20. Western Blot and relative band intensities of U87-MG and T98-G cells treated with LUT or NDGA. U87-MG (A) and T98-G (B) cells were cultivated with LUT or NDGA for 72h and total cell protein was extracted. Each lane represents a separately cultivated trial and contains 40 μ g of protein. Each band shows the relative expression of proMMP2 (72kD), activated MMP2 (MMP2: 62kD), proMMP14 (63kD) and MMP14 (60kD) normalized to Ponceau Red staining of the same membrane. The fibrosarcoma cell line HT1080 served as a positive control. A two-way ANOVA with a Bonferroni post-test was performed for U87-MG (C) and T98-G (D), and $p \leq 0.05$ was considered significant. N=3 in duplicates.

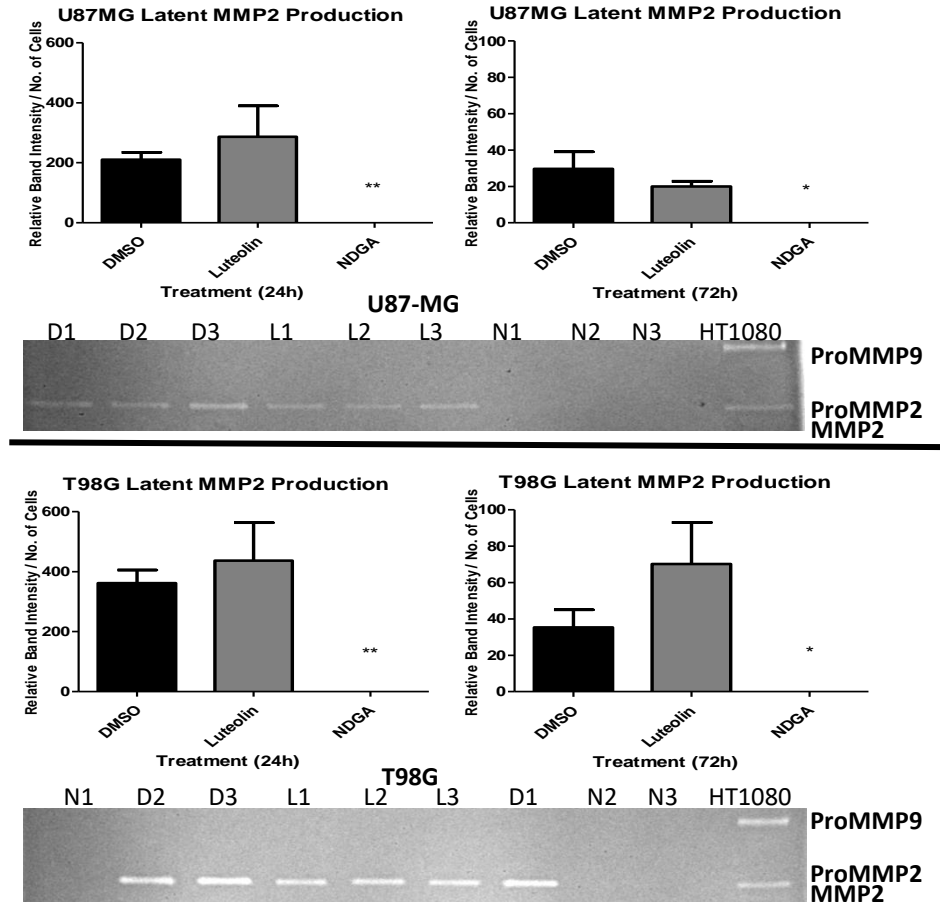


Figure R21. Gelatin Zymography and relative band intensities of GBM cells treated with LUT or NDGA. U87-MG (*above solid line*) and T98-G (*below solid line*) cells were cultivated with LUT or NDGA for 24h (serum-free medium) and 72h (serum-free medium during the last 24h period) and medium was collected. Each lane represents a separately cultivated trial. Each band shows the relative activity of proMMP2 (72kDa), activated MMP2 (MMP2: 62kDa), proMMP9 (92-82kDa) compared with the HT1080 fibrosarcoma cell line. Zymography values of relative ProMMP2 band intensity normalized by the number of cells present on the plate at the time of collection after 72h of treatment with 15-LOX inhibitors. *D1,D2,D3* = (DMSO *N*=1, 2, 3). *L1,L2,L3* (Luteolin *N*=1,2,3). *N1,N2,N3* (NDGA *N*=1,2,3). *B* (blank). *N*=3 in duplicate.

4.5. The Influence of COX and PGE₂ on 15-LOX-1 and MMPs

It is also known that there are some interactions between the LOX and COX pathways (94). Therefore, the influence of COX inhibition and PGE₂ on 15-LOX-1 and MMP2/ MMP14 expression and activity was examined. After U87-MG and T98-G cells were treated with a COX-1 inhibitor (SC560), a COX-2 inhibitor (NS398) or PGE₂ for 24 hours, 15-LOX-1 expression was unaltered by COX inhibitors, although there was a tendency to decrease ($p= 0.06$). However, exogenous PGE₂ significantly increased 15-LOX-1 expression in U87-MG, but not in T98-G (Figures R22 and R23).

The presence and activity of MMPs were also examined. Conventional RT-PCR and real time quantitative PCR demonstrated that COX inhibitors and PGE₂ did not influence MMP2 and MMP14 mRNA in U87-MG and T98-G cells (Figures R24 and R25). However, NS398 produced nearly a 3-fold increase of ProMMP2 mRNA in U87-MG (Figure R25). Western blotting further confirmed a significant increase in ProMMP2 caused by NS398 (Figure R26). No influence of COX treatments on MMP expression was observed in T98-G (Figure R26). PGE₂ did not influence MMP production in U87-MG, however, it did significantly increase ProMMP2 activity in T98-G (Figures R27 and R28). A significant decrease in MMP2 caused by SC560 was identified by both western blot and zymography in U87-MG (Figures R26 and R28).

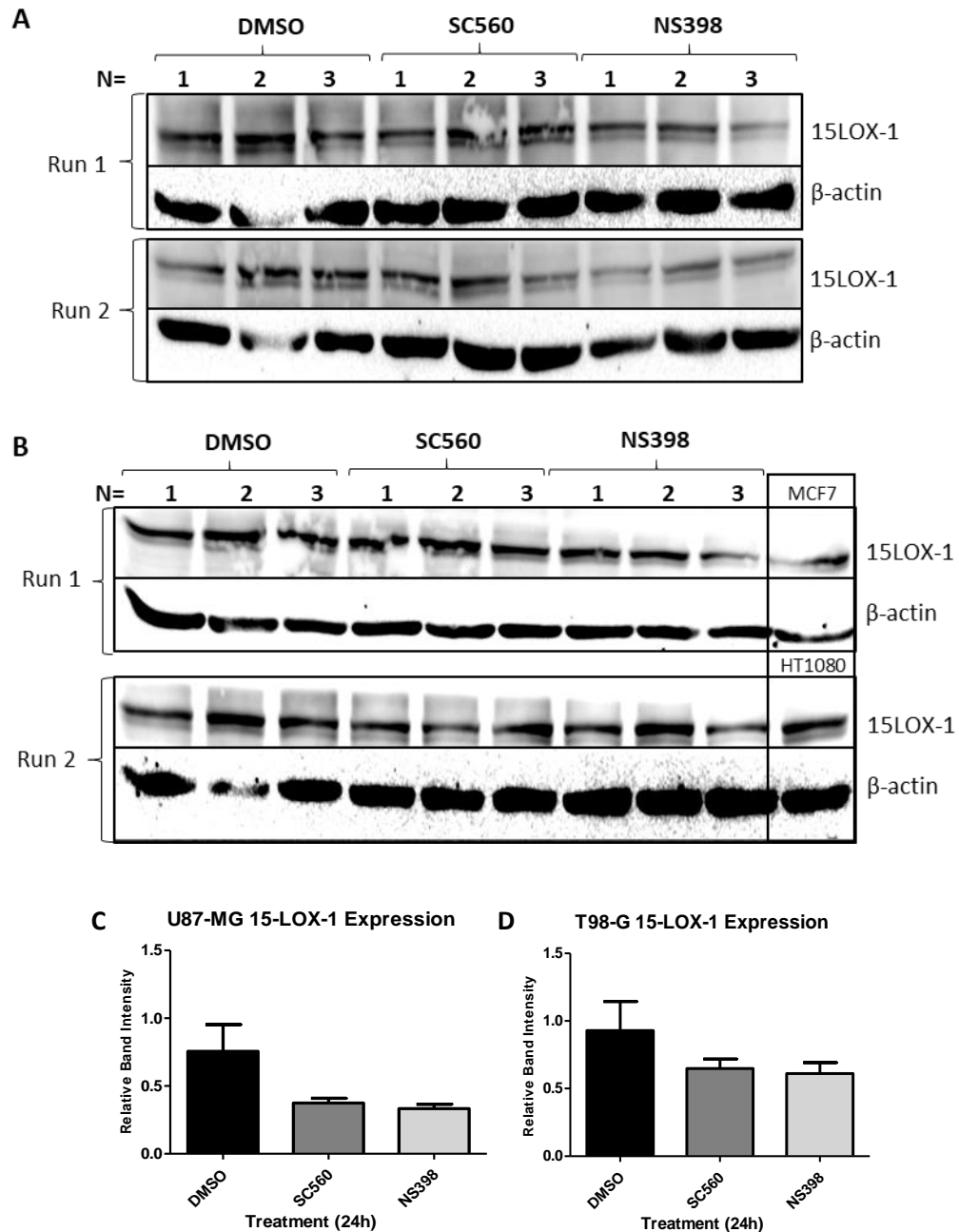


Figure R22. Western Blots of 15-LOX-1 expression after treatments with a COX-1 inhibitor (SC560) and a COX-2 inhibitor (NS398) for 24 hours. (A) U87-MG protein samples of treated cells. The Western Blot protocol was performed twice using fresh samples and new nitrocellulose membranes (Run 1; Run 2). Each membrane possesses three separate trials of cells incubated in each treatment (N=1,2,3). **(B)** T98-G protein samples of treated cells. The breast cancer cell line, MCF7, and fibrosarcoma cell line, HT1080, were used as positive controls. **(C)** U87-MG and **(D)** T98-G statistical analysis. The relative band intensities of 15-LOX-1 were normalized to the relative band intensities of the endogenous control, β -actin. An unpaired t-test with Welch's correction was performed and a p-value ≤ 0.05 was considered significant (*).

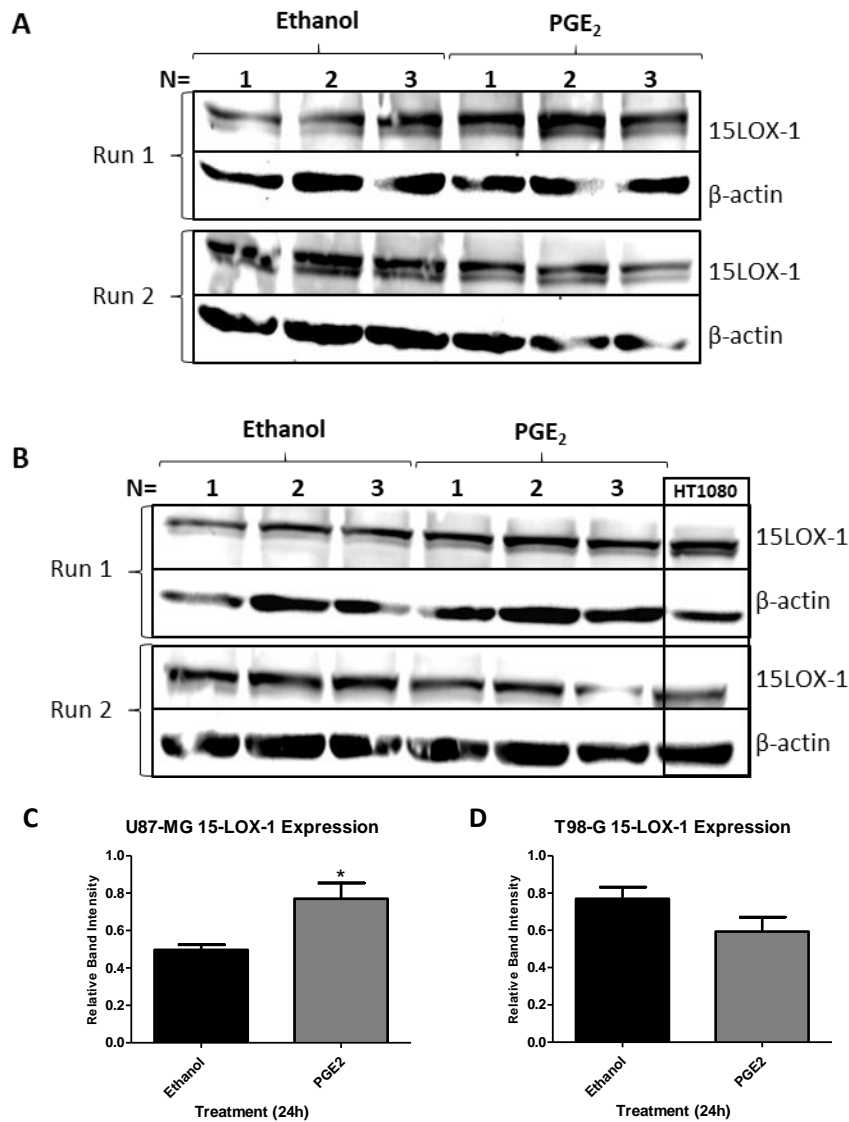


Figure R23. Western Blots of 15-LOX-1 expression after treatments with PGE₂ for 24 hours. (A) U87-MG protein samples of treated cells. The Western Blot protocol was performed 2 times using fresh samples and new nitrocellulose membranes (Run 1; Run 2). Each membrane possesses three separate trials of cells incubated in each treatment (N=1,2,3). (B) T98-G protein samples of treated cells. The fibrosarcoma cell line, HT1080, was used as a positive control. (C) U87-MG and (D) T98-G statistical analysis. The relative band intensities of 15-LOX-1 were normalized to the relative band intensities of the endogenous control, β-actin. An unpaired t-test with Welch's correction was performed and a p-value ≤ 0.05 was considered significant (*). N=3 in duplicate.

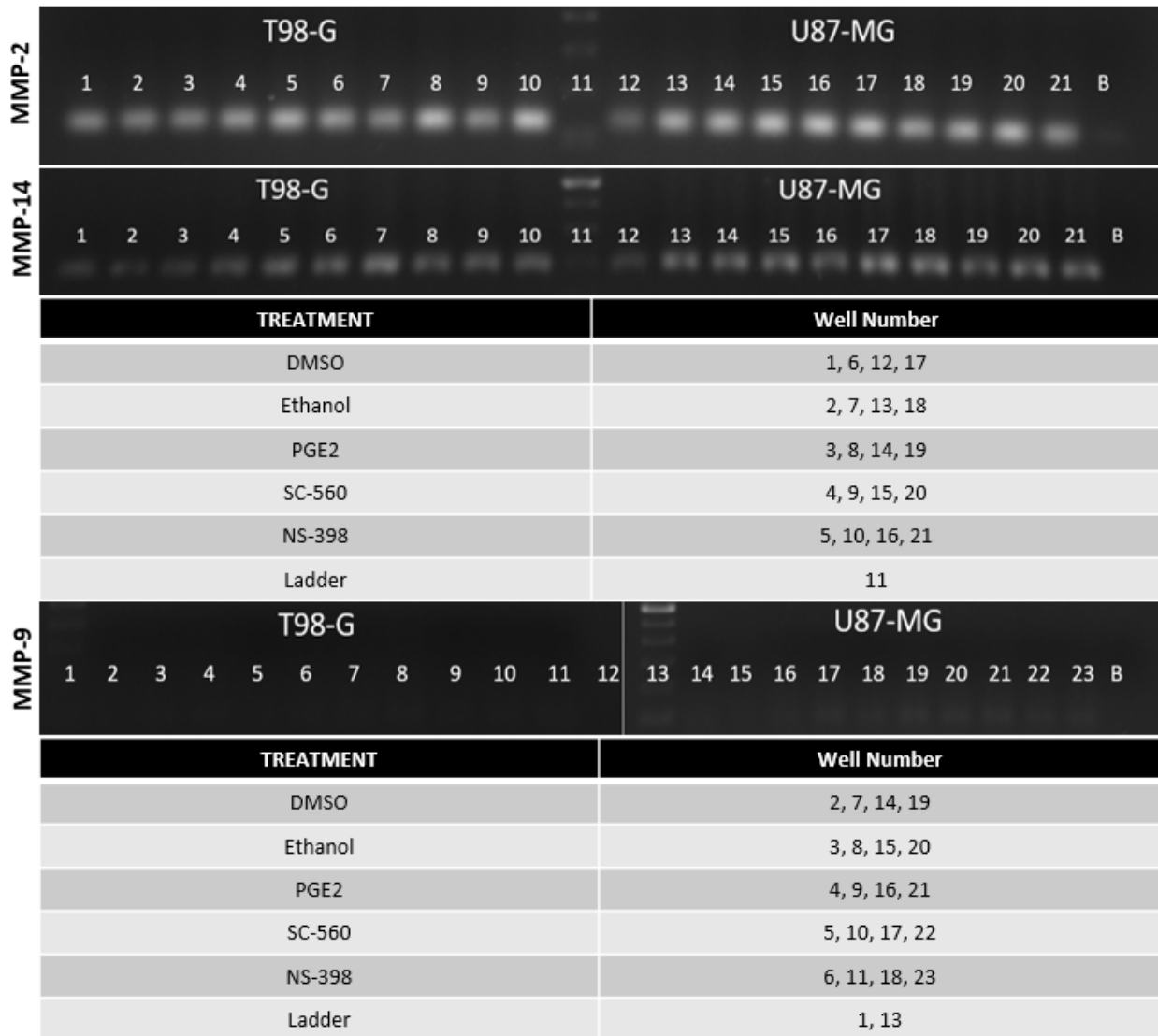


Figure R24. Conventional PCR expression of MMP-2, MMP-14, MMP-9 after 24 hours of treatment with PGE₂, SC560, NS398 or their respective controls in duplicates (N=2).

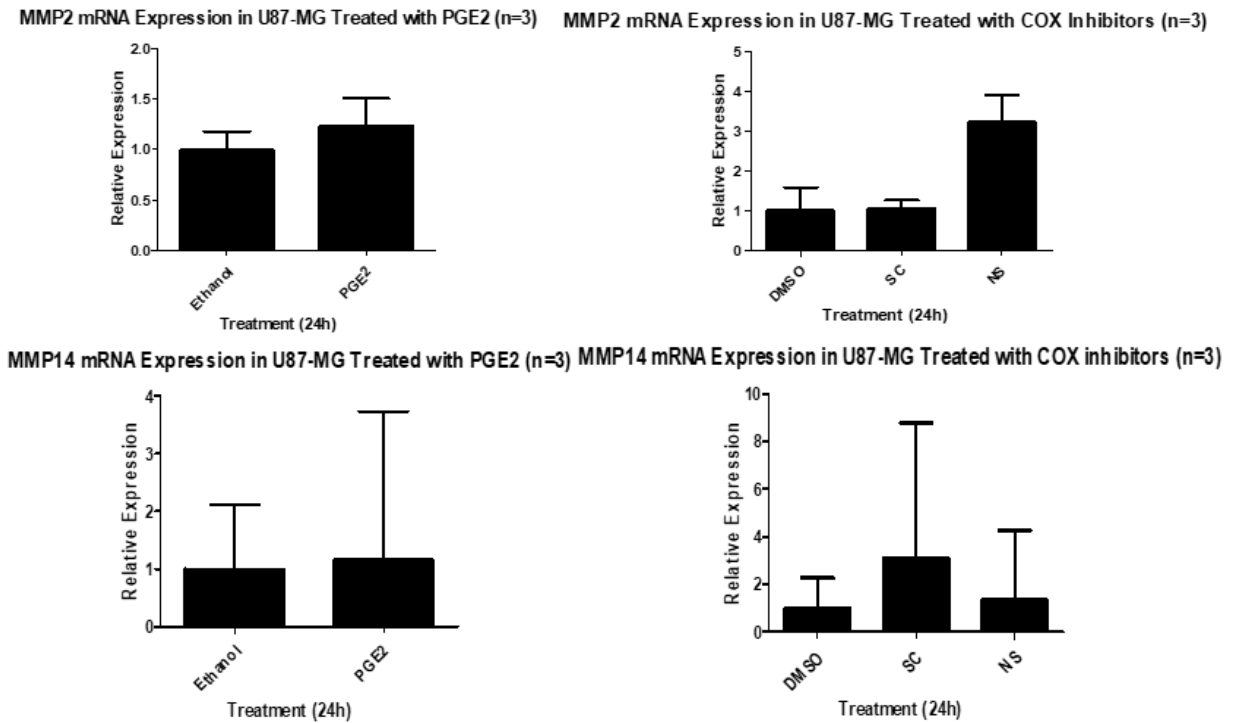


Figure R25. Quantitative Real Time PCR of MMP-2 and MMP-14 gene expression. MMP-9 was below the detectable limit. N=3 in duplicate.

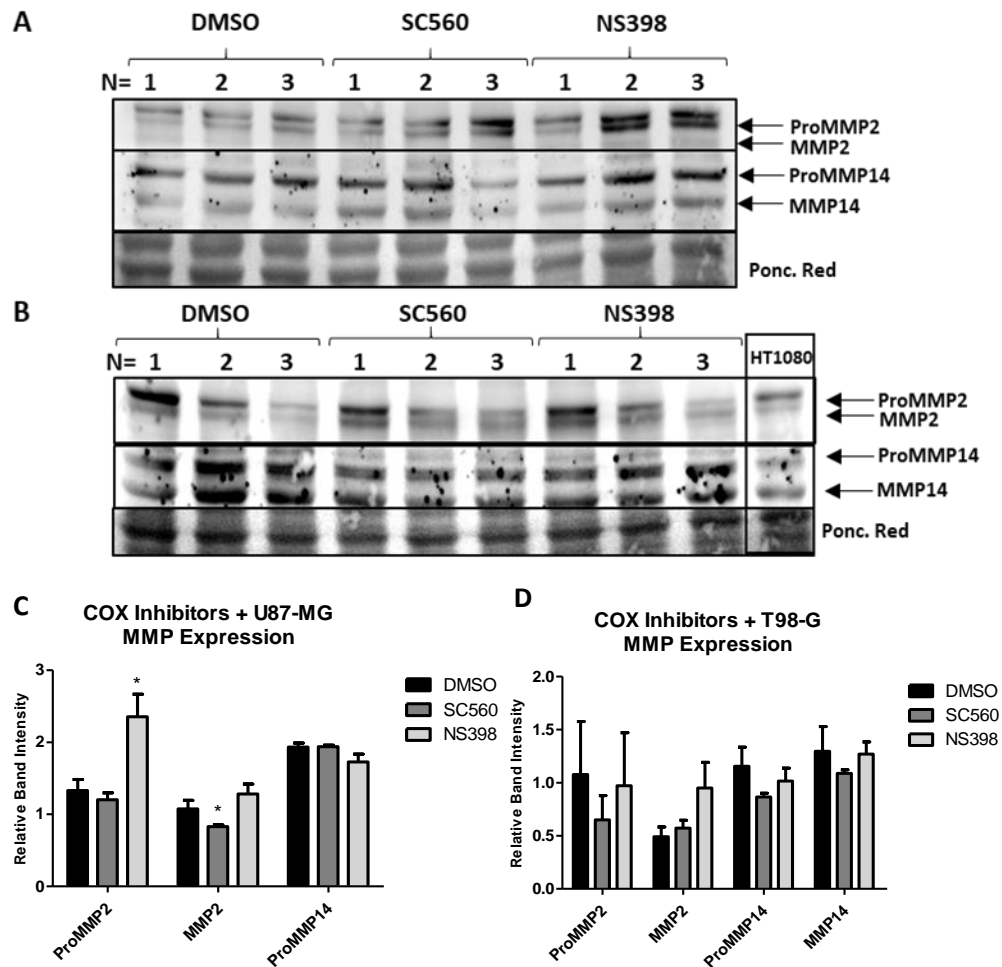


Figure R26. Western Blot and relative band intensities of MMPs in U87-MG and T98-G cells treated with SC560 or NS398. U87-MG cells were cultivated with SC560 or NS398 for 24h and total cell protein was extracted. Each lane represents a separately cultivated trial and contains 40 μ g of protein. Each band shows the relative expression of proMMP2 (72kDa), activated MMP2 (MMP2: 62kDa), proMMP14 (63kDa) and activated MMP14 (60kDa) normalized to Ponceau Red staining of the same membrane. A two-way ANOVA with a Bonferroni post-test was performed, and $p \leq 0.05$ was considered significant (*). N=3 in duplicate.

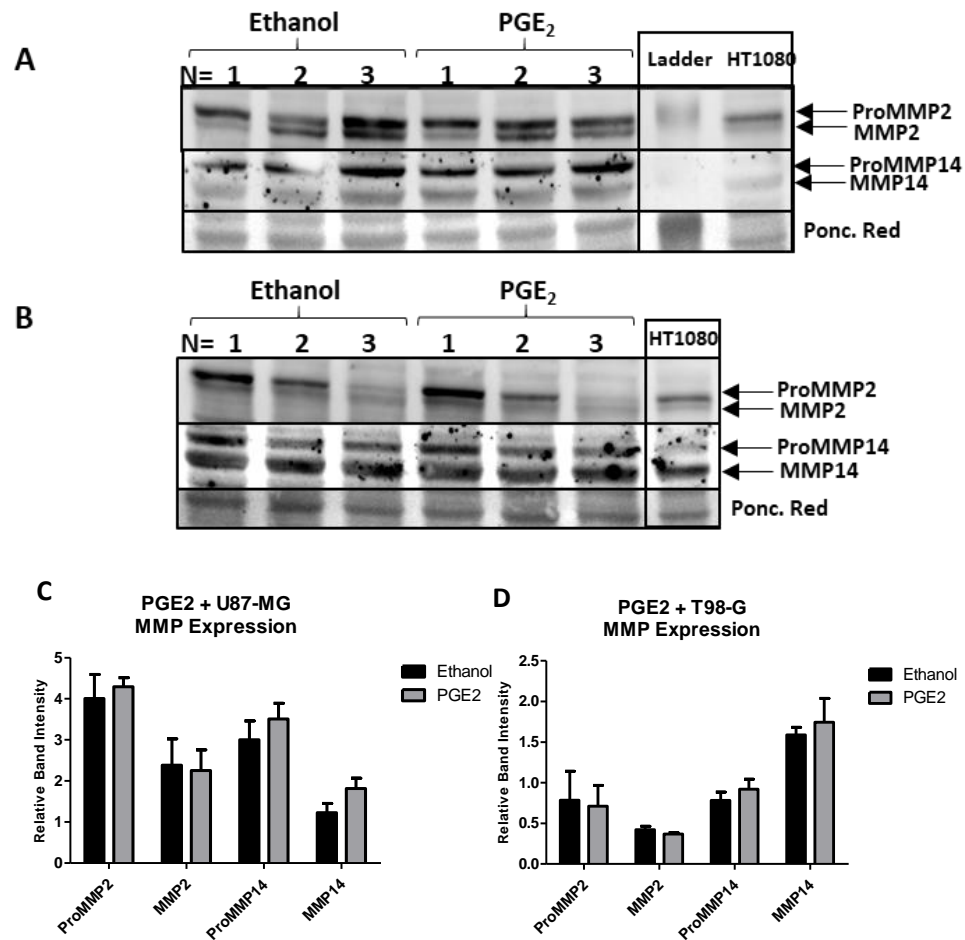


Figure R27. Western Blot and relative band intensities of U87-MG cells treated with PGE₂. U87-MG cells were cultivated with PGE₂ for 24h and total cell protein was extracted. Each lane represents a separately cultivated trial and contains 40μg of protein. Each band shows the relative expression of proMMP2 (72kDa), activated MMP2 (MMP2: 62kDa), proMMP14 (63kDa) and activated MMP14 (60kDa) normalized to Ponceau Red staining of the same membrane. A two-way ANOVA with a Bonferroni post-test was performed, and $p \leq 0.05$ was considered significant. N=3 in duplicate.

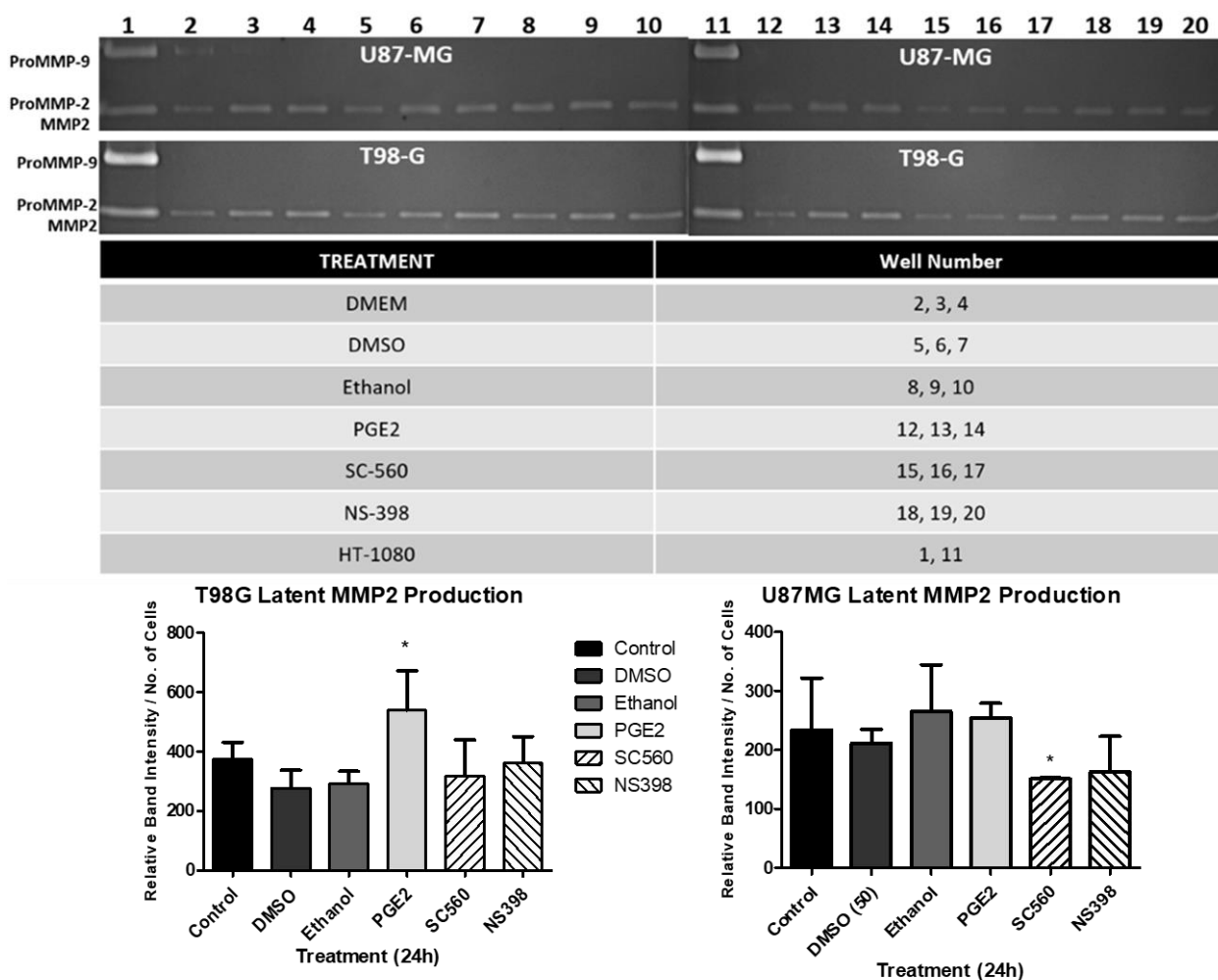


Figure R28. COX inhibitor Gelatin Zymogram [top] of serum-free medium of cell lines subjected to 24 hours of treatment with PGE₂, SC560, NS398 or their respective controls. Data analysis of relative band intensity normalized to the number cells present on the plate at the time of collection. N=3 in duplicate.

5 DISCUSSION

For decades, PUFA metabolism and signaling has been explored in cancer (95)(96). The synthesis of eicosanoids and other lipid mediators from the oxygenation of PUFAs has the means to modulate cell proliferation, cell adhesion, migration and angiogenesis by up-regulating or down-regulating other signaling molecules (38,41). All these cellular processes are involved in the inflammatory response and are also related to the development of tumors. However, the activities of lipid-oxidizing enzymes, such as lipoxygenases and cyclooxygenases, in cancer are still be explored intensively as a potential therapeutic strategy.

The LOX pathway is less described in the tumors of the central nervous system compared with COX. The aim of this study was to characterize the transcriptional profile of components of the 15-lipoxygenase pathway, including enzymes, receptors and metabolites. The data from this study and previously unpublished data (Figure S1) confirm the presence of the 15-LOX pathway and its potential role in GBM cell lines U87-MG and T98-G. Due to the heterogeneous profile of these two cell lines (Table R2), analyses were performed, where possible, comparing the influence of 15-LOX and its metabolites on GBM growth, migration and invasiveness; which was the second aim of this study.

5.1 15-LOX Pathway in GBM

Conventional RT-PCR and western blot analysis confirmed the presence of 15-LOX-1 along with the 13(S)-HODE, 9(S)-HODE and 15(S)-HETE receptors in the U87-MG and T98-G cell lines (Figures R3 and R9). Since this project was part of a larger project examining the expression and activity of range of lipid mediators present in glioblastoma cells, previous LC-MS/MS analyses identified the presence of 15-LOX metabolites as the most abundant lipid mediators in five GBM cell lines and patient samples compared to the production of other lipoxygenase isoforms (Figure S1). Despite possible non-enzymatic oxidation of LA (97), the varying amounts of 15-LOX products suggest that non-enzymatic synthesis is not exclusively responsible for the production of HODEs/15-HETE in these cells. Supplementary figures have been added exploring the findings of the Human Protein Atlas (HPA) and The Cancer Genome Atlas (TCGA) Databases that are pertinent to the present study (summarized in Table S1) (98)(99).

The Human Protein Atlas did not identify 15-LOX-1 or 15-LOX-2 in GBM cell lines or glioma samples with the primers and antibodies used (Figures S1 and S2). The TCGA database

identified both 15-LOX isoforms and observed a significant decrease in 15-LOX-1 mRNA expression between non-tumor and GBM samples, while no significant difference was observed in 15-LOX-2 mRNA expression (Figure S3). Survival curves did not demonstrate any changes between high and low expression of 15-LOX-1 or 15-LOX-2 among GBM patients (Figure S3). This suggests that 15-LOX metabolism may not be as directly involved in patient outcome as is, for example, PTEN; where lower expression significantly reduces patient survival (99). However, in a study with 48 prostatectomy samples, 15-LOX-1 expression positively correlated with tumor malignancy (60). Moreover, as the literature shows, cancer is a multifactorial disease and is influenced by an array of factors involved in genetics, proteomics and lipidomics (18). Thus, continued studies in 15-LOX are valid and necessary.

15-LOX metabolites require the presence of certain receptors to modulate cell activity. In this study, the more prominent HODE receptors were examined: peroxisome proliferator-activated receptor gamma (PPAR γ), PPAR beta/delta (PPAR β/δ) and GPR132. As described in Marion-Letellier *et al.*'s review (2016), PPAR γ possesses various functions: glucose and lipid metabolism; anti-inflammatory regulation; oxidative stress inhibition; improved endothelial function (100). This receptor is a promiscuous nuclear receptor with many potential ligands, including eicosanoids and other lipid mediators such as 13-HODE/9-HODE/15-HETE. In brain tissue, PPAR γ is present among several cell types such as astrocytes, microglial, oligodendrocytes and neurons (101). As reviewed by Youssef and Badr (2011), specific PPAR γ agonists in glioblastomas demonstrated promising antitumoral effects, however they were not reflected in *in vivo* contexts (102). In colorectal cancer, 13(S)-HODE and 9(S)-HODE have been proven to bind to PPAR γ , reducing cell growth and increasing apoptosis (103). Specifically, 13-HODE down-regulates PPAR β/δ signaling and upregulates PPAR γ activity in colorectal cells (104). Moreover, in human mesangial cells, 9(S)-HODE is capable of binding to PPAR γ to stimulate cell proliferation and ECM components such as type IV collagen (72). However, these relationships have not been explored in GBM.

PPAR γ mRNA expression in GBM cell lines varies in the literature. Kato *et al.* (2002) did not identify PPAR γ mRNA in T98-G or U251-MG (105). Meanwhile the HPA identified very little expression in U138-MG, weak expression in U87-MG cell lines and no expression in U251-MG. To compliment this data, the PPAR γ mRNA in the present study was not detected in U138-MG, and U251-MG bands were very weak, even after 40 amplification cycles. However, the present

study identified the mRNA in T98-G, which is contrary to Kato *et al.*'s study. Papi *et al.* (2009) identified PPAR γ in U87-MG and successfully activated it with different agonists implementing anti-tumoral effects (106). Morosetti *et al.* (2004) identified an increased expression of PPAR γ mRNA in U87-MG and A172 GBM cell lines compared to other GBM cell lines (107), which also corroborate the findings seen in Figure R3.

Although the cell lines diverged in their expression of PPAR γ mRNA, HPA patient samples had medium to high PPAR γ staining and the TCGA also identified PPAR γ mRNA in GBM samples. The high staining of PPAR γ in excised GBM samples could be due to the heterogenous mixture of nervous tissue cells, or the cell lines tested decreased their PPAR γ production when they were cultivated after being removed from their original host patients. However, TCGA did not report any significant changes between non-tumor samples and GBM samples nor was there any correlation identified between PPAR γ expression and patient survival time (Table S1). However, long-term PPAR γ activation, as was attempted in prostate cancer, could be a key therapeutic strategy (108,109).

It is known that PPAR γ is a suppressor of the interleukin 6 (IL-6)/STAT3 pathway (110)(111), and prostate cancer progression positively correlates with STAT3 expression (112). The IL6/STAT3 axis is a major pro-inflammatory pathway used by the immune system and is often manipulated by neoplastic cells (113). The use of PPAR γ agonists in GBM cells is known to reduce brain tumor stemness, cell proliferation and invasive capacity partially by phosphorylating STAT3 (114–116). In the TCGA database there is a very significant increase of STAT3 in GBM cells compared to non-tumoral human brain tissue. The abundant levels of 13-HODE found in GBM cell lines may be influencing GBM growth in a way that is similar to prostate cancer, by inhibiting PPAR γ activities and increasing STAT3 activation. Further investigation is required.

The expression of PPAR β/δ mRNA was identified in GBM cell lines (U87-MG, U251-MG, U138-MG) and glioma samples studied by the HPA, which match the results of this study (Figure R3). The TCGA identified a decrease in PPAR β/δ mRNA in GBM samples compared to non-tumor samples, and this decrease was correlated with decreased survival time (Figure S4). In the present study PPAR β/δ mRNA was abundant in the five GBM cell lines examined. PPAR β/δ is another receptor of which 13-HODE is a ligand. PPAR β/δ has demonstrated seemingly opposing roles in tumorigenesis. In various models of cancer, PPAR β/δ elicits pro-tumorigenic activities (117). Hsi

et al. (2001) demonstrated that 13-HODE is not only capable of binding to the generally anti-tumoral PPAR γ but it can also activate the extracellular signal-regulated kinase (ERK) pathway by increasing its phosphorylation to subsequently upregulate PPAR β/δ and phosphorylate PPAR γ , thus inhibiting PPAR γ (62). In prostate cancer cells (PC3) the highly expressed PPAR β/δ , when activated by pharmacological agonists, increases proliferation (118). However, 13(S)-HODE has also been reported in colorectal cancer cells as a ligand to PPAR β/δ , which when bound, decreases PPAR- δ activation, and down-regulates PPAR- δ expression, inducing apoptosis (70). In colorectal cancer, PPAR β/δ is a downstream transcriptional target of the Ras/mitogen-activated protein kinase (MAPK)/ERK pathway (119).

The MAP kinase pathway can be activated through G-protein receptor 132. GPR132 is a transmembrane stress-inducible receptor and is up-regulated when cells are exposed to genetically damaging agents. The activation of this receptor has been associated with intracellular calcium mobilization, inhibition of cAMP formation, and MAP kinase activation (120); all of which induce pro-tumorigenic activity. Similarly, the PGE₂ receptors EP2/EP4 also upregulate cAMP formation and pro-tumorigenic activity in GBM cells (121). Although an inverse, pro-apoptotic relationship between cAMP pathway activation and MAPK inhibition has been documented in GBM cells (122), this may be the result of other compensatory pathways being activated and further research is required.

9-HODE, another 15-LOX-derived lipid mediator found in our GBM cell lines (Supplemental Figure S1), is a ligand for both PPAR γ and GPR132 (97). Specifically, 9-HODE was detected in T98-G, which coincided with the more intense GPR132 RT-PCR band seen among the cell lines (Figure R3). This implies that in T-98G this 9-HODE/GPR132 pathway may be present, although examining the role of this pathway would require further investigation. In the present study, GPR132 mRNA was expressed, in varying degrees, in all five cell lines examined. The HPA identified mRNA only in U251-MG, but it did find abundant protein expression in normal brain tissue and some expression in GBM patient samples. Although the TCGA did not identify any changes in mRNA expression between non-tumor and GBM samples, it surprisingly correlated high GPR132 expression with improved survival time compared with low expression. It is possible that since GPR132 has a key pro-inflammatory role as a macrophage phagocytic receptor (123), its

upregulation correlated with increased patient survival may be due to the immune system's response to the tumor's presence and not necessarily directly involved in an anti-tumorigenic role.

Frasch *et al.* (2011) demonstrated that the activation of GPR132 in macrophages can also induce an increased synthesis of PGE₂ and its receptor, EP2 (124). Both PGE₂ and EP2 are expressed in GBM and actively increase cell migration as seen in a previous study (41). The PGE₂/EP4 pathway, up-regulated in the GBM cell lines studied (41), also induces EP4-dependent MAPK signaling in GBM (125). The endogenous 9-HODE/GPR132 pathway could be an inducer of the active PGE₂/EP2-EP4/MAPK signaling pathways in GBM and could be explored in future studies.

Another relationship worth mentioning is that found between the 15-Lipoxygenase gene and the p53 gene explored in the murine BALB/c embryo fibroblast cell lines transfected with human p53 wildtype and mutated genes by Kelavkar and Badr (1999) (126). They demonstrated that 15-LOX's gene (chromosome 17p13.3), which is in close proximity to p53's gene (chromosome 17p13.1), is upregulated by p53 mutants, resulting in pro-tumorigenic activity derived from 15-LOX products. Gain of function p53 mutations are found in 84% of GBM patients and 94% of GBM cell lines (127). Unpublished LC-MS/MS data from a previous project show that there are more 15-LOX products (13-HODE, 9-HODE, 15-HETE) in the p53 mutant cells lines U251-MG, U138-MG and T98-G, than in the p53 wildtype cell lines A172 and U87-MG (13-HODE only) (Figure S1). The different responses observed in this study between the p53 wildtype U87-MG cells and the p53 mutated T98-G cells could be influenced by mutated p53 upregulating 15-LOX activity in LA metabolism.

5.2 15-LOX Products and Cell Viability and Growth

Examining the MTT assay performed (Figure R4), 13-HODE and 9-HODE [0.1 and 1 μ M] appeared to have negatively influenced the ability of mitochondria to reduce MTT into formazan, and this limited mitochondrial activity implies reduced cell viability. However, higher concentrations of 13-HODE and 9-HODE (5 μ M) significantly increased cell count in U87-MG (Figures R5 and R6). Although this appears to be paradoxical, there is a possible explanation. It is noteworthy that in O'Donnell *et al.*'s study, mammalian 15-lipoxygenase was able to oxidize NADH (128). Stockert *et al.* (2012) demonstrated that MTT reduction into formazan occurs by dehydrogenases, like NADH, present in the cytosol or by those associated with the endoplasmic

reticulum (ER), and not in mitochondria (129). The oxidation of NADH due to 15-LOX could limit the efficiency of the MTT conversion. On the other hand, the presence of exogenous HODEs may compete with formazan for the electron donated by NADH, thus, producing a result that could be misinterpreted as reduced viability.

Exogenous treatments 13-HODE and 9-HODE causing tumor growth are contrary to what is found in other cancer models like colorectal, non-small cell lung cancer and breast cancer (68,103,130). However, in prostate cancer, these 15-LOX-1 products also act in a pro-tumorigenic way. Kelavkar *et al.* (2001) showed that the overexpression of 15-LOX-1 in prostate cancer cells (PC-3) increased tumorigenesis (131). Moreover, Hsi *et al.* (2002) demonstrated that PC-3 and LNCaP prostate cell lines generate more 13-HODE, and Spindler *et al.* (1997) treated PC-3 cells with exogenous 13-HODE and observed an increased MAP Kinase signaling and increased cell proliferation (62)(132). The large amounts of 13-HODE in the GBM cells lines examined and subsequent increases in cell growth suggest that GBM and prostate cancer models may activate similar pathways for growth and survival.

5.3 Lipoygenase Inhibitors and Influence on GBM

In order to understand the role of 15-LOX-1 (and its products) in GBM cell activities pharmacological inhibitors were applied. Two lipoygenase inhibitors were selected: Luteolin (LUT) and Nordihydroguaiaretic acid (NDGA). LUT, a dietary flavonoid, is commonly found in broccoli, carrots and chrysanthemum flowers, and is a proven 15-LOX-1 inhibitor (133). However, when U87-MG cells were treated with Luteolin, an insignificant decrease in cell count was observed (Figure R8). Although the inhibitory effect of LUT on U87-MG cell count has been described by Tsai *et al.* (2013) and Wang *et al.* (2017), the influential cytotoxic concentrations used in those studies ranged from 17.5 - 52.5 μ M and 80 - 100 μ M, respectively; which were much higher than those used in the present study (7.5 μ M and 15 μ M) (134)(135).

It is possible, according to Sadik *et al.* (2003), that flavonoids operate through various mechanisms such as iron-chelating and reduction when interacting with lipoygenases (133). Since LOXs mainly function through hydrogen abstraction of the substrate with the help of the iron in its active site, inhibitors targeting this reaction may operate through a variety of mechanisms, such as reduction, chelation, competition and/or allosteric interactions (136). According to Leopoldini *et al.*'s study (2004), LUT is one of the most stable flavonoids and due to its planar structure, it

requires the least amount of energy for electron transfer and hydrogen exchange (137). Rai *et al.* (2010) also noted that their very effective synthetic inhibitor of 15-LOX-1, called compound 1 (ML351), was a non-reducing inhibitor (136). Meanwhile, Leopoldini *et al.* (2004) also demonstrated that LUT is structurally more likely to be a proton donor (a non-reducing agent) than a reducing agent (137). In general, although the specific mechanism has yet to be described, it appears that by competing with LA, LUT blocks the H⁺ abstraction from occurring between LA and 15-LOX to form HODEs (138).

LUT did not alter the production of 15-LOX-1 in U87-MG or in T98-G (Figure R9). After observing that 13-HODE and 9-HODE treatments increased U87-MG cell counts (Figures R5 and R6), concomitant treatments of LUT plus 13-HODE or 9-HODE were performed (Figure R12). The goal was to see if LUT would interfere with the 15-LOX products' influence on cell count. Cell counts increased with the 13-HODE treatments at 72hr, independent of LUT's presence, compared with their respective controls. One possible explanation for this result is that the non-cytotoxic concentration of LUT used likely influences U87-MG and T98-G cell migration and invasive potential, as was seen in the present study (Figures R14 and R20) and also described by Cheng *et al.* (2013) (139). Moreover, Wang *et al.* (2014) demonstrated that LUT is a natural agonist of PPAR γ (140). As was previously mentioned, 13-HODE can interact with PPAR β/δ via MAPK/ERK to downregulate PPAR γ in prostate cancer cells (62). Therefore, if these GBM cells follow the patterns observed in the model of prostate cancer, the reduced PPAR γ expression caused by exogenous 13-HODE (which would limit cell death) may also have limited LUT's influence on PPAR γ -related downstream activities.

The other LOX inhibitor used in this study was Nordihydroguaiaretic acid (NDGA). NDGA, found in the creosote bush plant, is a nonselective redox-active compound and a pan-lipoxygenase inhibitor that scavenges reactive oxygen species (ROS), which are often products of LOXs, and is thus both an antioxidant and a LOX inhibitor (141). This inhibitor was used as another control to identify interference of other LOXs in these assays, and to identify the more specific activity of Luteolin on 15-LOX activity. As was observed in Figures R8, R9 and R10, its influence at the concentrations used was not overwhelming. Only in treatments with serum-free medium were the effects of NDGA extremely cytotoxic for both cell lines (Figures R10; R11). These

cytotoxic effects of NDGA have also been seen in T98-G and A172 cell lines, and the concentrations from this 1989 study were used in the present study (142).

The sensitivity of cells in serum-free medium toward LUT and NDGA may be due to the influence of the “albumin effect”. The “albumin effect”, as described by Rowland *et al.* (2008), occurs when albumin sequesters free long chain fatty acids and, thus, reduces their bioavailability (143). With the absence of albumin in the culture medium, the competition that LUT/ NDGA have for 15-LOX’s active site is reduced and inactivation is more effective. Moreover, as with any flavonoid, LUT can potentially influence other metabolic pathways including that of 15-LOX and LA/AA (140). This is possibly the reason why the treatments applied in serum-free medium were more cytotoxic than those in medium with serum (Figure R10 and R11). However, this does not exclude the possibility that the changes seen in the cells might be due to the lack of growth and survival factor normally found in the serum.

5.4 15-LOX and Migration

Some authors have debated concerning the validity of the “go-or-grow” hypothesis in glioma cells (144). This hypothesis suggests that cell migration and cell division are spatiotemporally distinct (145). Since T98-G cell growth was not as affected by exogenous HODEs as U87-MG was, it is possible that HODE treatments might have been influencing other pathways in T98-G such as those related to migration, as the go-or-grow hypothesis would suggest. A simple wound healing assay was performed over a 12-hour period with T98-G cells submitted to exogenous treatments of 13-HODE [5 μ M], 9-HODE [5 μ M], 15-HETE [1 μ M], LUT [15 μ M] and NDGA [40 μ M]. The images were then analyzed with ImageJ software and GraphPad Prism software to determine the difference of migration that occurred over the 12-hour period between the treated cells and control cells.

13-HODE surprisingly decreased T98-G cell migration, while 9-HODE and 15-HETE increased migration by 20% and 29%, respectively, yet were not statistically significant (Figure R11). There are a couple of possible explanations for these results. Concerning 13-HODE, it is possible that since it is capable of reducing tumor cell adhesion to endothelial cells (146), the mechanisms involved might be affecting T98-G cell migration. Another possibility is related to the fact that 13-HODE can bind to PPAR γ , which has been known to suppress glioma cell migration when activated (147).

Despite the lack of a statistically significant increase in migration caused by either 9-HODE or 15-HETE, this does not negate the possibility of an indirect influence on migration at a longer time interval (>12 hours). For example, endogenous/exogenous 15-HETE was identified as an angiogenic factor for ischemic nervous tissue (148). Furthermore, 9-HODE can stimulate type IV collagen production, as was observed in mesangial cells (72). Type IV collagen is an important component of brain ECM, and is expressed in glioblastoma tumor vasculature (149). It is also known that GBM cells can produce their own type IV collagen as ECM scaffolding for activities like migration/adhesion (150).

Finally, the present study also observed significant reductions in cell migration caused by LUT and NDGA treatments (62% and 29%, respectively) (Figure R11), as was similarly documented by other authors (134,151,152). Wang *et al.* (2017) demonstrated that through the p-IGF-1R/PI3K/AKT/mTOR signaling pathway, LUT can inhibit U251-MG and U87-MG cell migration (148).

5.5 Invasive Potential

Invasive potential, as defined in this study, is the production of matrix metalloproteases which contribute to making invasive behavior possible. According to the data found in the present study, MMP-2 and MMP-14 are clearly present within U87-MG and T98-G cells (Figures R16; R17; R20) and that MMP-2 is released into the ECM as was determined by zymography using the cells' serum-free medium (Figure R18). This data coincides with the findings of other authors as well (153)(154)(155). However, there is a controversy in the literature concerning MMP-9 expression in GBM cell lines. Hagemann *et al.* (2012), in their review of MMP expression in GBM, created a table summarizing the authors who reported the presence or absence of MMP-9 in GBM cell lines (155). According to the data presented in Figures R16 and R18, MMP-9 is not endogenously produced by either U87-MG or T98-G GBM cell lines. All zymograms were run with HT1080 samples as a positive control for MMP expression (83).

Exogenous treatments using 15-LOX-1 products, 9-HODE and 13-HODE, caused significant increases in MMP2 mRNA expression according to qRT-PCR data (Figure R19). Next, the influence of 15-LOX inhibition using LUT or NDGA on the invasive potential of GBM cells was examined. LUT did not influence MMP-2 or MMP-14 production or activity in U87-MG cells (Figures R20 and R21). The only other study to date examining the influence of LUT on the

invasive potential of the GBM cells lines used in this study, by Wang *et al.* (2017), demonstrated that the suppression of MMP-2 expression in U87-MG started from 10 μ M of LUT after 24 hours (135). However, Wang *et al.*'s study treated the cells with LUT for 24 hours in serum-free medium before western blot analysis. However, the present study, only examined MMP production in serum-free medium to measure the extracellular output from the cells. Intracellular MMP production remained under normal cultivation conditions (10% FBS) in order to compare the cellular responses to LUT more accurately.

Interestingly, T98-G cells responded differently from U87-MG. LUT caused a significant decrease in ProMMP-2 and MMP-2 production but did not limit MMP-2's activity (Figure R20). According to Jiang *et al.* (2013), LUT can inhibit MMP-2 production in MCF7 breast cancer cells starting at 40 μ M LUT (156). The influence of LUT on MMP production in T98-G has not been reported previously.

Concerning NDGA, the strong response of the cells, based on their morphology, to this LOX inhibitor in serum-free medium (Figures R10 and R11) appeared to have placed the cells into a possible state of quiescence/senescence; although this was not experimentally verified. Thus, extracellular MMP-2 was completely absent in both cell lines (Figure R21). Furthermore, NDGA had no effect on MMP-2 and MMP-14 production. However, when the T98-G cells that were treated for 72 hours (in 10% FBS) were collected and intracellular MMPs were extracted, western blotting identified a significant increase in ProMMP-2 and a significant decrease in ProMMP-14 (Figure R20). The increase in ProMMP-2 might be a response to the stressful environment. There are no reports in the literature to date describing NDGA's relationship with GBM cell invasion.

5.6 The Influence of COX on LA metabolism and Invasive Potential

Linoleic acid conversion by cyclooxygenase into 13-HpODE is possible but is much less common due to the efficiency and affinities of COX to AA and eicosapentaenoic acid (EPA) (157). Cells would require a supraphysiological amount of LA substrate (ex. 100 μ M LA (158)) to overcome COX-2's affinity for AA and EPA. Hoping to observe the effects of COX inhibition on MMP expression and activity, U87-MG and T98-G cells were inhibited with SC-560 (COX-1) and NS-398 (COX-2) and stimulated with the major COX-2 product, PGE₂ (Figure S9-S11).

After 24 hours of treatment with NS398, qRT-PCR demonstrated an increase in MMP2 mRNA and western blots also showed a significant increase in ProMMP-2 in U87-MG (Figures R25 and R26). COX-2 has been reported upregulating synthesis of MMP2 and its inhibition by NS398 also reduces MMP-2 activity (86). Therefore, the increase of the latent form of MMP-2 due to NS398 is reasonable.

COX-1 inhibition significantly decreased MMP-2 in U87-MG as demonstrated by both the western blots and the zymograms (Figure R26 and R28). Since COX-1 is ubiquitously expressed in many tissue types, and functions as a homeostatic catalyst of lipid formation for cell-cell signalling and angiogenesis, it is reasonable to expect a decrease in both active and latent MMP-2 expression (159). The PGE₂ treatment increased the release of MMP-2 into the extracellular environment of T98-G cells (Figure R28). It has been reported that PGE₂ can increase glioma cell migration as well as upregulate MMP-2 expression in endometriosis (41,86).

6 CONCLUSION

In conclusion, the 15-LOX-1/13-HODE pathway is present and active in GBM cell lines. Although 15-LOX-1/13-HODE may not call as much attention as other pathways like COX/PGE₂, the results of this study confirm that 15-LOX-1 products, 13-HODE and 9-HODE, do increase GBM cell growth, as well as influence GBM cell migration and invasive potential. Moreover, this study confirmed the presence of MMP-2 and absence of MMP-9 in the GBM cell lines examined, which is a controversy found in the literature. 15-LOX and its LA-derived metabolites exercise a certain pro-tumorigenic influence on the GBM cells examined *in vitro*. Further studies will clarify if these relationships positively correlate with malignancy or if this pathway could influence future therapies.

REFERENCES*

1. Cooper GM. The Development and Causes of Cancer. In: *The Cell: A Molecular Approach* [Internet]. 2nd ed. Sinauer Associates; 2000 [cited 2019 May 21]. Available from: <https://www.ncbi.nlm.nih.gov/books/NBK9963/>
2. Sudhakar a. History of Cancer, Ancient and Modern Treatment Methods Akulapalli. *J Cancer Sci Ther* [Internet]. 2010;1(2):1–4. Available from: <http://www.ncbi.nlm.nih.gov/pmc/articles/PMC2927383/pdf/nihms226784.pdf>
3. International Agency For Research on Cancer. *Cancer Tomorrow* [Internet]. [cited 2019 Mar 1]. Available from: http://gco.iarc.fr/tomorrow/graphic-bar?type=0&population=900&mode=population&sex=0&cancer=39&age_group=value&apc_male=0&apc_female=0
4. Alcantara Llaguno SR, Parada LF. Cell of origin of glioma: biological and clinical implications. *Br J Cancer* [Internet]. 2016 Dec 6 [cited 2019 Mar 1];115(12):1445–50. Available from: <http://www.ncbi.nlm.nih.gov/pubmed/27832665>
5. Ohgaki H, Kleihues P. The definition of primary and secondary glioblastoma. *Clin Cancer Res* [Internet]. 2013 Feb 15 [cited 2019 Mar 1];19(4):764–72. Available from: <http://www.ncbi.nlm.nih.gov/pubmed/23209033>
6. Louis DN, Perry A, Reifenberger G, von Deimling A, Figarella-Branger D, Cavenee WK, et al. The 2016 World Health Organization Classification of Tumors of the Central Nervous System: a summary. *Acta Neuropathol*. 2016;131(6):803–20.
7. Molenaar RJ, Radivoyevitch T, Maciejewski JP, van Noorden CJF, Bleeker FE. The driver and passenger effects of isocitrate dehydrogenase 1 and 2 mutations in oncogenesis and survival prolongation. *Biochim Biophys Acta - Rev Cancer* [Internet]. 2014 Dec 1 [cited 2019 Jun 5];1846(2):326–41. Available from: <https://www.sciencedirect.com/science/article/pii/S0304419X14000493?via%3Dihub>
8. Watanabe T, Nobusawa S, Kleihues P, Ohgaki H. IDH1 mutations are early events in the development of astrocytomas and oligodendrogliomas. *Am J Pathol* [Internet]. 2009 Apr [cited 2019 Mar 1];174(4):1149–53. Available from: <http://www.ncbi.nlm.nih.gov/pubmed/19246647>
9. Martinez-Lage M, Sahm F. Practical Implications of the Updated WHO Classification of Brain Tumors The New Classification and Its Implementation. *Semin Neurol*. 2018;38:11–8.
10. Ostrom QT, Gittleman H, Farah P, Ondracek A, Chen Y, Wolinsky Y, et al. CBTRUS statistical report: Primary brain and central nervous system tumors diagnosed in the United States in 2006–2010. *Neuro Oncol* [Internet]. 2013 Nov [cited 2019 Mar 1];15 Suppl 2(Suppl 2):ii1-56. Available from: <http://www.ncbi.nlm.nih.gov/pubmed/24137015>

*In agreement with: International Committee of Medical Journal Editors. [Internet]. Uniform requirements for manuscripts submitted to Biomedical Journal: sample references. [updated 2011 Jul 15]. Available from: <http://www.icmje.org>

11. Matias D, Balça-Silva J, da Graça GC, Wanjiru CM, Macharia LW, Nascimento CP, et al. Microglia/Astrocytes–Glioblastoma Crosstalk: Crucial Molecular Mechanisms and Microenvironmental Factors. *Front Cell Neurosci* [Internet]. 2018;12(August):1–22.
12. Das UN. Essential fatty acids and their metabolites as modulators of stem cell biology with reference to inflammation, cancer, and metastasis. *Cancer Metastasis Rev.* 2011;30(3–4):311–24.
13. Menter DG, Dubois RN. Prostaglandins in cancer cell adhesion, migration, and invasion. *Int J Cell Biol.* 2012;2012.
14. Das UN, Madhavi N. Effect of polyunsaturated fatty acids on drug-sensitive and resistant tumor cells in vitro. *Lipids Health Dis* [Internet]. 2011;10(1):159.
15. Pidgeon GP, Lysaght J, Krishnamoorthy S, Reynolds J V., O’Byrne K, Nie D, et al. Lipoxygenase metabolism: Roles in tumor progression and survival. *Cancer Metastasis Rev.* 2007;26(3–4):503–24.
16. Theeler BJ, Yung WKA, Fuller GN, De Groot JF. Moving toward molecular classification of diffuse gliomas in adults. *Neurology.* 2012;79(18):1917–26.
17. Gentric G, Mieulet V, Mehta-Grigoriou F. Heterogeneity in Cancer Metabolism: New Concepts in an Old Field. *Antioxid Redox Signal* [Internet]. 2017;26(9):462–85.
18. Hanahan D, Weinberg RA. Hallmarks of cancer: The next generation. *Cell* [Internet]. 2011;144(5):646–74. Available from: <http://dx.doi.org/10.1016/j.cell.2011.02.013>
19. Fouad YA, Aanei C. Revisiting the Hallmarks of Cancer. *Am J Cancer Res.* 2017;7(5):1016–36.
20. Pavlova NN, Thompson CB. THE EMERGING HALLMARKS OF CANCER METABOLISM Natalya. *Cell Metab.* 2016;23(1):27–47.
21. Kamphorst JJ, Cross JR, Fan J, de Stanchina E, Mathew R, White EP, et al. Hypoxic and Ras-transformed cells support growth by scavenging unsaturated fatty acids from lysophospholipids. *Proc Natl Acad Sci U S A.* 2013;110(22):8882–7.
22. Röhrig F, Schulze A. The multifaceted roles of fatty acid synthesis in cancer. *Nat Rev Cancer* [Internet]. 2016;16(11):732–49. Available from: <http://dx.doi.org/10.1038/nrc.2016.89>
23. Fillmore N, Mori J, Lopaschuk GD. Mitochondrial fatty acid oxidation alterations in heart failure, ischaemic heart disease and diabetic cardiomyopathy. *Br J Pharmacol* [Internet]. 2014 Apr [cited 2019 Mar 2];171(8):2080–90. Available from: <http://www.ncbi.nlm.nih.gov/pubmed/24147975>
24. Panov A, Orynbayeva Z, Vavilin V, Lyakhovich V. Fatty acids in energy metabolism of the central nervous system. *Biomed Res Int* [Internet]. 2014 [cited 2019 May 14];2014:472459. Available from: <http://www.ncbi.nlm.nih.gov/pubmed/24883315>
25. Tyurina YY, Poloyac SM, Tyurin VA, Kapralov AA, Jiang J, Anthonymuthu TS, et al. A mitochondrial pathway for biosynthesis of lipid mediators. *Nat Chem* [Internet].

- 2014;6(6):542–52. Available from: <http://www.nature.com/doi/10.1038/nchem.1924>
26. O'Banion MK. Prostaglandin E2 synthases in neurologic homeostasis and disease. *Prostaglandins Other Lipid Mediat* [Internet]. 2010;91(3–4):113–7. Available from: <http://dx.doi.org/10.1016/j.prostaglandins.2009.04.008>
 27. Harayama T, Riezman H. Understanding the diversity of membrane lipid composition. *Nat Rev Mol Cell Biol* [Internet]. 2018;19(5):281–96. Available from: <http://dx.doi.org/10.1038/nrm.2017.138>
 28. Yamashita A, Hayashi Y, Nemoto-Sasaki Y, Ito M, Oka S, Tanikawa T, et al. Acyltransferases and transacylases that determine the fatty acid composition of glycerolipids and the metabolism of bioactive lipid mediators in mammalian cells and model organisms. *Prog Lipid Res*. 2014;53(1):18–81.
 29. Bentsen H. Dietary polyunsaturated fatty acids, brain function and mental health. *Microb Ecol Health Dis* [Internet]. 2017 [cited 2019 Mar 1];28. Available from: <http://dx.doi.org/10.1080/16512235.2017.1281916>
 30. Park JB, Lee CS, Jang JH, Ghim J, Kim YJ, You S, et al. Phospholipase signalling networks in cancer. *Nat Rev Cancer* [Internet]. 2012;12(11):782–92. Available from: <http://dx.doi.org/10.1038/nrc3379>
 31. Yang L, Zhang H. Expression of Cytosolic Phospholipase A2 Alpha in Glioblastoma Is Associated With Resistance to Chemotherapy. *Am J Med Sci*. 2018;356(4):391–8.
 32. Wiktorowska-Owczarek A, Berezińska M, Nowak J. PUFAs: Structures, Metabolism and Functions. *Adv Clin Exp Med* [Internet]. 2015 [cited 2019 Mar 1];24(6):931–41. Available from: <http://www.ncbi.nlm.nih.gov/pubmed/26771963>
 33. Wang D, Dubois RN. Eicosanoids and cancer. 2011;10(3):181–93.
 34. Violette Said H, Ebtisam AAH. Synopsis of arachidonic acid metabolism: A review. *J Adv Res* [Internet]. 2018;11:23–32. Available from: <https://doi.org/10.1016/j.jare.2018.03.005>
 35. Warner TD, Mitchell JA. Cyclooxygenase-3 (COX-3): Filling in the gaps toward a COX continuum? *Proc Natl Acad Sci* [Internet]. 2002 Oct 15 [cited 2019 Mar 1];99(21):13371–3. Available from: <http://www.ncbi.nlm.nih.gov/pubmed/12374850>
 36. Sang N, Chen C. Lipid Signaling and Synaptic Plasticity. *Neurosci* [Internet]. 2006;12(5):425–34. Available from:
 37. Kostenis E, Ulven T. Emerging roles of DP and CRTH2 in allergic inflammation. *Trends Mol Med*. 2006;12(4):148–58.
 38. Sulciner ML, Gartung A, Gilligan MM, Serhan CN, Panigrahy D. Targeting lipid mediators in cancer biology. *Cancer Metastasis Rev*. 2018;37(2–3):557–72.
 39. Schneider C, Pratt DA, Porter NA, Brash AR. Control of oxygenation in lipoxygenase and cyclooxygenase catalysis. 2007;14(5):473–88.
 40. Simmons DL. Cyclooxygenase Isozymes: The Biology of Prostaglandin Synthesis and Inhibition. *Pharmacol Rev* [Internet]. 2004;56(3):387–437.

41. Gomes RN, Colquhoun A. E series prostaglandins alter the proliferative, apoptotic and migratory properties of T98G human glioma cells in vitro. *Lipids Health Dis* [Internet]. 2012;11(1):171.
42. Jiang J, Qiu J, Li Q, Shi Z. Prostaglandin E2 Signaling: Alternative Target for Glioblastoma? *Trends in cancer* [Internet]. 2017 [cited 2019 May 16];3(2):75–8. Available from: <http://www.ncbi.nlm.nih.gov/pubmed/28718447>
43. Manikandan P, Nagini S. Cytochrome P450 Structure, Function and Clinical Significance: A Review. *Arch Biochem Biophys* [Internet]. 2018;19(1):38–54.
44. Klingenberg M. Pigments of rat liver microsomes. *Arch Biochem Biophys*. 1958;75(2):376–86.
45. Omura T. Forty years of cytochrome P450. *Biochem Biophys Res Commun*. 1999;266(3):690–8.
46. Spector AA. Arachidonic acid cytochrome P450 epoxygenase pathway. *J Lipid Res* [Internet]. 2009;50(Supplement):S52–6. Available from: <http://www.jlr.org/lookup/doi/10.1194/jlr.R800038-JLR200>
47. Panigrahy D, Kaipainen A, Greene ER, Huang S. Cytochrome P450-derived eicosanoids: the neglected pathway in cancer. *Cancer Metastasis Rev* [Internet]. 2010 Dec [cited 2019 May 16];29(4):723–35. Available from: <http://www.ncbi.nlm.nih.gov/pubmed/20941528>
48. Guengerich FP, Munro AW. Unusual cytochrome P450 enzymes and reactions. *J Biol Chem*. 2013;288(24):17065–73.
49. Mitchell JA, Ahmetaj-Shala B, Kirkby NS, Wright WR, Mackenzie LS, Reed DM, et al. Role of prostacyclin in pulmonary hypertension. *Glob Cardiol Sci Pract* [Internet]. 2014 [cited 2019 Mar 1];2014(4):382–93. Available from: <http://www.ncbi.nlm.nih.gov/pubmed/25780793>
50. Brash AR. Lipoxygenases: Occurrence, Functions , Catalysis , and Acquisition of Substrate *. *J Bio Chem*. 1999;274(34):23679–83.
51. Haeggström JZ, Funk CD. Lipoxygenase and Leukotriene Pathways: Biochemistry, Biology, and Roles in Disease. *Chem Rev* [Internet]. 2011 Oct 12 [cited 2019 Mar 1];111(10):5866–98. Available from: <https://pubs.acs.org/doi/10.1021/cr200246d>
52. Funk CD. The molecular biology of mammalian lipoxygenases and the quest for eicosanoid functions using lipoxygenase-deficient mice. *Biochim Biophys Acta - Lipids Lipid Metab*. 1996;1304(1):65–84.
53. Savari S, Vinnakota K, Zhang Y, Sjölander A. Cysteinyl leukotrienes and their receptors: bridging inflammation and colorectal cancer. *World J Gastroenterol* [Internet]. 2014 Jan 28 [cited 2019 Mar 1];20(4):968–77. Available from: <http://www.ncbi.nlm.nih.gov/pubmed/24574769>
54. Mashima R, Okuyama T. The role of lipoxygenases in pathophysiology; new insights and future perspectives. *Redox Biol* [Internet]. 2015 Dec [cited 2019 Mar 1];6:297–310. Available from: <http://www.ncbi.nlm.nih.gov/pubmed/26298204>

55. Pergola C, Gerstmeier J, Mönch B, Çalışkan B, Luderer S, Weinigel C, et al. The novel benzimidazole derivative BRP-7 inhibits leukotriene biosynthesis in vitro and in vivo by targeting 5-lipoxygenase-activating protein (FLAP). *Br J Pharmacol* [Internet]. 2014 Jun [cited 2019 Mar 1];171(12):3051–64. Available from: <http://www.ncbi.nlm.nih.gov/pubmed/24641614>
56. Dobrian AD, Lieb DC, Cole BK, Taylor-Fishwick DA, Chakrabarti SK, Nadler JL. Functional and pathological roles of the 12- and 15-lipoxygenases. *Prog Lipid Res* [Internet]. 2011 Jan [cited 2019 Mar 1];50(1):115–31. Available from: <http://www.ncbi.nlm.nih.gov/pubmed/20970452>
57. Kutzner L, Goloshchapova K, Heydeck D, Stehling S, Kuhn H, Schebb NH. Mammalian ALOX15 orthologs exhibit pronounced dual positional specificity with docosahexaenoic acid. *Biochim Biophys Acta - Mol Cell Biol Lipids* [Internet]. 2017;1862(7):666–75. Available from: <http://dx.doi.org/10.1016/j.bbalip.2017.04.001>
58. Il Lee S, Zuo X, Shureiqi I. 15-Lipoxygenase-1 as a tumor suppressor gene in colon cancer: is the verdict in? *Cancer Metastasis Rev* [Internet]. 2011 Dec [cited 2019 Mar 1];30(3–4):481–91. Available from: <http://www.ncbi.nlm.nih.gov/pubmed/22037943>
59. Wu Y, Fang B, Yang XQ, Wang L, Chen D, Krasnykh V, et al. Therapeutic molecular targeting of 15-lipoxygenase-1 in colon cancer. *Mol Ther*. 2008;16(5):886–92.
60. Kelavkar UP, Nixon JB, Cohen C, Dillehay D, Eling TE, Badr KF. Overexpression of 15-lipoxygenase-1 in PC-3 human prostate cancer cells increases tumorigenesis. *Carcinogenesis*. 2001;22(11):1765–73.
61. Xu XC, Shappell SB, Liang Z, Song S, Menter D, Subbarayan V, et al. Reduced 15S-Lipoxygenase-2 Expression in Esophageal Cancer Specimens and Cells and Upregulation In Vitro by the Cyclooxygenase-2 Inhibitor, NS398. *Neoplasia*. 2003;5(2):121–7.
62. Hsi LC, Wilson LC, Eling TE. Opposing effects of 15-lipoxygenase-1 and -2 metabolites on MAPK signaling in prostate: Alteration in peroxisome proliferator-activated receptor ?? *J Biol Chem*. 2002;277(43):40549–56.
63. Jiang WG, Watkins G, Douglas-Jones A, Mansel RE. Reduction of isoforms of 15-lipoxygenase (15-LOX)-1 and 15-LOX-2 in human breast cancer. *Prostaglandins Leukot Essent Fat Acids*. 2006;74(4):235–45.
64. Tang S, Bhatia B, Maldonado CJ, Yang P, Newman RA, Liu J, et al. Evidence that arachidonate 15-lipoxygenase 2 is a negative cell cycle regulator in normal prostate epithelial cells. *J Biol Chem*. 2002;277(18):16189–201.
65. Villacorta L, Schopfer FJ, Zhang J, Freeman BA, Chen YE. PPARgamma and its ligands: therapeutic implications in cardiovascular disease. *Clin Sci (Lond)* [Internet]. 2009 Feb [cited 2019 Mar 2];116(3):205–18. Available from: <http://www.ncbi.nlm.nih.gov/pubmed/19118492>
66. Naruhn S, Meissner W, Adhikary T, Kaddatz K, Klein T, Watzer B, et al. 15-hydroxyeicosatetraenoic acid is a preferential peroxisome proliferator-activated receptor beta/delta agonist. *Mol Pharmacol* [Internet]. 2010 Feb 1 [cited 2019 Mar 2];77(2):171–84.

Available from: <http://www.ncbi.nlm.nih.gov/pubmed/19903832>

67. Vijil C, Hermansson C, Jeppsson A, Bergström G, Hultén LM. Arachidonate 15-lipoxygenase enzyme products increase platelet aggregation and thrombin generation. *PLoS One* [Internet]. 2014 [cited 2019 Mar 1];9(2):e88546. Available from: <http://www.ncbi.nlm.nih.gov/pubmed/24533104>
68. Yuan H, Li M-Y, Ma LT, Hsin MKY, Mok TSK, Underwood MJ, et al. 15-Lipoxygenases and its metabolites 15(S)-HETE and 13(S)-HODE in the development of non-small cell lung cancer. *Thorax* [Internet]. 2010;65(4):321–6.
69. Çimen I, Tunçay S, Banerjee S. 15-Lipoxygenase-1 expression suppresses the invasive properties of colorectal carcinoma cell lines HCT-116 and HT-29. *Cancer Sci*. 2009;100(12):2283–91.
70. Shureiqi I, Jiang W, Zuo X, Wu Y, Stimmel JB, Leesnitzer LM, et al. The 15-lipoxygenase-1 product 13-S-hydroxyoctadecadienoic acid down-regulates PPAR-delta to induce apoptosis in colorectal cancer cells. *Proc Natl Acad Sci U S A* [Internet]. 2003;100(17):9968–73. Available from: <http://www.pnas.org/content/100/17/9968.full>
71. Hattori T, Obinata H, Ogawa A, Kishi M, Tatei K, Ishikawa O, et al. G2A plays proinflammatory roles in human keratinocytes under oxidative stress as a receptor for 9-hydroxyoctadecadienoic acid. *J Invest Dermatol*. 2008;128(5):1123–33.
72. Negishi M, Shimizu H, Okada S, Kuwabara A, Okajima F, Mori M. 9HODE stimulates cell proliferation and extracellular matrix synthesis in human mesangial cells via PPARgamma. *Exp Biol Med (Maywood)* [Internet]. 2004 Nov [cited 2019 Mar 2];229(10):1053–60. Available from: <http://www.ncbi.nlm.nih.gov/pubmed/15522842>
73. Obinata H, Hattori T, Nakane S, Tatei K, Izumi T. Identification of 9-hydroxyoctadecadienoic acid and other oxidized free fatty acids as ligands of the G protein-coupled receptor G2A. *J Biol Chem* [Internet]. 2005 Dec 9 [cited 2019 Mar 2];280(49):40676–83. Available from: <http://www.ncbi.nlm.nih.gov/pubmed/16236715>
74. Guo L, Zhang X, Zhou D, Okunade AL, Su X. Stereospecificity of fatty acid 2-hydroxylase and differential functions of 2-hydroxy fatty acid enantiomers. *J Lipid Res* [Internet]. 2012 Jul [cited 2019 May 19];53(7):1327–35. Available from: <http://www.ncbi.nlm.nih.gov/pubmed/22517924>
75. Jackson C, Ruzevick J, Phallen J, Belcaid Z, Lim M. Challenges in immunotherapy presented by the glioblastoma multiforme microenvironment. *Clin Dev Immunol*. 2011.
76. Boucher BJ. Matrix metalloproteinase protein inhibitors: highlighting a new beginning for metalloproteinases in medicine. *Met Med*. 2016;3:75–9.
77. Schiera G, Di Liegro CM, Di Liegro I. Molecular Determinants of Malignant Brain Cancers: From Intracellular Alterations to Invasion Mediated by Extracellular Vesicles. *Int J Mol Sci* [Internet]. 2017 Dec 20 [cited 2019 Mar 2];18(12). Available from: <http://www.ncbi.nlm.nih.gov/pubmed/29261132>
78. Vempati P, Karagiannis ED, Popel AS. A biochemical model of matrix metalloproteinase 9 activation and inhibition. *J Biol Chem*. 2007;282(52):37585–96.

79. Itoh Y, Binner S, Nagase H. Steps involved in activation of the complex of pro-matrix metalloproteinase 2 (progelatinase A) and tissue inhibitor of metalloproteinases (TIMP)-2 by 4-aminophenylmercuric acetate [Internet]. Vol. 308, *Biochem. J.* 1995 [cited 2019 Mar 2]. Available from: <https://www.ncbi.nlm.nih.gov/pmc/articles/PMC1136975/pdf/biochemj00062-0274.pdf>
80. Koo B-H, Kim YH, Han JH, Kim D-S. Dimerization of matrix metalloproteinase-2 (MMP-2): functional implication in MMP-2 activation. *J Biol Chem* [Internet]. 2012 Jun 29 [cited 2019 Mar 2];287(27):22643–53. Available from: <http://www.ncbi.nlm.nih.gov/pubmed/22577146>
81. Parks WC, Wilson CL, Lopez-Boado YS. Matrix metalloproteinases as modulators of inflammation. *Nat Rev Immunol.* 2004;4:617–29.
82. Itoh Y. Membrane-type matrix metalloproteinases: Their functions and regulations. *Matrix Biol.* 2015;44–46:207–23.
83. Toth M, Fridman R. Assessment of Gelatinases (MMP-2 and MMP-9 by Gelatin Zymography. *Methods Mol Med* [Internet]. 2001 [cited 2019 Mar 2];57:163–74. Available from: <http://www.ncbi.nlm.nih.gov/pubmed/21340898>
84. Daniele A, Abbate I, Oakley C, Casamassima P, Savino E, Casamassima A, et al. Clinical and prognostic role of matrix metalloproteinase-2, -9 and their inhibitors in breast cancer and liver diseases: A review. *Int J Biochem Cell Biol* [Internet]. 2016;77:91–101.
85. Lee J, Banu SK, Subbarao T, Starzinski-Powitz A, Arosh JA. Selective inhibition of prostaglandin E2 receptors EP2 and EP4 inhibits invasion of human immortalized endometriotic epithelial and stromal cells through suppression of metalloproteinases. *Mol Cell Endocrinol* [Internet]. 2011 Jan 30 [cited 2019 Mar 2];332(1–2):306–13.
86. Jana S, Chatterjee K, Ray AK, DasMahapatra P, Swarnakar S. Regulation of Matrix Metalloproteinase-2 Activity by COX-2-PGE2-pAKT Axis Promotes Angiogenesis in Endometriosis. *PLoS One* [Internet]. 2016 [cited 2019 Mar 2];11(10):e0163540. Available from: <http://www.ncbi.nlm.nih.gov/pubmed/27695098>
87. Wu MY, Lin TH, Chiu YC, Liou HC, Yang R Sen, Fu WM. Involvement of 15-lipoxygenase in the inflammatory arthritis. *J Cell Biochem.* 2012;113(7):2279–89.
88. Liu Y, Zhang H, Yan L, Du W, Zhang M, Chen H, et al. MMP-2 and MMP-9 contribute to the angiogenic effect produced by hypoxia/15-HETE in pulmonary endothelial cells. *J Mol Cell Cardiol* [Internet]. 2018 Aug [cited 2019 Mar 2];121:36–50. Available from: <http://www.ncbi.nlm.nih.gov/pubmed/29913136>
89. Chabane N, Zayed N, Benderdour M, Martel-Pelletier J, Pelletier J-P, Duval N, et al. Human articular chondrocytes express 15-lipoxygenase-1 and -2: potential role in osteoarthritis. *Arthritis Res Ther* [Internet]. 2009 [cited 2019 Mar 2];11(2):R44. Available from: <http://www.ncbi.nlm.nih.gov/pubmed/19296842>
90. Ferreira MT, Gomes RN, Panagopoulos AT, Gonçalves de Almeida F, Veiga JCE, Colquhoun A. Opposing roles of PGD 2 in GBM. *Prostaglandins Other Lipid Mediat.* 2017;(In Press).

91. Marshall OJ. PerlPrimer: Cross-platform, graphical primer design for standard, bisulphite and real-time PCR. *Bioinformatics*. 2004;20(15):2471–2.
92. Auld DS. [14] Removal and replacement of metal ions in metallopeptidases. *Methods Enzymol* [Internet]. 1995 Jan 1 [cited 2019 May 30];248:228–42.
93. Livak KJ, Schmittgen TD. Analysis of Relative Gene Expression Data Using Real-Time Quantitative PCR and the $2^{-\Delta\Delta CT}$ Method. *Methods* [Internet]. 2001;25(4):402–8.
94. Reddy KK, Vidya Rajan VK, Gupta A, Aparoy P, Reddanna P. Exploration of binding site pattern in arachidonic acid metabolizing enzymes, Cyclooxygenases and Lipoxygenases. *BMC Res Notes* [Internet]. 2015;8(1):152.
95. SHUSTER CW. Effects of oxidized fatty acids on ascites tumor metabolism. *Proc Soc Exp Biol Med* [Internet]. 1955 Nov [cited 2019 Mar 5];90(2):423–6. Available from: <http://www.ncbi.nlm.nih.gov/pubmed/13273469>
96. Iuchi K, Ema M, Suzuki M, Yokoyama C, Hisatomi H. Oxidized unsaturated fatty acids induce apoptotic cell death in cultured cells. *Mol Med Rep* [Internet]. 2019 Feb 5 [cited 2019 Mar 5];19(4):2767–73.
97. Vangaveti VN, Shashidhar VM, Rush C, Malabu UH, Rasalam RR, Collier F, et al. Hydroxyoctadecadienoic acids regulate apoptosis in human THP-1 cells in a PPAR γ -dependent manner. *Lipids*. 2014;49(12):1181–92.
98. Uhlen M, Fagerberg L, Hallstrom BM, Lindskog C, Oksvold P, Mardinoglu A, et al. Tissue-based map of the human proteome. *Science* (80-) [Internet]. 2015;347(6220):1260419–1260419.
99. McLendon R, Friedman A, Bigner D, Van Meir EG, Brat DJ, M. Mastrogiannakis G, et al. Comprehensive genomic characterization defines human glioblastoma genes and core pathways. *Nature* [Internet]. 2008 Oct 23 [cited 2019 Mar 7];455(7216):1061–8. Available from: <http://www.nature.com/doi/10.1038/nature07385>
100. Marion-Letellier R, Savoye G, Ghosh S. Fatty acids, eicosanoids and PPAR gamma. *Eur J Pharmacol* [Internet]. 2016 Aug 15 [cited 2019 Mar 5];785:44–9. Available from: <https://www.sciencedirect.com/science/article/pii/S0014299915303423?via%3Dihub>
101. Heneka MT, Landreth GE. PPARs in the brain. *Biochim Biophys Acta - Mol Cell Biol Lipids* [Internet]. 2007 Aug 1 [cited 2019 Mar 5];1771(8):1031–45. Available from:
102. Youssef J, Badr M. Peroxisome proliferator-activated receptors and cancer: challenges and opportunities. *Br J Pharmacol* [Internet]. 2011 Sep [cited 2019 Mar 5];164(1):68–82. Available from: <http://www.ncbi.nlm.nih.gov/pubmed/21449912>
103. Cabral M, Martín-Venegas R, Moreno JJ. Differential cell growth/apoptosis behavior of 13-hydroxyoctadecadienoic acid enantiomers in a colorectal cancer cell line. *Am J Physiol Gastrointest Liver Physiol* [Internet]. 2014;307(6):G664-71. Available from: <http://www.ncbi.nlm.nih.gov/pubmed/25035111>
104. Chang J, Jiang L, Wang Y, Yao B, Yang S, Zhang B, et al. 12/15 lipoxygenase regulation of colorectal tumorigenesis is determined by the relative tumor levels of its metabolite 12-

- HETE and 13-HODE in animal models. *Oncotarget*. 2015;
105. Kato M, Nagaya T, Fujieda M, Saito K, Yoshida J, Seo H. Expression of PPAR γ and its ligand-dependent growth inhibition in human brain tumor cell lines. *Jpn J Cancer Res* [Internet]. 2002 Jun [cited 2019 Mar 5];93(6):660–6. Available from: <http://www.ncbi.nlm.nih.gov/pubmed/12079514>
 106. Papi A, Tatenhorst L, Terwel D, Hermes M, Kummer MP, Orlandi M, et al. PPAR γ and RXR γ ligands act synergistically as potent antineoplastic agents *in vitro* and *in vivo* glioma models. *J Neurochem* [Internet]. 2009 Jun 1 [cited 2019 Mar 7];109(6):1779–90.
 107. Morosetti R, Servidei T, Mirabella M, Rutella S, Mangiola A, Maira G, et al. The PPAR γ ligands PGJ2 and rosiglitazone show a differential ability to inhibit proliferation and to induce apoptosis and differentiation of human glioblastoma cell lines. *Int J Oncol* [Internet]. 2004 Aug 1 [cited 2019 Mar 5];25(2):493–502.
 108. Mueller E, Smith M, Sarraf P, Kroll T, Aiyer A, Kaufman DS, et al. Effects of ligand activation of peroxisome proliferator-activated receptor gamma in human prostate cancer. *Proc Natl Acad Sci U S A* [Internet]. 2000 Sep 26 [cited 2019 Mar 5];97(20):10990–5. Available from: <http://www.ncbi.nlm.nih.gov/pubmed/10984506>
 109. Robbins GT, Nie D. PPAR gamma, bioactive lipids, and cancer progression. *Front Biosci (Landmark Ed)* [Internet]. 2012 Jan 1 [cited 2019 Mar 5];17:1816–34. Available from: <http://www.ncbi.nlm.nih.gov/pubmed/22201838>
 110. Ju KD, Lim JW, Kim H. Peroxisome Proliferator-activated Receptor-gamma Inhibits the Activation of STAT3 in Cerulein-stimulated Pancreatic Acinar Cells. *J cancer Prev* [Internet]. 2017 Sep [cited 2019 Mar 7];22(3):189–94. Available from: <http://www.ncbi.nlm.nih.gov/pubmed/29018784>
 111. Wang LH, Yang XY, Zhang X, Huang J, Hou J, Li J, et al. Transcriptional Inactivation of STAT3 by PPAR γ Suppresses IL-6-Responsive Multiple Myeloma Cells. *Immunity* [Internet]. 2004 Feb 1 [cited 2019 Mar 7];20(2):205–18.
 112. Moreira D, Zhang Q, Hossain DMS, Nechaev S, Li H, Kowolik CM, et al. TLR9 signaling through NF- κ B/RELA and STAT3 promotes tumor-propagating potential of prostate cancer cells. *Oncotarget* [Internet]. 2015 Jul 10 [cited 2019 Mar 7];6(19):17302–13. Available from: <http://www.ncbi.nlm.nih.gov/pubmed/26046794>
 113. Hodge DR, Hurt EM, Farrar WL. The role of IL-6 and STAT3 in inflammation and cancer. *Eur J Cancer* [Internet]. 2005 Nov 1 [cited 2019 Mar 7];41(16):2502–12. Available from:
 114. Im C-N. Combination Treatment with PPAR γ Ligand and Its Specific Inhibitor GW9662 Downregulates BIS and 14-3-3 Gamma, Inhibiting Stem-Like Properties in Glioblastoma Cells. *Biomed Res Int* [Internet]. 2017 [cited 2019 Mar 5];2017:5832824. Available from: <http://www.ncbi.nlm.nih.gov/pubmed/28642874>
 115. Chearwae W, Bright JJ. PPAR γ agonists inhibit growth and expansion of CD133+ brain tumour stem cells. *Br J Cancer* [Internet]. 2008 Dec 16 [cited 2019 Mar 7];99(12):2044–53. Available from: <http://www.ncbi.nlm.nih.gov/pubmed/19018263>

116. Wan Z, Shi W, Shao B, Shi J, Shen A, Ma Y, et al. Peroxisome proliferator-activated receptor γ agonist pioglitazone inhibits β -catenin-mediated glioma cell growth and invasion. *Mol Cell Biochem* [Internet]. 2011 Mar 9 [cited 2019 Mar 7];349(1–2):1–10. Available from: <http://link.springer.com/10.1007/s11010-010-0637-9>
117. Tachibana K, Yamasaki D, Ishimoto K, Doi T. The role of PPARs in cancer. *PPAR Res*. 2008.
118. Stephen RL, Gustafsson MCU, Jarvis M, Tatoud R, Marshall BR, Knight D, et al. Activation of Peroxisome Proliferator-Activated Receptor δ Stimulates the Proliferation of Human Breast and Prostate Cancer Cell Lines. *Cancer Res* [Internet]. 2004 May 1 [cited 2019 Mar 5];64(9):3162–70. Available from: <http://www.ncbi.nlm.nih.gov/pubmed/15126355>
119. Shao J, Sheng H, DuBois RN. Peroxisome proliferator-activated receptors modulate K-Ras-mediated transformation of intestinal epithelial cells. *Cancer Res* [Internet]. 2002 Jun 1 [cited 2019 Mar 5];62(11):3282–8. Available from: <http://www.ncbi.nlm.nih.gov/pubmed/12036946>
120. Obinata H, Hattori T, Nakane S, Tatei K, Izumi T. Identification of 9-hydroxyoctadecadienoic acid and other oxidized free fatty acids as ligands of the G protein-coupled receptor G2A. *J Biol Chem*. 2005;280(49):40676–83.
121. Qiu J, Li Q, Bell KA, Yao X, Du Y, Zhang E, et al. Small-molecule inhibition of prostaglandin E receptor 2 impairs cyclooxygenase-associated malignant glioma growth. *Br J Pharmacol* [Internet]. 2019 Jun 29 [cited 2019 May 30];176(11):1680–99.
122. Daniel PM, Filiz G, Mantamadiotis T. Sensitivity of GBM cells to cAMP agonist-mediated apoptosis correlates with CD44 expression and agonist resistance with MAPK signaling. *Cell Death Dis* [Internet]. 2016;7(12):e2494. Available from: <http://www.nature.com/doi/10.1038/cddis.2016.393>
123. Peter C, Waibel M, Radu CG, Yang L V, Witte ON, Schulze-Osthoff K, et al. Migration to apoptotic “find me” signals is mediated via the phagocyte receptor G2A. *J Biol Chem* [Internet]. 2008 Feb 29 [cited 2019 Mar 5];283(9):5296–305. Available from: <http://www.ncbi.nlm.nih.gov/pubmed/18089568>
124. Frasch SC, Fernandez-Boyanapalli RF, Berry KZ, Leslie CC, Bonventre J V., Murphy RC, et al. Signaling via macrophage G2A enhances efferocytosis of dying neutrophils by augmentation of rac activity. *J Biol Chem*. 2011;286(14):12108–22.
125. Jiang J, Qiu J, Li Q, Shi Z. Prostaglandin E2 Signaling: Alternative Target for Glioblastoma? *Trends in Cancer*. 2017;3(2):75–8.
126. Kelavkar UP, Badr KF. Effects of mutant p53 expression on human 15-lipoxygenase-promoter activity and murine 12/15-lipoxygenase gene expression: evidence that 15-lipoxygenase is a mutator gene. *Proc Natl Acad Sci U S A* [Internet]. 1999;96(8):4378–83.
127. Zhang Y, Dube C, Gibert M, Cruickshanks N, Wang B, Coughlan M, et al. The p53 Pathway in Glioblastoma. *Cancers (Basel)* [Internet]. 2018 Sep 1 [cited 2019 Mar 5];10(9). Available from: <http://www.ncbi.nlm.nih.gov/pubmed/30200436>

128. O'donnell VB, Kühn H. Co-oxidation of NADH and NADPH by a mammalian 15-lipoxygenase: inhibition of lipoxygenase activity at near-physiological NADH concentrations. *Biochem J* [Internet]. 1997 Oct 1 [cited 2019 Mar 5];327 (Pt 1)(Pt 1):203–8. Available from: <http://www.ncbi.nlm.nih.gov/pubmed/9355754>
129. Stockert JC, Blázquez-Castro A, Cañete M, Horobin RW, Villanueva Á. MTT assay for cell viability: Intracellular localization of the formazan product is in lipid droplets. *Acta Histochem* [Internet]. 2012 Dec 1 [cited 2019 Mar 5];114(8):785–96.
130. Tavakoli-Yaraki M, Karami-Tehrani F. Apoptosis induced by 13-S-hydroxyoctadecadienoic acid in the breast cancer cell lines, MCF-7 and MDA-MB-231. *Iran J Basic Med Sci.* 2013;16(4):653–9.
131. Kelavkar U, Glasgow W, Eling TE. The effect of 15-lipoxygenase-1 expression on cancer cells. *Curr Urol Rep.* 2002;3(3):207–14.
132. Spindler SA, Sarkar FH, Sakr WA, Blackburn ML, Bull AW, Lagattuta M, et al. Production of 13-Hydroxyoctadecadienoic Acid (13-HODE) by Prostate Tumors and Cell Lines. *Biochem Biophys Res Commun* [Internet]. 1997 Oct 29 [cited 2019 Mar 7];239(3):775–81.
133. Sadik CD, Sies H, Schewe T. Inhibition of 15-lipoxygenases by flavonoids: Structure-activity relations and mode of action. *Biochem Pharmacol.* 2003;65(5):773–81.
134. Tsai Y-D, Chen H-J, Hsu H-F, Lu K, Liang C-L, Liliang P-C, et al. Luteolin inhibits proliferation of human glioblastoma cells via induction of cell cycle arrest and apoptosis. *J Taiwan Inst Chem Eng* [Internet]. 2013;44(6):837–45.
135. Wang Q, Wang H, Jia Y, Ding H, Zhang L, Pan H. Luteolin reduces migration of human glioblastoma cell lines via inhibition of the p-IGF-1R/PI3K/AKT/mTOR signaling pathway. *Oncol Lett.* 2017;14(3):3545–51.
136. Rai G, Kenyon V, Jadhav A, Schultz L, Armstrong M, Jameson JB, et al. Discovery of potent and selective inhibitors of human reticulocyte 15-lipoxygenase-1. *J Med Chem* [Internet]. 2010 Oct 28 [cited 2019 Mar 5];53(20):7392–404. Available from: <http://www.ncbi.nlm.nih.gov/pubmed/20866075>
137. Leopoldini M, Prieto Pitarch I, Russo N, Toscano M. Structure, conformation, and electronic properties of apigenin, luteolin, and taxifolin antioxidants. A first principle theoretical study. *J Phys Chem A.* 2004;108(1):92–6.
138. Ribeiro D, Freitas M, Tomé SM, Silva AMS, Porto G, Cabrita EJ, et al. European Journal of Medicinal Chemistry Inhibition of LOX by flavonoids : a structure e activity relationship study. *Eur J Med Chem* [Internet]. 2014;72:137–45. Available from: <http://dx.doi.org/10.1016/j.ejmech.2013.11.030>
139. Cheng W-Y, Chiao M-T, Liang Y-J, Yang Y-C, Shen C-C, Yang C-Y. Luteolin inhibits migration of human glioblastoma U-87 MG and T98G cells through downregulation of Cdc42 expression and PI3K/AKT activity. *Mol Biol Rep* [Internet]. 2013 Sep [cited 2019 Jun 2];40(9):5315–26. Available from: <http://www.ncbi.nlm.nih.gov/pubmed/23677714>
140. L. W, B. W, E.-M. P-W, M. B, X. L, C. M, et al. Natural product agonists of peroxisome

- proliferator-activated receptor gamma (PPARgamma): A review. *Biochem Pharmacol* [Internet]. 2014;92(1):73–89.
141. Hernández-Damián J, Andérica-Romero AC, Pedraza-Chaverri J. Paradoxical cellular effects and biological role of the multifaceted compound nordihydroguaiaretic acid. *Arch Pharm (Weinheim)*. 2014;347(10):685–97.
 142. Wilson DE, DiGianfilippo A, Ondrey FG, Anderson KM, Harris JE. Effect of nordihydroguaiaretic acid on cultured rat and human glioma cell proliferation. *J Neurosurg* [Internet]. 1989 Oct 1 [cited 2019 Mar 5];71(4):551–7. Available from: <https://thejns.org/view/journals/j-neurosurg/71/4/article-p551.xml>
 143. Rowland A, Elliot DJ, Knights KM, Mackenzie PI, Miners JO. The “albumin effect” and in vitro-in vivo extrapolation: sequestration of long-chain unsaturated fatty acids enhances phenytoin hydroxylation by human liver microsomal and recombinant cytochrome P450 2C9. *Drug Metab Dispos* [Internet]. 2008 May 1 [cited 2019 May 31];36(5):870–7. Available from: <http://www.ncbi.nlm.nih.gov/pubmed/18256202>
 144. Giese A, Loo MA, Tran N, Haskett D, Coons SW, Berens ME. Dichotomy of astrocytoma migration and proliferation. *Int J Cancer* [Internet]. 1996 Jul 17 [cited 2019 Mar 6];67(2):275–82.
 145. Garay T, Juhász É, Molnár E, Eisenbauer M, Czirók A, Dekan B, et al. Cell migration or cytokinesis and proliferation?--revisiting the “go or grow” hypothesis in cancer cells in vitro. *Exp Cell Res* [Internet]. 2013;319(20):3094–103. Available from: <http://www.ncbi.nlm.nih.gov/pubmed/23973668>
 146. Bastida E, Bertomeu MC, Haas TA, Almirall L, Lauri D, Orr FW, et al. Regulation of tumor cell adhesion by intracellular 13-HODE: 15-HETE ratio. *J Lipid Mediat* [Internet]. [cited 2019 Mar 6];2(5):281–93. Available from: <http://www.ncbi.nlm.nih.gov/pubmed/1966807>
 147. Seufert S, Coras R, Tränkle C, Zlotos DP, Blümcke I, Tatenhorst L, et al. PPAR gamma activators: Off-target against glioma cell migration and brain invasion. *PPAR Res*. 2008.
 148. Wang D, Liu Y, Chen L, Li P, Qu Y, Zhu Y, et al. Key role of 15-LO/15-HETE in angiogenesis and functional recovery in later stages of post-stroke mice. *Sci Rep* [Internet]. 2017 Apr 24 [cited 2019 Mar 6];7:46698. Available from: <http://www.ncbi.nlm.nih.gov/pubmed/28436420>
 149. MCCOMB RD, MOUL JM, BIGNER DD. Distribution of Type VI Collagen in Human Gliomas. *J Neuropathol Exp Neurol* [Internet]. 1987 Nov 1 [cited 2019 May 31];46(6):623–33.
 150. Bouterfa H, Darlapp AR, Klein E, Pietsch T, Roosen K, Tonn JC. Expression of different extracellular matrix components in human brain tumor and melanoma cells in respect to variant culture conditions. *J Neurooncol* [Internet]. 1999 Aug [cited 2019 Jun 6];44(1):23–33. Available from: <http://www.ncbi.nlm.nih.gov/pubmed/10582665>
 151. Sun H, Bian X, Chen Y, Shi J. [The effect of nordihydroguaiaretic acid on endothelial cell migration induced by glioma cells]. *Zhonghua bing li xue za zhi = Chinese J Pathol*

- [Internet]. 2000 Feb [cited 2019 Mar 6];29(1):30–3. Available from: <http://www.ncbi.nlm.nih.gov/pubmed/11866889>
152. Li X, Fan S, Pan X, Xiaokaiti Y, Duan J, Shi Y, et al. Nordihydroguaiaretic acid impairs prostate cancer cell migration and tumor metastasis by suppressing neuropilin 1. *Oncotarget* [Internet]. 2016 Dec 27 [cited 2019 Mar 6];7(52):86225–38. Available from: <http://www.ncbi.nlm.nih.gov/pubmed/27863391>
 153. Koul D, Parthasarathy R, Shen R, Davies M a, Jasser S a, Chintala SK, et al. Suppression of matrix metalloproteinase-2 gene expression and invasion in human glioma cells by MMAC/PTEN. *Oncogene* [Internet]. 2001;20(46):6669–78. Available from: <http://www.ncbi.nlm.nih.gov/pubmed/11709701>
 154. Cesarini V, Martini M, Ricci Vitiani L, Luca Gravina G, Di Agostino S, Graziani G, et al. Type 5 phosphodiesterase regulates glioblastoma multiforme aggressiveness and clinical outcome. *Oncotarget* [Internet]. 2017;8(grade I):13223–39. Available from: <http://www.oncotarget.com/abstract/14656%0Ahttp://www.ncbi.nlm.nih.gov/pubmed/28099939>
 155. Hagemann C. A complete compilation of matrix metalloproteinase expression in human malignant gliomas. *World J Clin Oncol* [Internet]. 2012;3(5):67.
 156. Ying J, Kun-Peng X, Hong-Nan H, Li-Meng W, Wei Z, Ming-Jie X. Inhibitory effect of luteolin on the angiogenesis of chick chorioallantoic membrane and invasion of breast cancer cells via downregulation of AEG-1 and MMP-2. *Acta Physiol Sin* [Internet]. 2013 [cited 2019 Jun 2];65(5):513–8.
 157. Laneuville O, Breuer DK, Xu N, Huang ZH, Gage DA, Watson JT, et al. Fatty acid substrate specificities of human prostaglandin-endoperoxide H synthase-1 and -2. Formation of 12-hydroxy-(9Z, 13E/Z, 15Z)- octadecatrienoic acids from alpha-linolenic acid. *J Biol Chem* [Internet]. 1995 Aug 18 [cited 2019 Mar 7];270(33):19330–6. Available from: <http://www.ncbi.nlm.nih.gov/pubmed/7642610>
 158. Fujimoto Y, Yonemura T, Sakuma S. Role of linoleic Acid hydroperoxide preformed by cyclooxygenase-1 or -2 on the regulation of prostaglandin formation from arachidonic Acid by the respective enzyme. *J Clin Biochem Nutr* [Internet]. 2008 Sep [cited 2019 Mar 7];43(2):65–8. Available from: <http://www.ncbi.nlm.nih.gov/pubmed/18818754>
 159. Lipari L, Mauro A, Gallina S, Tortorici S, Buscemi M, Tetè S, et al. Expression of Gelatinases (MMP-2, MMP-9) and Cyclooxygenases (COX-1, COX-2) in Some Benign Salivary Gland Tumors. *Int J Immunopathol Pharmacol* [Internet]. 2012 Jan 1 [cited 2019 Mar 7];25(1):107–15.
 160. Soler J, Saura P, García-López D, Masgrau L, Lluch JM, González-Lafont À. How Can Linoleic Acid Be the Preferential Substrate of the Enzyme 15-Lipoxygenase-1? A QM/MM Approach. *J Phys Chem B*. 2016;120(8):1950–60.

APPENDIX - SUPPLEMENTARY DATA

This project is part of a larger project examining the expression and activity of various lipid mediators present in glioblastoma cells. Previous LC/EIS-MS/MS identified the presence of 15-LOX metabolites as the most abundant lipid mediators in five GBM cell lines and patient samples compared to the other lipoxygenase isoforms (Figure S1).

Examining the Human Protein Atlas (HPA) and The Cancer Genome Atlas (TCGA) Databases, the following figures compliment and support the findings of this study. The Human Protein Atlas did not identify 15-LOX-1 or 15-LOX-2 in GBM cell lines or glioma samples with the primers and antibodies used (Figures S2 and S3). The TCGA database demonstrated a significant decrease in 15-LOX-1 mRNA between non-tumor and GBM samples, while no significant difference was observed in 15-LOX-2 mRNA (Figure S4). Survival curves did not demonstrate any changes between high and low expression of 15-LOX-1 or 15-LOX-2 among GBM patients (Figure S4). The expression of PPAR β/δ mRNA and protein was identified in GBM cell lines and glioma samples according to HPA. Decreased mRNA was also observed in GBM samples compared to non-tumor samples and was correlated with decreased survival (Figure S5).

Regarding MMP expression in GBM, the Human Protein Atlas demonstrated the presence of MMP-2 and MMP-14 mRNA and protein expression in normal brain tissue, GBM cell lines and glioma patient samples (Figures S6 and S7). MMP-9 was not identified in any of the tissues (Figure S8). The TCGA database identified a significantly increased expression of MMP-2, MMP-14 and MMP-9 mRNA between non-tumor and GBM samples. Decreased survival was observed among GBM patients with high expression of MMP-2 (Figure S9). A summary of the findings may be found in Table S1.

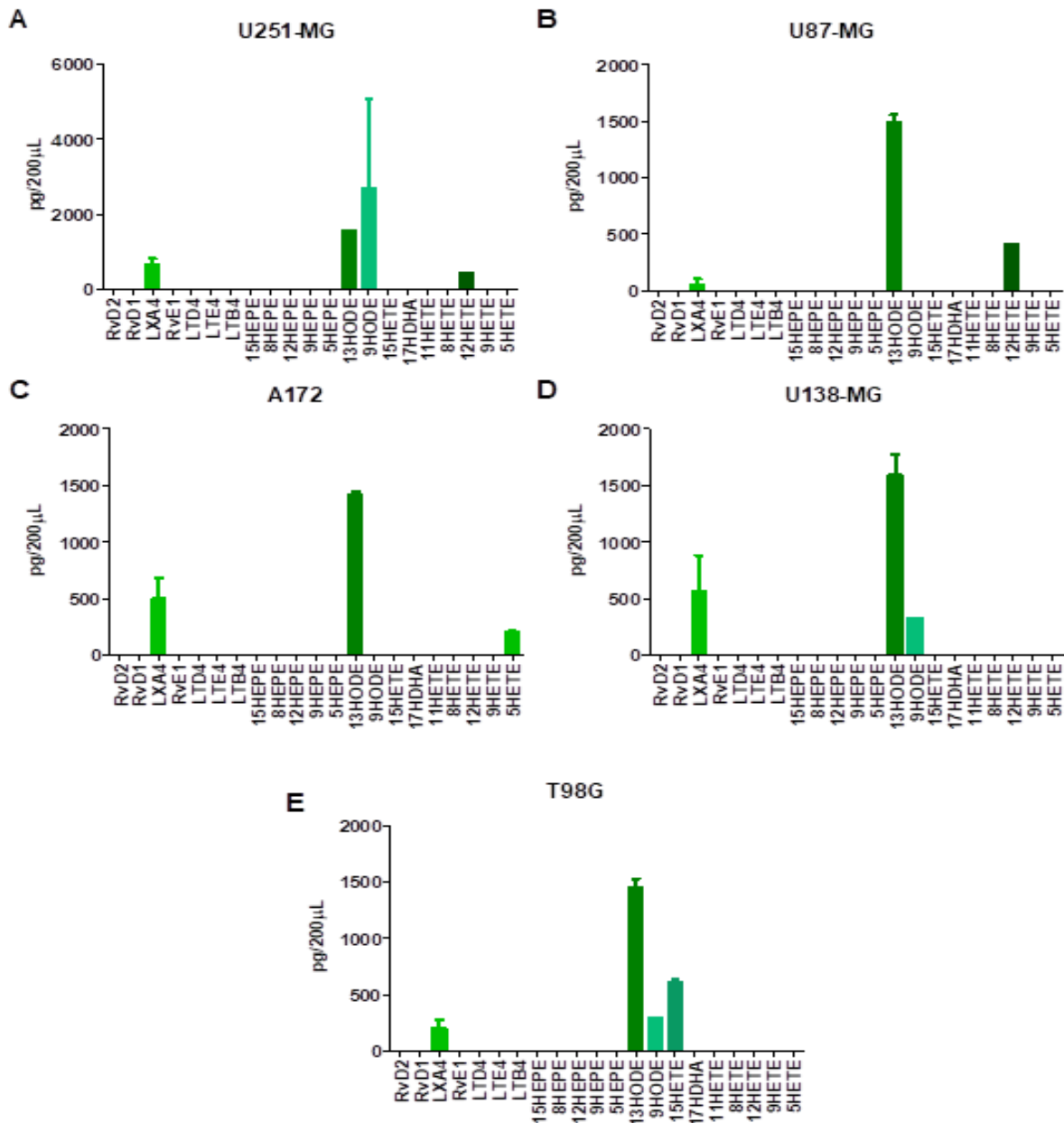


Figure S1. LC\ESI-MS/MS of the products: RvD2, RvD1, LXA4, RvE1, LTD4, LTE4, LTB4, 15-HEPE, 8-HEPE, 12-HEPE, 9-HEPE, 5-HEPE, 13-HODE, 9-HODE, 15-HETE, 17-HDHA, 11-HETE, 8-HETE, 12-HETE, 9-HETE, 5-HETE in the cell lines U-251MG (A), U-87MG (B), A172 (C), U-138MG (D) and T98G (E). N=3.

Source: Souza, FC. Eicosanoids as new therapeutic targets in the treatment of human glioblastoma [Thesis (Doctor from Department of Cell and Developmental Biology)] – Institute of Biomedical Sciences, University of Sao Paulo, Sao Paulo; 2017.

15-LOX-1

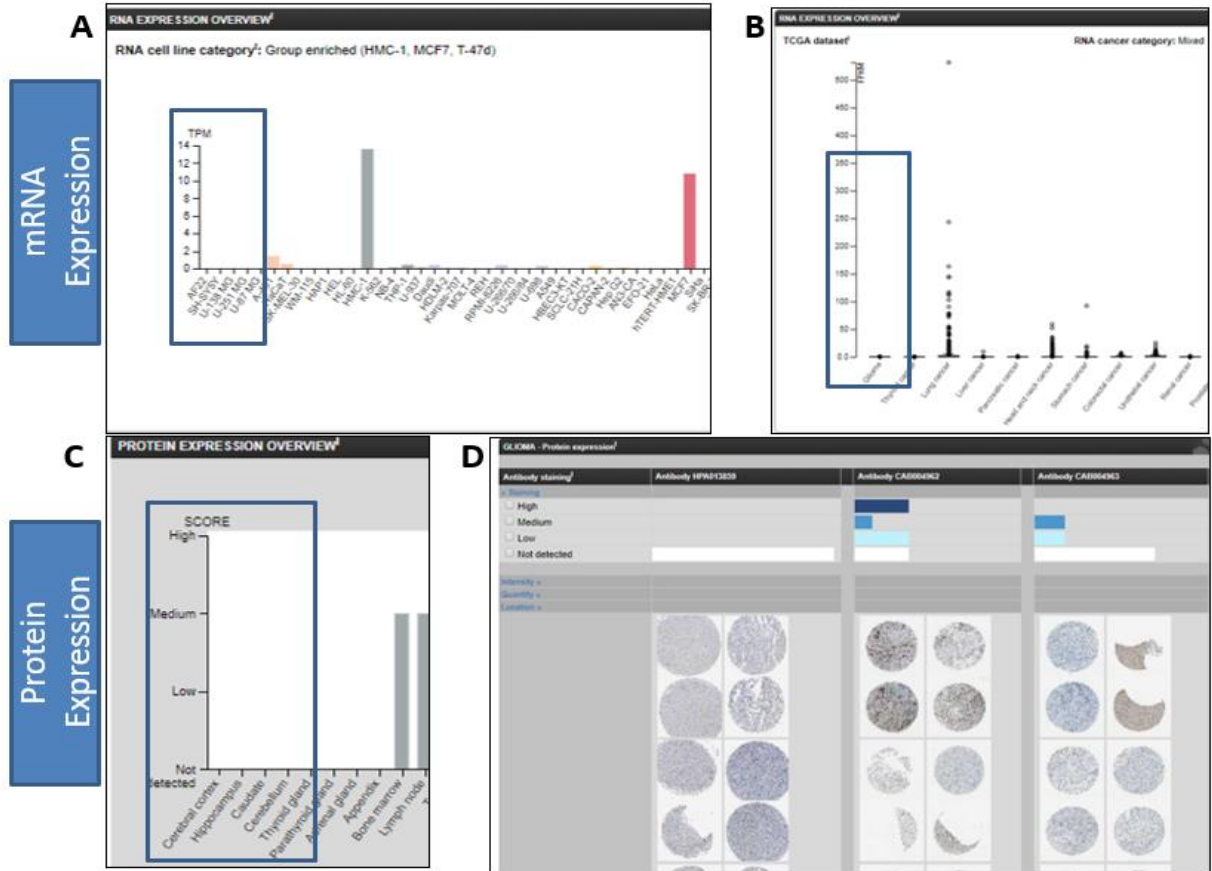


Figure S2. 15-LOX-1 mRNA and protein expression observed by the Human Protein Atlas Project. A) mRNA was not observed in GBM cell lines U138-MG, U251-MG and U87-MG. B) mRNA was not observed in glioma samples. C) Protein Expression was not observed in normal brain tissue. D) Partial protein expression was observed in GBM patient samples.

15-LOX-2

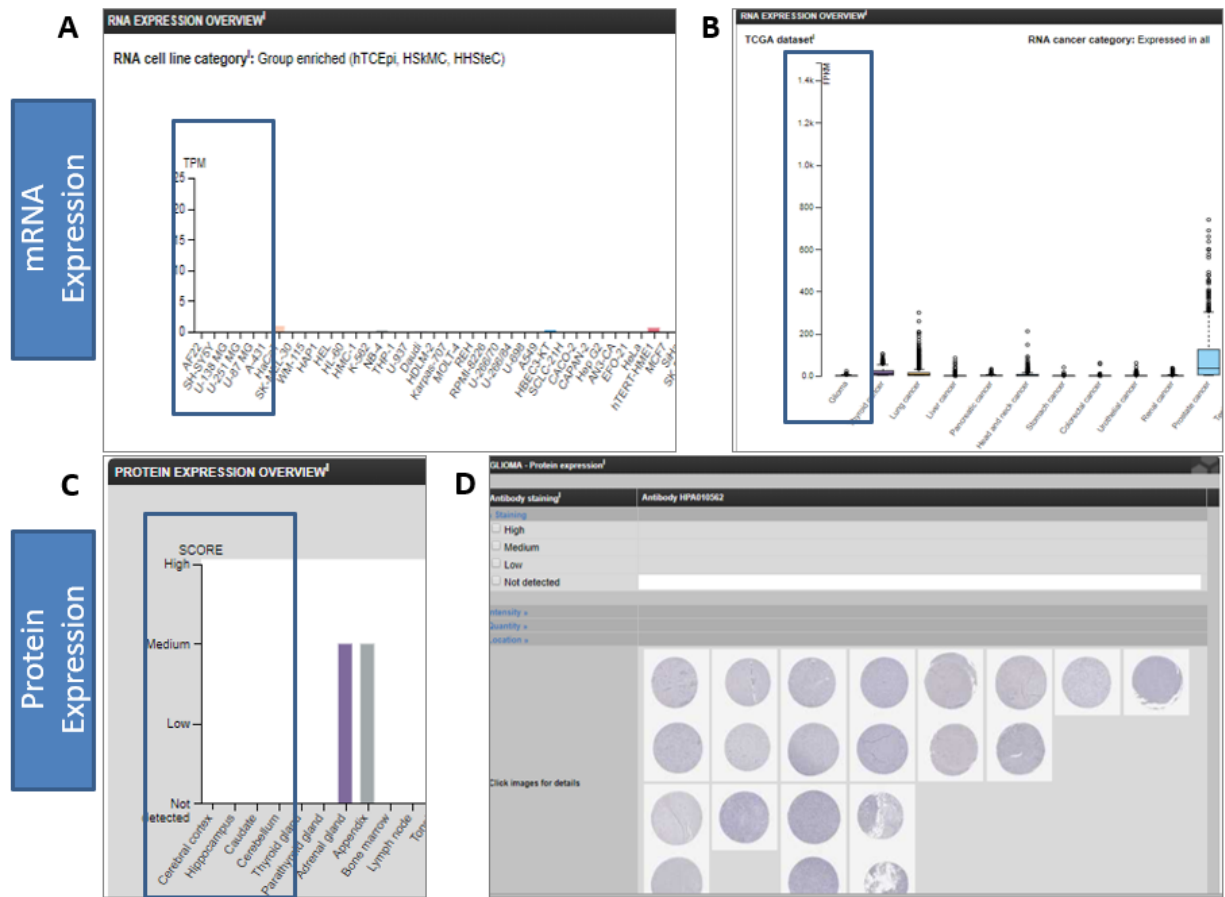


Figure S3. 15-LOX-2 mRNA and protein expression observed by the Human Protein Atlas Project. A) mRNA was not observed in GBM cell lines U138-MG, U251-MG and U87-MG. B) mRNA was not observed in glioma samples. C) Protein expression was not observed in normal brain tissue. D) No protein expression was observed in GBM patient samples.

TCGA

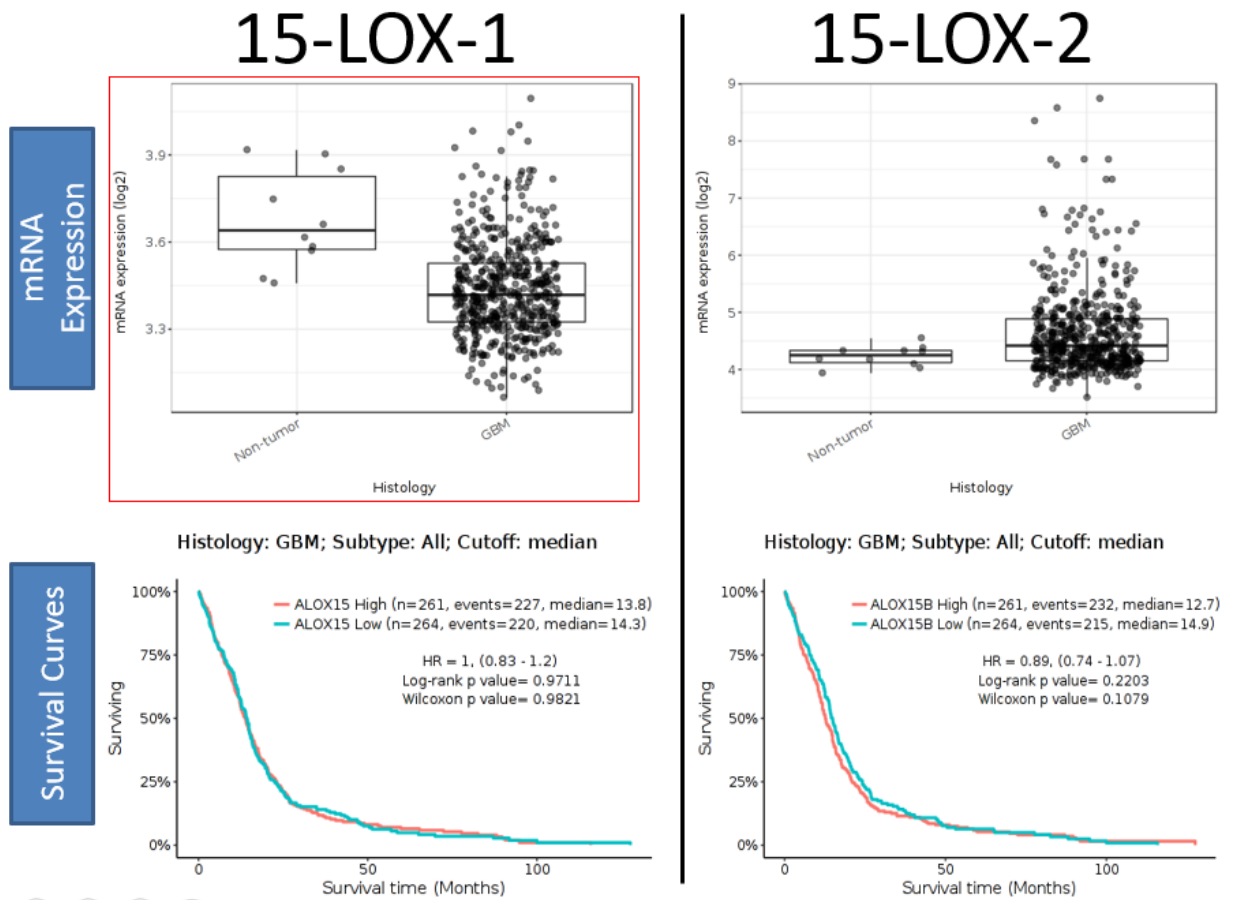
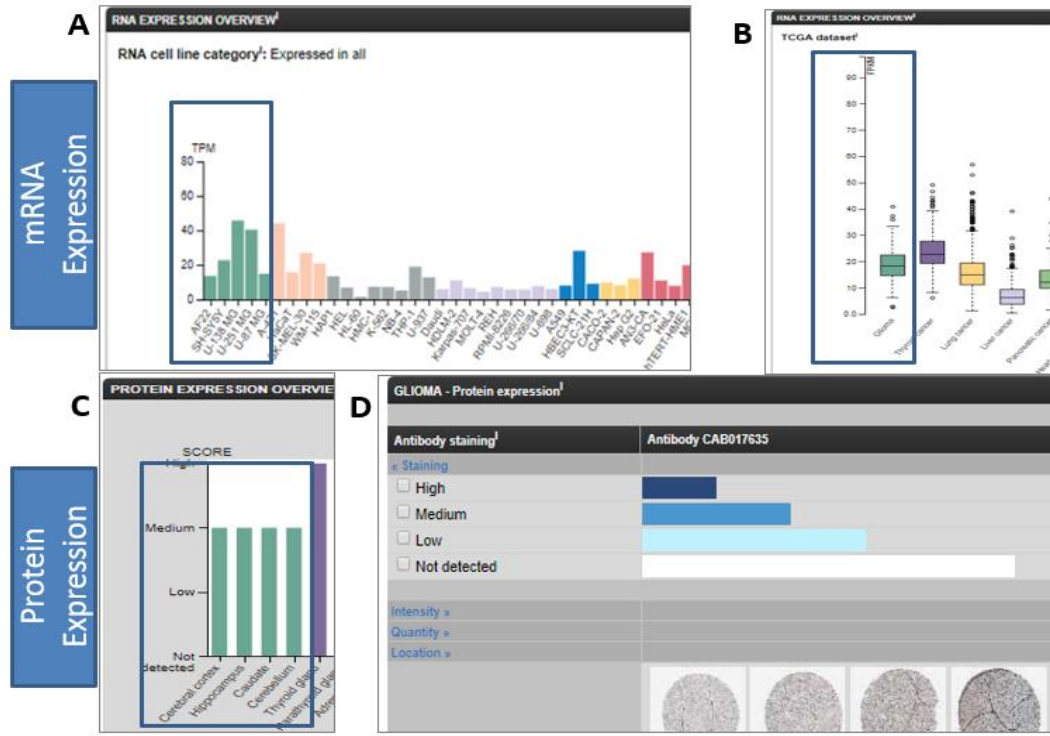


Figure S4. TCGA database information concerning 15-LOX-1 and 15-LOX-2 mRNA expression and survival curves. 15-LOX-1 mRNA is significantly decreased in GBM cells compared to non-tumor tissue. Survival curves were not altered by the high or low expression of 15-LOX-1 or 15-LOX-2.

PPAR β/δ



TCGA PPAR β/δ

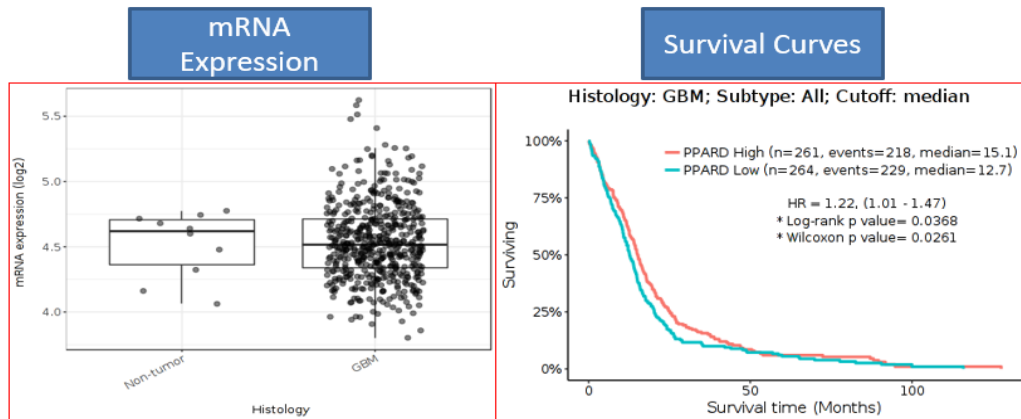


Figure S5. PPAR beta/delta mRNA and protein expression observed by the HPA [top] and TCGA [bottom]. A) mRNA was observed in GBM cell lines U138-MG, U251-MG and U87-MG. B) mRNA was observed in glioma samples. C) Protein expression was observed in normal brain tissue. D) Protein expression was observed in GBM patient samples. TCGA: mRNA was significantly decreased in GBM samples compared to non-tumor samples and decreased expression was associated with decreased survival.

MMP14

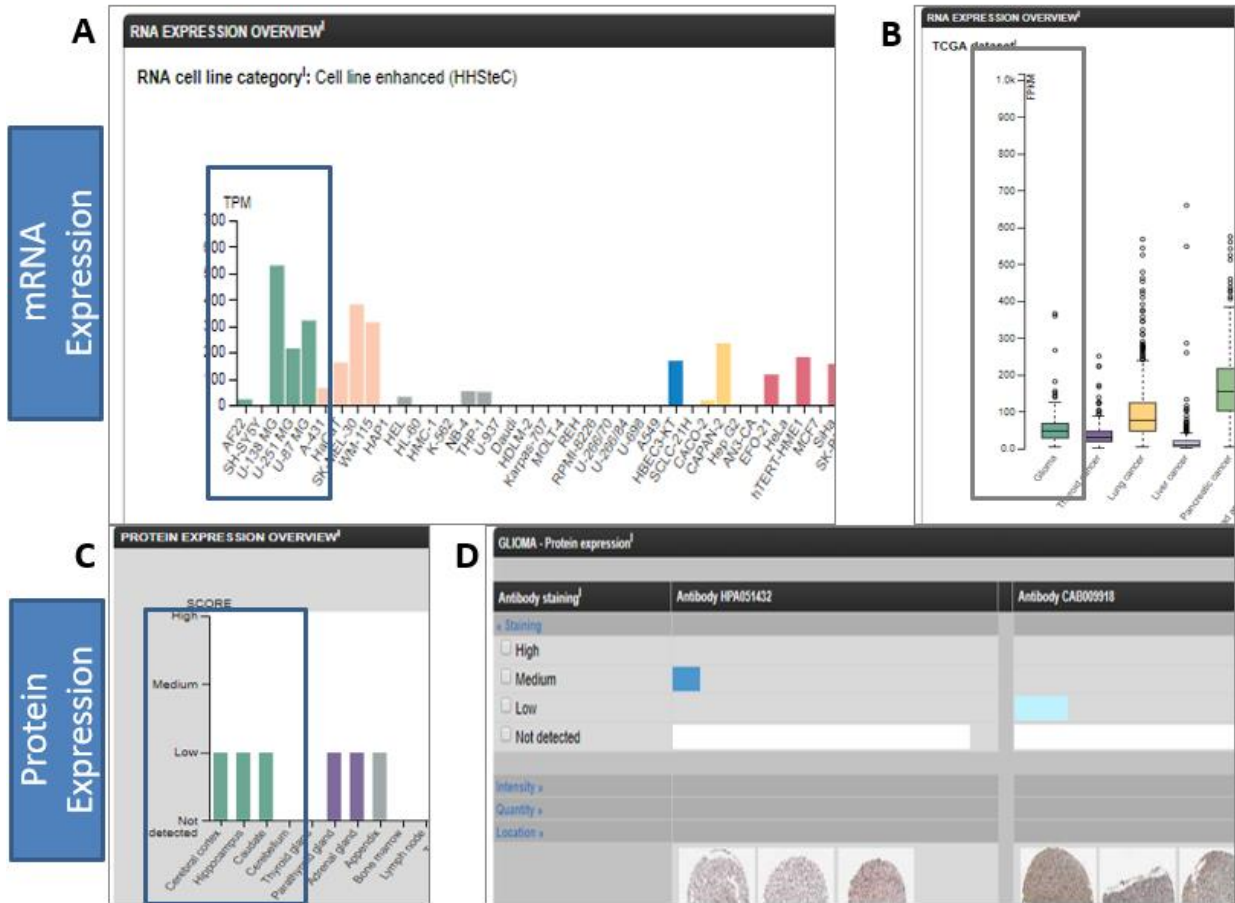


Figure S7. MMP-14 mRNA and protein expression observed by the Human Protein Atlas Project. A) mRNA was observed in GBM cell lines U138-MG, U251-MG and U87-MG. B) mRNA was identified in glioma samples. C) Protein expression was observed in the cerebral cortex, hippocampus and caudate, but not in the cerebellum. D) Very low to medium protein expression was observed in GBM patient samples.

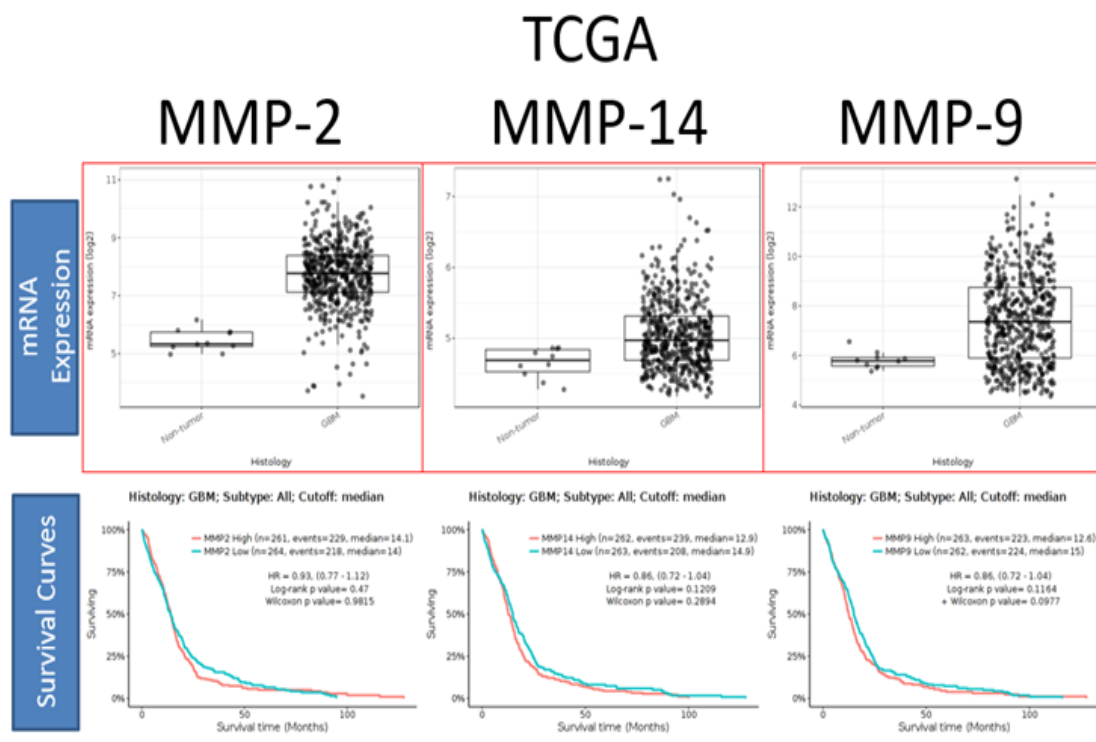


Figure S9. TCGA database information concerning MMP-2, MMP-14, MMP-9 mRNA expression and survival curves. The mRNAs of all three MMPs were significantly increased in GBM cells compared to non-tumor tissue [top row]. No significant correlation between MMP-2, MMP-14 and MMP-9 expression and survival were observed [bottom row].

Table S1. Summary of mRNA/ protein expression identified by the Human Protein Atlas and TCGA Databases, accessed beginning from September, 2018.

Protein	Protein Expression (Normal Brain Tissue)	mRNA present (no. / 3 GBM Cell Lines tested)	mRNA found in Glioma Samples	Protein Expression (in Glioma samples)	*TCGA: mRNA	†TCGA: Survival
15-LOX-1	-	-	-	-	↓	-
15-LOX-2	-	-	-	-	-	-
PPAR γ	√	√ (1)	-	√	-	-
PPAR β / δ	√	√ (3)	√	√	↓	↑
GPR132	√	√ (1)	√	√	-	↑
MMP-2	√	√ (3)	√	√	↑	↓
MMP-14	√	√ (3)	√	√	↑	-
MMP-9	-	√ (1)	-	-	↑	-

*TCGA: significantly increased (↑) or decreased (↓) mRNA expression in GBM samples compared with non-tumor samples.

†TCGA: survival curves that displayed a significant increase (↑) or decrease (↓) in survival correlated with mRNA expression.

√ = confirmed

- = information not available